The influence of melt flux and crustal processing on Re-Os isotope systematics of ocean island basalts: constraints from Galápagos

Gibson, S.A.[1], Dale, C.W.[2], Geist, D.J.[3], Day J.A.[1], Brügmann, G.[4] & Harpp, K.[5]

[1]Dept of Earth Sciences, University of Cambridge, Cambridge, UK sally@esc.cam.ac.uk
[2] Dept of Earth Sciences, Durham University, Durham, UK
[3] National Science Foundation, Earth Sciences Division, 4201 Wilson Blvd., Arlington, VA 22230, USA
[4]Curt-Engelhorn-Zentrum Archäometrie, Mannheim, Germany
[5]Geology Department, Colgate University, Hamilton, New York, USA

Corresponding author: Sally Gibson sally@esc.cam.ac.uk

Accepted for publication in EPSL

Word count: 6502

Main manuscript: 9 figures & 1 table
Supplementary file: 1 consisting of: 8 supplementary figures, 4 tables (sample info, microprobe data, standards and full whole rock data set) and 2 text files (Full description of Re-Os techniques & data sources used to compile figures)

Highlights (85 characters)

- High MgO Galápagos basalts exhibit a range of $^{187}Os/^{188}Os$ comparable to global OIB
- $^{187}Os/^{188}Os$ of Galápagos basalts broadly correlates with distance from plume stem
- $^{187}Os/^{188}Os$ of Galápagos basalts is influenced by melt flux to the crust
- Os threshold value for crustal contamination in OIB varies with setting
- Some regions of lower oceanic crust may have higher ^{187}Os than previously found

Abstract

New rhenium-osmium data for high-MgO (>9 wt. %) basalts from the Galápagos Archipelago reveal a large variation in $^{187}Os/^{188}Os$ (0.1304 to 0.173), comparable with the range shown by primitive global ocean island basalts (OIBs). Basalts with the least radiogenic $^{187}Os/^{188}Os$ occur closest to the Galápagos plume stem: those in western Galápagos have low $^{187}Os/^{188}Os$, moderate $^{87}Sr/^{86}Sr$, $^{143}Nd/^{144}Nd$, $^{206}Pb/^{204}Pb$ and high $^{3}He/^{4}He$ whereas basalts in the south also have low $^{187}Os/^{188}Os$ but more radiogenic $^{87}Sr/^{86}Sr$, $^{143}Nd/^{144}Nd$, $^{206}Pb/^{204}Pb$ and $^{3}He/^{4}He$. Our new Os isotope data are consistent with the previously established spatial zonation of the common global isotopic mantle reservoir "C" and ancient recycled oceanic crust in the mantle plume beneath western and southern parts of Galápagos, respectively.

Galápagos basalts with the most radiogenic $^{187}Os/^{188}Os$ (up to 0.1875) typically have moderate MgO (7-9 wt. %) and low Os (<50 pg g^{-1}) but have contrastingly unenriched Sr, Nd and Pb isotope signatures. We interpret this decoupling of chalcophile and lithophile isotopic systems as due to assimilation of young Pacific lower crust during crystal fractionation. Mixing models show the assimilated crust must have higher contents of Re and Os, and more radiogenic $^{187}Os/^{188}Os$ (0.32), than previously proposed for oceanic gabbros. We suggest the inferred, exceptionally-high radiogenic ^{187}Os of the Pacific crust may be localised and due to sulfides precipitated from hydrothermal systems established at the Galápagos Spreading Centre.

High $^{187}Os/^{188}Os$ Galápagos basalts are found where plume material is being dispersed laterally away from the plume stem to the adjacent spreading centre (*i.e.* in central and NE parts of the archipelago). The extent to which crustal processing influences $^{187}Os/^{188}Os$ appears to be primarily controlled by melt flux: as distance from the stem of the Galápagos plume increases, the melt flux decreases and crustal assimilation becomes proportionally greater, accounting for co-variations in Os and $^{187}Os/^{188}Os$. The Os concentration threshold below which the $^{187}Os/^{188}Os$ of Galápagos basalts are contaminated (100 pg g^{-1}) is higher than the canonical value (<50 pg g^{-1}) assumed for many other global OIBs (e.g. for Iceland, Grande Comores and Hawaii). This most likely reflects the low overall melt flux to the crust from the Galápagos plume, which has only a moderate excess temperature and buoyancy flux. Our findings have

implications for the interpretation of $^{187}Os/^{188}Os$ ratios in other ocean island settings, especially those where large variations in $^{187}Os/^{188}Os$ have been linked to heterogeneity in mantle lithology or sulfide populations: the effect of crustal contamination on $^{187}Os/^{188}Os$ may be greater than previously recognised, particularly for basalts associated with weak, low melt flux mantle plumes, such as Tristan, Bouvet, Crozet and St Helena.

Keywords: Osmium isotopes, ocean island basalts, Galápagos, mantle plume, crustal contamination, pyroxenite.

1. Introduction

Models invoking lithological heterogeneity of the convecting mantle have been widely adopted to explain elemental and isotopic variations in suites of ocean-island basalts (OIBs). Nevertheless, evidence for the extent of this heterogeneity remains contentious, especially the contribution of melts derived from recycled oceanic crust, *i.e.* pyroxenite/eclogite, compared to interaction of melts with the modern oceanic lithosphere. One approach adopted to quantify this lithological heterogeneity in OIB source regions utilizes the chalcophile ^{187}Re-^{187}Os isotopic system, which is distinct from lithophile radiogenic isotopic systems (*i.e.* Sr, Nd, Pb and Hf) because of the large difference in compatibilities of the parent and daughter elements during mantle melting: on a bulk scale, rhenium is moderately incompatible and osmium is strongly compatible [*Allègre and Luck*, 1980]. Decay of ^{187}Re to ^{187}Os causes oceanic crust with high Re/Os (*i.e.* gabbro and basalt) to rapidly develop supra-chondritic ^{187}Os/^{188}Os isotopic ratios while peridotite melt residues in the lithospheric mantle have low Re/Os and unradiogenic ^{187}Os/^{188}Os. Radiogenic ^{187}Os/^{188}Os is therefore believed to be a particularly sensitive indicator of ancient recycled crust, and coupled correlations of Os isotopic ratios with those of Sr-Nd-Pb and O have been interpreted as evidence of mixing of melts from peridotite and subducted oceanic crust in the convecting mantle, *e.g.* Reisberg *et al.* [1993], Hauri *et al.* [1996], Class *et al.* [2009], Day *et al.* [2009].

Osmium is highly-compatible during sulfide fractionation from primary magmas [*Burton et al.*, 2002], and the low Os (<50 pg g^{-1}) of oceanic basalts makes their ^{187}Os/^{188}Os ratios particularly susceptible to shallow level contamination either by: gabbros in the lower oceanic crust (Os=55 pg g^{-1}, initial ^{187}Os/^{188}Os =0.142; e.g. [*Peucker-Ehrenbrink et al.*, 2012]); interaction with seawater (Os=0.01 pg g^{-1},^{187}Os/^{188}Os =1.06; [*Levasseur et al.*, 1998]) or seawater-altered crust [*Gannoun et al.*, 2007]. While upper oceanic crust can acquire a high initial ^{187}Os/^{188}Os (0.173 [*Peucker-Ehrenbrink et al.*, 2003]) it typically has a low Os content (<20 pg g^{-1}; [*Gannoun et al.*, 2007]) and assimilation of young material of this type has a limited effect on the Os isotopic ratios of primitive basalts. The elevated ^{187}Os/^{188}Os ratios of low Os (<50 pg g^{-1}) oceanic basalts emplaced through young crust (<25 Ma; *e.g.* Iceland, Azores, Pitcairn; Skovgaard et al. [2001], Eisele [2002], Widom [1996]) have been attributed to contamination by seawater, assimilation of shallow-level volcanic crust or marine sediments whereas the elevated ^{187}Os/^{188}Os ratios of low Os (<50 pg g^{-1}) basalts emplaced through 'old' oceanic

crust have been linked to assimilation of lower crust with highly-radiogenic $^{187}Os/^{188}Os$, (*e.g.* Canary Islands and Grande Comore; Class [2009], Day et al. [2010]) .

Attempts to constrain the composition of recycled material in the convecting mantle have focussed on $^{187}Os/^{188}Os$ of OIBs with high MgO and Os contents, *e.g.* Bennett *et al.* [2000], Hauri et al. [1996], Lassiter & Hauri [1998], Dale *et al.* [2009b], Debaille *et al.* [2009], Day *et al.* [2009], Yang *et al.* [2013]. Nevertheless, Harvey *et al.* [2011] proposed that the broad spectrum of Os and $^{187}Os/^{188}Os$ displayed by high Os (>40 pg g^{-1}) OIBs results from sequential melting of different sulphide populations in the convecting mantle, rather than lithological heterogeneities, and the causes of variability in $^{187}Os/^{188}Os$ of OIBs therefore remain unclear.

We present the first osmium isotopic ratios, together with Re and Os contents, of recent, high-MgO (>7 wt. %) basalts in the Galápagos Archipelago. Lavas in this region exhibit large variations in elemental and Sr-Nd-Pb-Hf and He isotopic ratios that are widely believed to result from melting of different reservoirs in the upwelling Galápagos mantle plume (e.g. [*White et al.*, 1993; *Hoernle et al.*, 2000; *Harpp and White*, 2001]). We combine our Re-Os data with published geochemical analyses of Galápagos basalts, and the results of geophysical investigations, in order to explain regional differences in Os isotopes. Our findings for Galápagos, where detailed information about the underlying crust and plume structure is readily available, provide new constraints on the causes of variability in Os isotope systematics for global oceanic basalts.

2. Summary of the tectonic setting and volcanic activity in Galápagos

The Galápagos hotspot is located 160 km to 250 km south of the Galápagos Spreading Centre (GSC, Figure 1) and the region is an archetypal example of plume-ridge interaction. The thickness of the Galápagos lithosphere and plume structure have been described in recent investigations and are known in as much, if not greater, detail than any other archipelago. Body wave studies have shown that at depths >200 km the mantle plume stem resides beneath western Galápagos, which coincides with the region of most active volcanism [*Villagómez et al.*, 2014]. At shallower depths material is laterally dispersed from the plume stem towards the GSC. The distribution of historic volcanism on islands between the plume stem and ridge is largely controlled by local variations in lithospheric thickness and a confined NE channel of high-temperature,

low-viscosity flow embedded within the normal advection and spreading of the plume [*Gibson et al.*, 2015].

Galápagos volcanism is dominated by mildly alkaline and tholeiitic basalts with sub-ordinate trachytes and rhyolites and activity broadly decreases in age from <4 Ma in the east of the archipelago to <1 Ma in the west [*White et al.*, 1993; *Geist et al.*, 2014]. The different shield volcanoes on Isabela (Volcans Cerro Azul, Sierra Negra, Alcedo, Darwin, Wolf & Ecuador) and the volcano on Fernandina have the largest calderas up to 9 km in diameter, and are built on strong, thick lithosphere [*Feighner and Richards*, 1994]. The western volcanoes are supplied by a greater melt flux than currently occurs further east in the archipelago [*Geist et al.*, 1998].

Large regional variations in elemental ratios and Sr, Nd, Pb, Hf and He isotope compositions of Galápagos basalts have been attributed to spatial zonation in the underlying mantle plume (e.g. [*White et al.*, 1993; *Hoernle et al.*, 2000; *Harpp and White*, 2001]. Harpp & White [2001] identified four isotopically-distinct Galápagos mantle reservoirs: PLUME, which occurs in western Galápagos and resembles the common ("C") global plume reservoir; Depleted Galápagos Mantle, which is prevalent in central and eastern Galápagos and similar to global depleted mantle; and isotopically enriched Floreana (FLO) and Wolf-Darwin components, found in southern and northwestern Galápagos, respectively. The FLO reservoir is thought to contain ancient, altered oceanic crust that has been isolated in the convecting mantle [*Harpp et al.*, 2014].

3. Methods

Olivine grains were analysed for major and some trace elements using a Cameca SX 100 in the Department of Earth Sciences, University of Cambridge. Whole-rock powders with published major element analyses were digested and then analysed for a range of trace elements on a PerkinElmer Elan DRC II quadrupole Inductively Coupled Plasma (ICP) – Mass Spectrometer (MS) in the Department of Earth Sciences, University of Cambridge and for Sr, Nd and Pb isotopes using a ThermoFinnigan Neptune Multi-collector ICP-MS in the Department of Earth Sciences, Durham University (see Supplementary File and Gibson et al. [2012] for detailed descriptions of techniques).

Re-Os analyses were undertaken on subsets of samples at the Max-Planck-Institut für Chemie, Mainz in 2000 and in the Department of Earth Sciences, Durham

University in 2013. In both cases, 1.5 to 2 g of sample powder was digested and equilibrated with a ^{190}Os-^{185}Re spike using ~16 mol l^{-1} HNO_3 and ~12 mol l^{-1} HCl, in 3:2 or 2:1 proportions (see Supplementary File for further details of digestion techniques). Osmium was loaded onto Pt filaments and analysed as OsO_3^- by negative-thermal ionisation mass spectrometry (N-TIMS) using either a Finnigan MAT 262 (Mainz) or a ThermoFinnigan Triton (Durham). All relevant masses were measured sequentially using an axial secondary electron multiplier. Data were corrected offline for oxygen isotope interferences, spike-unmixing and mass fractionation (using $^{192}Os/^{188}Os$ ratios of 3.082678 (Mainz) and 3.08271 (Durham); these different values are insignificant at the level of precision required and measured on $^{187}Os/^{188}Os$. Counts on mass 233 ($^{185}ReO_3^-$) were typically insignificant for the precision required (<5 counts per second), with no correlation with mass 235, and thus no Re correction was made. Repeated analyses of Os in-house standard solutions gave average $^{187}Os/^{188}Os$ values of 0.10696 ± 0.00005 for 35 pg loads (n = 73) and 0.16108 ± 0.00016 for 10 pg aliquots (n = 23) at Mainz and Durham, respectively. At Mainz, Re was analysed on a Finnigan MAT 262 N-TIMS. Repeated measurements of a Johnson Matthey Re standard gave an external uncertainty of 0.1% (2 s.d.; n=57). At Durham, Re was measured on a ThermoFinnigan Element 2 ICP–MS. A Romil standard Re solution (1 ng g^{-1}) was analysed during each session to quantify the mass fractionation and a correction applied; this effect was always < 2% on the sample concentration. Total procedural blanks for Mainz were 0.2 - 1.5 pg Os, 0.1 - 0.5 pg Re (n = 8) with $^{187}Os/^{188}Os$ of 0.14 - 0.17 and Durham 0.25 - 1.9 pg Os, 0.5 - 1.2 pg Re (n = 3) with $^{187}Os/^{188}Os$ of 0.145 - 0.17.

4. Osmium isotope ratios of Galápagos basalts

4.1 Samples

Twenty-three samples, encompassing the full Sr-, Nd- and Pb-isotopic range displayed by Galápagos basalts, were analysed for $^{187}Os/^{188}Os$. We focused on the most primitive samples available from each island, specifically those with high bulk-rock Ni contents because of the similar behaviour of Os and Ni during crystal fractionation, albeit due to compatibility in different phases (Os in sulfides and Cr-spinel, Ni in silicate phases [*Burton et al.*, 2000]). In most cases we analysed samples with >200 µg g^{-1} Ni, >9 wt. % MgO and Mg# (Mg/Mg+Fe) =>0.6, exceptions were islands in NE Galápagos where the

most primitive basalts have <100 μg g^{-1} Ni, 7 to 9 wt. % MgO and Mg#=0.5 to 0.63 (Figure S1).

Ni and Cu sulphides are rare in Galapagos basalts but when present occur as either ~ 10 μm inclusions in olivine or as ~ 10 μm rounded globules in the matrix glass (Figure S2). In the samples from western and southern Galápagos (Fernandina, Isabela, Roca Redonda, Floreana) olivine occurs as both euhedral phenocrysts and large, strained macrocrysts with undulose extinction but in central (Santiago) and NE Galápagos (Pinta and Genovesa) it is predominantly present as euhedral phenocrysts (Table S1). Since olivine in Galápagos basalt is associated with Cr-spinel or sulfide inclusions, we have examined the possible effects of loss and accumulation of this phase on bulk-rock compositions. Co-variations between bulk-rock Mg# and forsterite content of the olivines suggest they are in equilibrium with the host magma at crustal pressures (Figure S3) and, importantly, the samples (with the exception of R9512) have not undergone extensive loss or accumulation of olivine.

4.2 Os and Re contents of Galápagos basalts

Osmium contents of Galápagos basalts range from 15 to 552 pg g^{-1} (Table 1) and generally exhibit a positive correlation with MgO, Ni and Cr (Figure 2). Exceptions are: the Roca Redonda sample (R9512) that has low Os (32 pg g^{-1}) given its high MgO (17.4 wt. %), Ni (510 μg g^{-1}) and Cr contents (625 μg g^{-1}); and a Volcan Darwin sample (E64) that has high Os (553 pg g^{-1}) and modest MgO (9.44 wt. %; Table 1). The co-variation of Os with MgO, Ni and Cr shown by Galápagos basalts is more systematic than has been observed for lavas from other OIBs and we attribute the relationship between Ni, MgO and Os to coupled crystallization of silicates and sulfides. We have used our whole-rock data with fractional crystallisation equations to calculate a bulk partition coefficient (D) for an early crystallising assemblage of olivine, Cr-spinel and sulfide. The best fit to our observed data is for a D_{Os} of ~15 (Figure 2). This is much greater than the estimated $D_{Os}^{olivine}$ of 0.51 [*Burton et al.*, 2002] and represents preferential partitioning of Os into sulfides, rather than simply into olivine, during the early stages of fractional crystallisation (e.g. Jackson & Shirey [2011]).

Galápagos basalts exhibit a relatively large variation in Re (80 to 910 pg g^{-1}, Table 1), which displays a scattered correlation with both MgO and Ni contents. The highest Re contents occur in submarine Fernandina basalts (western Galápagos); the

wide range in Re contents of other Galápagos basalts -- and variability with respect to Cu (which has similar compatibility Figure S4) -- may be due to Re loss during sub-aerial degassing [*Bennett et al.*, 2000].

4.3 $^{187}Os/^{188}Os$ characteristics of Galápagos basalts

The $^{187}Os/^{188}Os$ compositions of Galápagos basalts vary from 0.130 to 0.1875 (γOs = 0.5 to 45, where γOs= ([$^{187}Os/^{188}Os_{sample(t)}/^{187}Os/^{188}Os_{PUM(t)}$]-1) x 100 and PUM(t) is present-day primitive mantle= 0.1296 [*Meisel et al.*, 2001]; Table 1). Despite local and sometimes intra-island variations in $^{187}Os/^{188}Os$, *e.g.* Volcan Ecuador (Table 1) there is a broadly-systematic regional variation in Os isotopic ratios (Figure 1b). Recently erupted basalts (<1 Ma) with relatively unradiogenic $^{187}Os/^{188}Os$ ratios occur in: (i) western Galápagos (Roca Redonda and Fernandina), near the leading edge of the Galápagos plume and on the platform margins and (ii) 1.5 Ma to 779 ka flows on Floreana which, assuming a velocity of the Nazca plate of 20 km Myr^{-1}, would have been located near the southern margin of the plume stem at the time of their emplacement [*Harpp et al.*, 2014].

The most radiogenic $^{187}Os/^{188}Os$ ratios occur in recent basalts from central and NE Galápagos (Figure 1b). High $^{187}Os/^{188}Os$ ratios were measured in basalts with >50 pg g^{-1} Os from eastern Santiago (up to 0.155) and northern Isabela (Volcan Ecuador; 0.153). Even more radiogenic $^{187}Os/^{188}Os$ ratios (up to 0.1875) were measured in basalts with <50 pg g^{-1} Os on Genovesa, Pinta and Santa Cruz. While $^{187}Os/^{188}Os$ exhibits a broad inverse relationship with MgO (Figure 2) and Os content, we note that Galápagos lavas with similar MgO contents exhibit a large inter-island variation in $^{187}Os/^{188}Os$. For example, Fernandina submarine basalts with ~11 wt. % MgO have $^{187}Os/^{188}Os$ ratios of 0.133, while < 1Ma basalts from Isla Santiago (70 km east in central Galápagos) with comparable MgO and Os contents have $^{187}Os/^{188}Os$ ranging from 0.142 to 0.163 (Table 1).

The combined relatively unradiogenic $^{187}Os/^{188}Os$ (0.1329-0.1342), moderate $^{143}Nd/^{144}Nd$ (0.51292-0.51296) and $^{206}Pb/^{204}Pb$ (19.05-19.1), high $^{3}He/^{4}He$ (up to 29 R/Ra) and $\delta^{18}O$ (5.6 ±1‰) of Fernandina basalts [*White et al.*, 1993; *Geist et al.*, 1998; *Harpp and White*, 2001; *Kurz et al.*, 2009] support the hypothesis that their parental melts are derived from "C" like, primitive, lower mantle (Figure 3) and suggests that their Os systematics are most likely controlled by sulfide in this mantle source (cf.

Harvey et al., 2011). Similarly, we interpret the unradiogenic $^{187}Os/^{188}Os$ (0.1304) of the Roca Redonda picrite as evidence that, despite significant accumulated olivine ($Fo_{83.3}$ [*Vidito et al.*, 2013]) and apparent stalling of the parental melt in the crust, it has reached the surface with little crustal interaction.

Harpp & White [2001] showed that in Sr- Nd- and Pb-isotopic space the FLO (Floreana) mantle reservoir in southern Galápagos lies on a hyperbolic mixing curve between PLUME and global subducted, altered 2 Ga oceanic crust (HIMU). The $^{187}Os/^{188}Os$ ratios of Floreana basalts vary from 0.130-0.141. The sample with the least radiogenic $^{187}Os/^{188}Os$ (0.13014; FLO3-106) has moderately radiogenic $^{143}Nd/^{144}Nd$ (0.5130) and $^{206}Pb/^{204}Pb$ (19.89). By extrapolating to the previously estimated $^{206}Pb/^{204}Pb$ of the FLO endmember (21.2 [*Harpp and White*, 2001]) on Figure 4 we infer this reservoir has a $^{187}Os/^{188}Os$ ratio of 0.147. The two most radiogenic Floreana basalts (E110 and FL-3; $^{187}Os/^{188}Os$ = 0.139-0.141) have similar $^{206}Pb/^{204}Pb$ ratios (19.8-20) and plot on a mixing curve between melts of Galápagos FLO and PLUME reservoirs and an endmember with high $^{187}Os/^{188}Os$.

Surprisingly, the Os isotopic ratios of central and NE Galápagos basalts exhibit broadly negative and positive correlations with Sr and Nd isotopic ratios, respectively (Figure 3). These basalts have MORB-like Sr and Nd isotopic ratios, with unradiogenic Pb, but their $^{187}Os/^{188}Os$ are more radiogenic (0.147-0.188) than present-day MORB (0.126-0.14 [*Gannoun et al.*, 2007]), primitive upper mantle (0.1296 [*Meisel et al.*, 2001] and global OIBs derived from the "C" plume reservoir (0.1245-0.1314 [*Tejada et al.*, 2015]). Similar relationships between Pb and Os isotopic ratios of global OIBs with >30-40 pg g^{1} Os have been interpreted as mixing of primitive enriched "C"-like plume melts with ancient recycled pyroxenite (e.g. [*Lassiter and Hauri*, 1998; *Skovgaard et al.*, 2001; *Day et al.*, 2009]). Although this interpretation cannot be completely ruled out, we note that the combined unradiogenic Sr-, Pb- and radiogenic Nd-isotope characteristics of some central and NE Galápagos basalts are not consistent with a significant contribution from ancient recycled oceanic crust. Melting of this mantle reservoir would result in basalts with combined radiogenic $^{206}Pb/^{204}Pb$ and $^{187}Os/^{188}Os$ ratios, similar to those that we have identified at Floreana (Figure 4). Thus, the origin of these isotopic covariations in global OIB remains unclear. Here we present an alternative mechanism for generating the radiogenic Os signature, based on a greater understanding of magma

flux and lithospheric structure at Galápagos.

5. What is the cause of large inter-island variations in Os isotope ratios of Galápagos basalts?

Variable extents of melting of different sulfide populations in the convecting mantle [*Harvey et al.*, 2011], could generate variations in $^{187}Os/^{188}Os$ that are decoupled from those of lithophile isotopes in Galápagos basalts. For example, higher degree melting close to the plume stem might result in more Os-rich melts with less radiogenic Os, than more distal melts. Such a model could account for the variable $^{187}Os/^{188}Os$ in basalts with similar Os contents close to the plume stem, but not the wide range of $^{187}Os/^{188}Os$ displayed by Galápagos basalts as a whole. On a plot of $^{206}Pb/^{204}Pb$ versus $^{187}Os/^{188}Os$, Galápagos basalts exhibit a broad negative correlation (Figure 4), which implies they contain melts with high $^{187}Os/^{188}Os$ and low $^{206}Pb/^{204}Pb$. The source of the radiogenic Os must have high time-averaged Re/Os and the most plausible explanation is that it is either (i) ancient subducted oceanic crust in the convecting mantle, or (ii) 5 to 15 Ma Pacific crust.

While the Sr-, Nd-, Hf-, Pb- and Os-isotopic ratios of Floreana basalts are consistent with at least some ancient subducted material undergoing melting in the Galápagos plume, a number of lines of evidence suggest that $^{187}Os/^{188}Os$ of other Galápagos magmas result instead from assimilation of Pacific crust. First, the regional variability in $^{187}Os/^{188}Os$ shows a negative correlation (r=-0.61) with proposed lithological variations (*i.e.,* pyroxenite or peridotite) in the Galápagos plume based on the parameterisation of elemental concentrations (Mg, Fe, Ni and Mn) in olivine ([*Vidito et al.*, 2013], Figure S6 & S7). Second, Galápagos basalts display broad systematic variations in $^{187}Os/^{188}Os$ with indices of crystal fractionation, *e.g.* MgO (r=-0.87) and Ni (r=-0.83), implying that the variability in $^{187}Os/^{188}Os$ post-dates melt generation in the mantle. Finally, the spatial zonation in Os isotopes of Galápagos basalts can be directly linked to variations in the melt flux from the Galápagos plume in to the crust (see below).

The sensitivity of $^{187}Os/^{188}Os$ ratios of oceanic basalts to assimilation of crustal material is highly dependent upon magmatic Os contents (Figure S8). Previous investigations have shown that OIBs with 30 to 50 pg g^{-1} Os are especially susceptible

(e.g. [*Reisberg et al.*, 1993; *Eisele et al.*, 2002; *Class et al.*, 2009]. Thus, while crustal assimilation might explain the radiogenic $^{187}Os/^{188}Os$ of low-Os Galápagos basalts, it does not readily account for elevated $^{187}Os/^{188}Os$ in some basalts with higher Os contents (50 to 100 pg g^{-1}; Figure 6). Moreover, not all low-Os basalts have high $^{187}Os/^{188}Os$ and, as we described above, the Galápagos sample with the least radiogenic $^{187}Os/^{188}Os$ (Roca Redonda) has one of the lowest Os contents.

6. The origin of regional variations in crustal contamination of Galápagos plume-derived melts

Our conclusion that radiogenic Os isotope ratios of Galápagos basalts primarily reflect crustal assimilation is consistent with findings from whole-rock [*Saal et al.*, 2007] and melt-inclusion data [*Peterson et al.*, 2014]. Saal *et al.* [2007] noted that some Galápagos basalts erupted east of 91 °W have positive Sr anomalies on normalised multi-element plots, and suggested they are evidence of crustal contamination in basalts erupted distal to the present-day plume stem. Our new Os isotope data show, however, that some basalts which lack a positive Sr anomaly have radiogenic $^{187}Os/^{188}Os$ and may also have assimilated oceanic crust, such as alkaline basalts on western Santiago (Figures 5 and S5). Their relatively high Sr, Pb, and Eu concentrations obscure any evidence of a crustal contribution on normalised multi-element plots, but osmium isotopes are a more sensitive indicator of assimilation. Because of the multiple causes of Sr variability in Galápagos basalts the overall correlation of Sr with $^{187}Os/^{188}Os$ is weak (Figure S6).

The variability in $^{187}Os/^{188}Os$ of Galápagos basalts does not directly correlate with age and hence thickness of the underlying Pacific crust but subtle regional variations in lower crust composition potentially exert a control on the crustal processing of plume-derived melts (Figures 1 & 5). Much of the Galápagos platform is underlain by crust more than twice as thick as that currently forming on the GSC above ambient temperature mantle [*Feighner and Richards*, 1994; *Canales et al.*, 2002]. The thickest Galápagos crust (up to 18 km) occurs beneath the western part of the platform, above the present-day plume stem [*Feighner and Richards*, 1994]. The lower 6-8 km of this is likely dominated by mafic and ultramafic intrusions emplaced in ridge-generated crust [*Richards et al.*, 2013]. Away from the plume stem and east of ~91 °W (Figure 1) the crust is thinner (8 – 12 km) and weaker [*Feighner and Richards*, 1994]. The young

(~5 Ma) crust beneath the northeast of the archipelago was created when the Galápagos plume was located near the GSC and most likely consists of wehrlitic and gabbroic material, similar to that thought to form the basement of the Cocos and Carnegie ridges [*Sallarès et al.*, 2003].

6.1 Modelling the effects of crustal processing on $^{187}Os/^{188}Os$ of Galápagos magmas

With the exception of E64 (Volcan Darwin) and R9512 (Roca Redonda), Galápagos basalts fall on predicted fractional crystallisation trends on MgO versus Os plots (Figure 2), and show no evidence of having accumulated an Os-rich phase. We have therefore used the equations of Nishimura [2012] to model assimilation fractional crystallisation (AFC) and thereby assess the effects of crustal interaction on both Os contents and $^{187}Os/^{188}Os$ ratios of Galápagos basalts (Figure 6). While our AFC models assume a bulk D_{Os} of 15, and that whole-rock compositions are representative of parental melts (Section 3), they are compromised by $^{187}Re/^{188}Os$ and $^{187}Os/^{188}Os$ ratios of oceanic crust for which published data are limited [*Gannoun et al.*, 2016].

Young upper crust in the Nazca plate as sampled by DSDP 504B can acquire high initial $^{187}Os/^{188}Os$ (0.173) but has a low mean Os content (23 pg g^{-1}; Peucker-Ehrenbrink et al. [2003]) and assimilation of such material would have little effect on the Os isotopic ratios of Galápagos basalts with 100's of pg g^{-1} Os (Figure 6a). DSDP 504B did not penetrate lower crust, and there are no Re-Os data for gabbros from here or elsewhere in the Pacific, so we have used the hypothetical composition of global average lower oceanic crust proposed by Peucker-Ehrenbrink *et al.* [2012] in our AFC models. While this has high Os (55 pg g^{-1}), moderate Re (427 pg g^{-1}) but unradiogenic $^{187}Os/^{188}Os$ (0.142), relative to upper crust, AFC models (Figure 6a) show this also cannot satisfactorily explain the radiogenic $^{187}Os/^{188}Os$ of Galápagos basalts. Radiogenic in-growth of ^{187}Os for 10 Ma crust with MORB-like $^{187}Os/^{188}Os_i$ (0.128) would only cause a small increase in $^{187}Os/^{188}Os$ (to 0.1345), which is lower than the ratio observed in most of the basalts, including some with Os in excess of 50 pg g^{-1} (Figure 6a).

We also used the composition of high Re/Os lower oceanic crust from the SW Indian Ridge (DSDP 735B; Blusztajn *et al.* [2000]) in our AFC models (Figure 6b). This contains 9 pg g^{-1} Os and 2153 pg g^{-1} Re, and is hence relatively evolved [*Gannoun et al.*, 2016] so that the amount of ^{187}Os generated by radiogenic in-growth is large, and the

$^{187}Os/^{188}Os$ of crust with an initial ratio of 0.128 increases over a 10 Ma time interval to 0.3205. While this high Re/Os lower oceanic crust can be used to satisfactorily model the range of Os and $^{187}Os/^{188}Os$ ratios in some basalts from western and southern Galápagos, contamination by crust of this composition cannot account for the combined high Os and radiogenic $^{187}Os/^{188}Os$ in the majority of samples (Figure 6b). This is because in AFC models there is a trade-off between the rate of assimilation to fractionation (r_a) and the Os content of both the crust and magma: the amount of fractional crystallisation predicted by our models requires that, even for gabbros with $^{187}Re/^{188}Os$ as high as those reported by Blusztajn *et al.* [2000], any plausible contaminant for Galápagos basalts must have >~50 pg g^{-1} Os (Figure 6). The fact that the $^{187}Os/^{188}Os_{10Ma}$ ratio of the postulated crustal contaminant for NE Galápagos basalts is more radiogenic (0.25 to 0.3) and the Os content higher (50 to 100 pg g^{-1}) than observed in the limited number of analyses of gabbros from lower oceanic crust [*Blusztajn et al.*, 2000; *Dale et al.*, 2007; *Peucker-Ehrenbrink et al.*, 2012] is an important finding from our study. We now explore mechanisms that might potentially cause an increase in the Re and Os contents of the crustal contaminant.

The origin of the $^{187}Os/^{188}Os$ variability of oceanic crust is not well understood (see Gannoun *et al*. [2016]) but significant amounts of Re (up to 75%) may reside in silicate phases [*Dale et al.*, 2009a] and cumulate magnetite [*Righter et al.*, 1998]. Sulfides (*e.g.* chalcopyrite, pentlandite, pyrrhotite, pyrite) are the major host of crustal Os (>90%) and also some Re [*Dale et al.*, 2009a], and variable assimilation of these minerals may well explain some of the Galápagos Re-Os data. Since magmatic sulfides have high Os but relatively low Re/Os, and unlikely to produce the elevated $^{187}Os/^{188}Os$ of a plausible contaminant, we suggest that the sulfides precipitated from S-rich hydrothermal fluids. Hydrothermal activity is evident in the upper parts of the oceanic crust -- including in DSDP 504B [*Bach et al.*, 2003] -- and alteration affects up to 40 % of gabbros [*Nicolas et al.*, 2003].

According to Peucker-Ehrenbrink et al. [2003] 'neither Holes 504B or 735B are representative of altered oceanic crust in general' and it is therefore unsurprising that the published Re-Os data for these sites do not correspond to crust assimilated by Galápagos basalts. In the light of there being no appropriate end member composition in the current $^{187}Os/^{188}Os$ oceanic crust database we used a series of hypothetical

compositions. A best fit to the observed $^{187}Os/^{188}Os$ ratios of basalts from central, northeastern and eastern Galápagos was obtained in AFC models using a hypothetical, hydrothermal sulfide-rich gabbro with 100 pg g^{-1} Os, $^{187}Os/^{188}Os$ of 0.3, r_a values ranging from ~0.2 to 0.6 and 30 to 40% fractional crystallisation (Figure 6a). If the Os content of the crust is only 50 pg g^{-1}, then the maximum r_a increases to 0.8 but the amount of fractional crystallisation decreases slightly to <30% (Figure 6c). While the maximum estimated r_a for high-MgO Galápagos basalts is between 0.6 and 0.8, those with high $^{187}Os/^{188}Os$ from the west of the archipelago undergo less fractionation (20%) than those in the east (40%) for similar amounts of assimilation (Figure 6a), *i.e.* crustal contamination is more sporadic but occurs at higher MgO contents and temperatures nearer the plume stem. The result of the model involving a contaminant with high Os (100 pg g^{-1}) is in agreement with AFC models which have shown that the amount of assimilation is limited by the thermal energy of the magma and for most cases maximum assimilation rates are attained very rapidly, *i.e.* at low amounts of fractional crystallisation [*Bohrson and Spera*, 2001]. Our estimates of assimilation assume bulk crustal melting: selective melting of sulfides would reduce the amount of fractionation required only as long as the melt is under-saturated in this phase, which is not the case for Galápagos (Figure 2 and S2).

Mixing curves between isotopically different Galápagos melts and lower crust in $^{187}Os/^{188}Os$ and $^{87}Sr/^{86}Sr$ space (Figure 3) reveal that, even with a contaminant containing 100 pg g^{-1} Os, assimilation of ~40% highly-radiogenic oceanic crust would be required to explain the Os isotopic characteristics of Galápagos basalts with the most elevated $^{187}Os/^{188}Os$ and lowest $^{87}Sr/^{86}Sr$ ratios. This crust must also have a very high Re concentration, or at least have gained radiogenic ^{187}Os through alteration. The predicted amounts of contamination for some Galápagos basalts are high but are consistent with the findings of Kvassnes & Grove [2008] who showed that ascending parental MORB magmas are capable of melting significant amounts (50 wt. %) of gabbroic lower crust, while simultaneously crystallising olivine and subsequently plagioclase. Estimates of assimilation from Os in SW Indian Ridge MORB – which possess similarly radiogenic $^{187}Os/^{188}Os$ to Galápagos – give lower values of around 10% assimilation [*Yang et al.*, 2013], but this is due to a model with only 15 pg g^{-1} Os in the melt and the most radiogenic lower crust value (0.467) from Blusztajn et al. [2000]. We envisage that primitive Galápagos-plume related magmas are ~ 75°C hotter than

MORB and, given reasonable residence times and magma chamber geometries, would be readily able to melt lower crust.

6.2 The importance of plume melt flux on $^{187}Os/^{188}Os$ of Galápagos basalts

Our findings show that the variability of $^{187}Os/^{188}Os$ in Galápagos is to a large extent regionally controlled and related to both mantle and crustal processes (Figure 7). This relationship has not previously been observed in OIBs. The most crustally-contaminated Galápagos magmas occur where there is a low magmatic flux, *i.e.* where plume material is being dispersed laterally, and there is significantly less upwelling (~2 cm yr^{-1}) than at the plume stem (~7 cm yr^{-1}), such as at E. Santiago, Genovesa & Pinta (Figure 1 & S5; [*Saal et al.*, 2000]). Volcanoes in the west of the archipelago are built on the massive Galápagos Platform, which is constructed entirely of regionally extensive lava flows, and enormous volumes of plume derived magma have already passed through the crust by the time the central volcanoes (e.g. Fernandina) began their construction. The relatively low volumes of melt generated by passive adiabatic decompression of plume material beneath the northern and eastern islands [*Gibson et al.*, 2015] would encourage the development of small lower-crustal magma chambers with low volume to surface ratios. Magmatic plumbing systems involving a low flux of melt from the Galápagos plume are likely to be complex, with magmas following new ascent paths through the lithosphere, rather than previously established flow channels. These conditions would encourage assimilation of surrounding gabbro. Indeed, the elevated Os isotopic ratios of high-MgO Galápagos melts show that many were contaminated as soon as they began their migration through the crust, *i.e.* prior to undergoing extensive cooling and crystal fractionation. In this respect our findings differ from those of Saal *et al.* [2007] who used more-highly fractionated, plagioclase-saturated, MORB-like melt compositions to model the geochemical variations that might result from diffusive interaction of Galápagos melts with plagioclase in the lower crust.

Our $^{187}Os/^{188}Os$ data suggest that assimilation of oceanic crust by Galápagos plume-derived melts is sporadic on short length scales, *i.e.* individual volcanic centres. The regional variations in $^{187}Os/^{188}Os$ are best accounted for by differences in the extent of assimilation and fractional crystallisation. The observation that Galápagos basalts with the least enriched Sr-, Nd- and Pb-isotopic ratios have undergone the greatest amounts of crustal contamination is due to: (i) the off axis location of the Galápagos plume stem; and (ii) relatively thin lithosphere above the site of channelled

plume flow to the ridge [*Gibson et al.*, 2015]. It is the low melt flux that causes magmas to stall, cool and fractionate, and this explains the lack of lavas with primitive major-element compositions. Nevertheless, our study has shown that while assimilation of hydrothermally-altered lower crust increases $^{187}Os/^{188}Os$ ratios of Galápagos basalts, Sr-, Nd- and Pb-isotopic ratios are relatively unaffected by this process (because of the relatively small isotopic difference between primary melt and contaminant) and retain the signatures of their mantle source regions (cf. Figure 3).

7. Comparison of Galápagos Re-Os data with global OIBs

In general, a broad positive correlation exits between $^{187}Os/^{188}Os$ of global OIBs with high Os (>50 pg g^{-1}) and the age of the underlying lithosphere (Figure 8). For OIBs formed on old lithosphere, such as Hawaii, Canaries and Cook Austral, the high $^{187}Os/^{188}Os$ could be due to either: (i) older, thicker lithosphere limiting the amount of adiabatic decompression melting in the underlying mantle plume and therefore enhancing the effect of any pyroxenite melting relative to peridotite, or (ii) assimilation of 'old' crust with more radiogenic $^{187}Os/^{188}Os$. On Figure 8 it is clear that some high Os Galápagos basalts have more radiogenic $^{187}Os/^{188}Os$ than basalts formed on young lithosphere (<50 Ma) such as at Iceland, the Azores and Pitcairn, and as discussed above we attribute this to assimilation of crust during relatively early stages of crystallisation at Galápagos.

While the $^{187}Os/^{188}Os$ ratios of oceanic crust are typically assumed to correlate with age, due to decay of ^{187}Re, the elevated $^{187}Os/^{188}Os$ ratios of some recent Galápagos basalts are testimony to the assimilation of young (<10 Ma), hydrothermal sulfide-bearing, Re- and Os-rich lower oceanic crust. Our AFC models suggest that this has a more radiogenic Os isotopic signature than previously supposed in studies of oceanic basalts, which have assumed $^{187}Os/^{188}Os$ ratios of fresh gabbro for lower oceanic crust, e.g. Yang *et al.* [2013]. This finding has fundamental implications for how Re-Os data are interpreted. For example, the involvement of high Re/Os recycled ancient mafic components (eclogite/pyroxenite) in the convecting mantle to explain the radiogenic $^{187}Os/^{188}Os$ of many Os-rich global OIBs (e.g. [*Lassiter and Hauri*, 1998; *Skovgaard et al.*, 2001; *Class et al.*, 2009; *Day et al.*, 2009]) need not be so strongly invoked if assimilation of even young oceanic crust may overprint the Os isotopic signature of magmas with Os contents ≤100 pg g^{-1}. What remains uncertain is whether or not gabbro with radiogenic

$^{187}Os/^{188}Os$ is restricted to hydrothermally-altered, sulfide-rich crust that formed at spreading centres or may also occur in plume-formed crust generated away from mid-ocean ridges. The marked increase in Os isotopic ratios with distance from the upwelling plume stem that we observe in Galápagos has not been reported from other global suites of oceanic basalts and may depend on the near-ridge setting of Galápagos and also the unique widespread distribution of active volcanism in the archipelago. Nevertheless, changes in Os isotopic ratios related to temporal variations in melt flux have been inferred for both Iceland [*Skovgaard et al.*, 2001; *Debaille et al.*, 2009] and Hawaii [*Gaffney et al.*, 2005].

Galápagos basalts are exceptional in that, although erupted in a near-ridge setting, they have radiogenic $^{187}Os/^{188}Os$ at relatively high MgO and Os contents (100 pg g^{-1}; Figures 8 & 9), which suggests contamination occurs at an earlier stage in crustal processing than has been identified in many other OIBs. The volume flux of melt estimated for the present-day Galápagos plume (2.8 ±1.6 m^3/s) is less than half that of Hawaii (5.0 ±3.7 m^3/s) and Iceland (9.2 ±6.7 m^3/s; Sallares & Charvis [2003]) and we suggest this controls the introduction of crustal Os into OIBs with moderate to high Os contents. Furthermore, the Galápagos plume generates less melt than near-axis hotspots such as the Azores, Pitcairn and Iceland because it impacts beneath thicker lithosphere. An important first order observation is that many Galápagos basalts with radiogenic $^{187}Os/^{188}Os$ were erupted from volcanoes located distal to the plume stem (*i.e.* region of greatest upwelling; Figure 1 & S5) and we anticipate these will have magma chambers supplied by the lowest melt flux. Moreover, the distinct isotopic signature [*White et al.*, 1993] and olivine chemistry ([*Vidito et al.*, 2013]) of each Galápagos volcano suggest they are each underlain by a relatively small magma chamber in comparison to Hawaii and Iceland.

8. Conclusions

Our new Re-Os isotopic data for Galápagos basalts reveal a large systematic regional variation in $^{187}Os/^{188}Os$ composition, which represents both mantle and crustal processes. Basalts recently erupted near the western margin of the Galápagos platform (Fernandina and Roca Redonda) and at the leading edge of the hotspot track are the least radiogenic ($^{187}Os/^{188}Os$ ~0.130). This is consistent with the presence of a mantle reservoir in the Galápagos plume resembling the "C"-like global plume component. In

Os-Pb isotopic space, basalts from Floreana fall on a mixing curve between global "C" and HIMU mantle reservoirs and confirm that ancient recycled crust with elevated $^{187}Os/^{188}Os$ and $^{206}Pb/^{204}Pb$ is melting in the southern part of the upwelling Galápagos plume [*Harpp et al.*, 2014]. These findings concur with previous studies that have suggested the Galápagos plume is compositionally zoned (e.g. [*White et al.*, 1993; *Hoernle et al.*, 2000]).

A key finding is that basalts with radiogenic $^{187}Os/^{188}Os$ were erupted from volcanoes distal to the main zone of Galápagos plume upwelling, where plume material is laterally dispersed, i.e. in central and northeast parts of the archipelago. There is no correlation of $^{187}Os/^{188}Os$ with purported lithological variations in the Galápagos plume [*Vidito et al.*, 2013] but positive correlations of $^{187}Os/^{188}Os$ with indices of crystal fractionation (Os, Ni, Cr and MgO) suggest that large variations in $^{187}Os/^{188}Os$ are related to lithospheric processing, involving assimilation of lower oceanic crust during crystal fractionation, rather than mantle melting. In order to account for the observed variability in Os isotopic ratios we suggest that ridge-formed oceanic crust underlying Galápagos is enriched in radiogenic ^{187}Os, probably in the form of Os- and Re-rich hydrothermal sulfides. Such material, or simply older oceanic crustal material, may also explain the elevated $^{187}Os/^{188}Os$ of some other OIBs, including those that have been linked to melting of ancient pyroxenitic material.

The potential of Galápagos mantle plume-derived melts to assimilate Pacific lower crust is influenced by the melt flux and crustal residence times, which themselves are dependent upon the density difference between magma and crust. The lower melt flux of the Galápagos plume relative to the Hawaiian and Icelandic plumes may account for the early onset of contamination (expressed by MgO and Os contents) in ascending melts. Our findings from Galápagos show that, provided the rate of assimilation to crystal fractionation is low (<0.2), a threshold bulk-rock Os content of 30-50 pg g^{-1} is an appropriate contamination filter for melts which have ascended through the estimated young lower oceanic crust of Peucker-Ehrenbrink *et al.* [2012]. If, however, the oceanic crust has a greater concentration of Os, higher $^{187}Os/^{188}Os$ ratio, or the rate of assimilation to crystal fractionation is much higher, then the contamination filter threshold should be set at a greater Os content.

The causes of the large variability in $^{187}Os/^{188}Os$ that we have identified in Galápagos basalts have important implications for $^{187}Os/^{188}Os$ in global OIBs associated with weak mantle plumes (e.g. those at the end of long-lived hot spot tracks) and also off-axis mantle plumes, such as Tristan da Cunha, Bouvet, Crozet and St Helena. We urge caution in attributing radiogenic $^{187}Os/^{188}Os$ in basalts, especially associated with these hotspots, solely to lithological heterogeneity (recycled oceanic crust) in the convecting mantle, particularly in low Os basalts.

Acknowledgements

We thank the Galápagos National Park authorities for permission to collect samples in the Archipelago. We are grateful to Julia Griffin and Iris Buisman for help with electron microprobe analyses and Geoff Nowell for assistance with Sr, Nd and Pb isotope determinations. We thank Jason Harvey and Cornelia Class for their thorough and constructive reviews of an earlier draft of this manuscript. The research was funded by NERC RG57434 (SAG) and EAR-1145271 (DG).

References

Allègre, C. J., and J.-M. Luck (1980), Osmium isotopes as petrogenetic and geological tracers, *Earth Planet. Sci. Lett.*, *48*(1), 148–154, doi:10.1016/0012-821X(80)90177-6.

Bach, W., B. Peucker-Ehrenbrink, S. R. Hart, and J. S. Blusztajn (2003), Geochemistry of hydrothermally altered oceanic crust: DSDP/ODP Hole 504B – Implications for seawater-crust exchange budgets and Sr- and Pb-isotopic evolution of the mantle, *Geochem. Geophys. Geosystems*, *4*(3), 8904, doi:10.1029/2002GC000419.

Beattie, P., C. Ford, and D. Russell (1991), Partition coefficients for olivine-melt and orthopyroxene-melt systems, *Contrib. Mineral. Petrol.*, *109*(2), 212–224, doi:10.1007/BF00306480.

Bennett, V. C., M. D. Norman, and M. O. Garcia (2000), Rhenium and platinum group element abundances correlated with mantle source components in Hawaiian picrites: sulphides in the plume, *Earth Planet. Sci. Lett.*, *183*(3–4), 513–526, doi:10.1016/S0012-821X(00)00295-8.

Blusztajn, J., S. R. Hart, G. Ravizza, and H. J. B. Dick (2000), Platinum-group elements and Os isotopic characteristics of the lower oceanic crust, *Chem. Geol.*, *168*(1–2), 113–122, doi:10.1016/S0009-2541(00)00186-8.

Bohrson, W. A., and F. J. Spera (2001), Energy-constrained open-system magmatic processes II: Application of energy-constrained assimilation–fractional crystallization (EC-AFC) model to magmatic systems, *J. Petrol.*, *42*(5), 1019–1041, doi:10.1093/petrology/42.5.1019.

Burton, K. W., P. Schiano, J.-L. Birck, C. J. Allègre, M. Rehkämper, A. N. Halliday, and J. B. Dawson (2000), The distribution and behaviour of rhenium and osmium amongst mantle minerals and the age of the lithospheric mantle beneath Tanzania, *Earth Planet. Sci. Lett.*, *183*(1–2), 93–106, doi:16/S0012-821X(00)00259-4.

Burton, K. W., A. Gannoun, J.-L. Birck, C. J. Allègre, P. Schiano, R. Clocchiatti, and O. Alard (2002), The compatibility of rhenium and osmium in natural olivine and their behaviour during mantle melting and basalt genesis, *Earth Planet. Sci. Lett.*, *198*(1–2), 63–76, doi:10.1016/S0012-821X(02)00518-6.

Canales, J. P., G. Ito, R. S. Detrick, and J. M. Sinton (2002), Crustal thickness along the western Galápagos Spreading Center and the compensation of the Galápagos hotspot swell, *Earth Planet. Sci. Lett.*, *203*(1), 311–327.

Class, C., S. L. Goldstein, and S. B. Shirey (2009), Osmium isotopes in Grande Comore lavas: A new extreme among a spectrum of EM-type mantle endmembers, *Earth Planet. Sci. Lett.*, *284*(1–2), 219–227, doi:10.1016/j.epsl.2009.04.031.

Dale, C. W., A. Gannoun, K. W. Burton, T. W. Argles, and I. J. Parkinson (2007), Rhenium–osmium isotope and elemental behaviour during subduction of oceanic crust and the implications for mantle recycling, *Earth Planet. Sci. Lett.*, *253*(1–2), 211–225, doi:10.1016/j.epsl.2006.10.029.

Dale, C. W., K. W. Burton, D. G. Pearson, A. Gannoun, O. Alard, T. W. Argles, and I. J. Parkinson (2009a), Highly siderophile element behaviour accompanying subduction of oceanic crust: Whole rock and mineral-scale insights from a high-pressure terrain, *Geochim. Cosmochim. Acta*, *73*(5), 1394–1416, doi:10.1016/j.gca.2008.11.036.

Dale, C. W., D. G. Pearson, N. A. Starkey, F. M. Stuart, R. M. Ellam, L. M. Larsen, J. G. Fitton, and C. G. Macpherson (2009b), Osmium isotopes in Baffin Island and West Greenland picrites: Implications for the $^{187}Os/^{188}Os$ composition of the convecting mantle and the nature of high $^{3}He/^{4}He$ mantle, *Earth Planet. Sci. Lett.*, *278*(3–4), 267–277, doi:10.1016/j.epsl.2008.12.014.

Danyushevsky, L. V., and P. Plechov (2011), Petrolog3: Integrated software for modeling crystallization processes, *Geochem. Geophys. Geosystems*, *12*(7), Q07021, doi:10.1029/2011GC003516.

Day, J. M. D., D. G. Pearson, C. G. Macpherson, D. Lowry, and J.-C. Carracedo (2009), Pyroxenite-rich mantle formed by recycled oceanic lithosphere: Oxygen-osmium isotope evidence from Canary Island lavas, *Geology*, *37*(6), 555–558.

Day, J. M. D., D. G. Pearson, C. G. Macpherson, D. Lowry, and J. C. Carracedo (2010), Evidence for distinct proportions of subducted oceanic crust and lithosphere in

HIMU-type mantle beneath El Hierro and La Palma, Canary Islands, *Geochim. Cosmochim. Acta*, *74*(22), 6565–6589, doi:10.1016/j.gca.2010.08.021.

Debaille, V., R. G. Trønnes, A. D. Brandon, T. E. Waight, D. W. Graham, and C.-T. A. Lee (2009), Primitive off-rift basalts from Iceland and Jan Mayen: Os-isotopic evidence for a mantle source containing enriched subcontinental lithosphere, *Geochim. Cosmochim. Acta*, *73*(11), 3423–3449, doi:10.1016/j.gca.2009.03.002.

Eisele, J., M. Sharma, S. J. G. Galer, J. Blichert-Toft, C. W. Devey, and A. W. Hofmann (2002), The role of sediment recycling in EM-1 inferred from Os, Pb, Hf, Nd, Sr isotope and trace element systematics of the Pitcairn hotspot, *Earth Planet. Sci. Lett.*, *196*(3–4), 197–212, doi:10.1016/S0012-821X(01)00601-X.

Feighner, M. A., and M. A. Richards (1994), Lithospheric structure and compensation mechanisms of the Galápagos Archipelago, *J. Geophys. Res.-Solid Earth*, *99*(B4), 6711–6729.

Gaffney, A. M., B. K. Nelson, L. Reisberg, and J. Eiler (2005), Oxygen–osmium isotope systematics of West Maui lavas: A record of shallow-level magmatic processes, *Earth Planet. Sci. Lett.*, *239*(1–2), 122–139, doi:10.1016/j.epsl.2005.07.027.

Gannoun, A., K. W. Burton, I. J. Parkinson, O. Alard, P. Schiano, and L. E. Thomas (2007), The scale and origin of the osmium isotope variations in mid-ocean ridge basalts, *Earth Planet. Sci. Lett.*, *259*(3–4), 541–556, doi:10.1016/j.epsl.2007.05.014.

Gannoun, A., K. W. Burton, J. M. D. Day, J. Harvey, P. Schiano, and I. Parkinson (2016), Highly siderophile element and Os isotope systematics of volcanic rocks at divergent and convergent plate boundaries and in intraplate settings, *Rev. Mineral. Geochem.*, *81*(1), 651–724, doi:10.2138/rmg.2016.81.11.

Geist, D. J., T. Naumann, and P. Larson (1998), Evolution of Galápagos magmas: Mantle and crustal fractionation without assimilation, *J. Petrol.*, *39*(5), 953–971.

Geist, D. J., D. J. Fornari, M. D. Kurz, K. S. Harpp, A. Soule, M. Perfit, and A. M. Koleszar (2006), Submarine Fernandina: Magmatism at the leading edge of the Galápagos hot spot, *Geochem. Geophys. Geosystems*, *7*, doi:0.1029/2006GC001290.

Geist, D. J., H. Snell, H. Snell, C. Goddard, and M. D. Kurz (2014), A palaeogeographic model of Galápagos Islands and biogeographicaland evolutionary implications, , *The Galápagos: A Natural Laboratory for the Earth Sciences. AGU Monograph*, 145–166.

Gibson, S. A., and D. J. Geist (2010), Geochemical and geophysical mapping of lithospheric thickness variations beneath Galápagos, *Earth Planet. Sci. Lett.*, *300*, 275–286, doi:10.1016/j.epsl.2010.10.002.

Gibson, S. A., D. J. Geist, J. A. Day, and C. W. Dale (2012), Short wavelength heterogeneity in the Galápagos plume: evidence from compositionally-diverse basalts on Isla Santiago, *Geochem. Geophys. Geosystems*, doi:10.1029/2012GC004244.

Gibson, S. A., D. J. Geist, and M. A. Richards (2015), Mantle plume capture and outflow during Galápagos plume-ridge interaction, *Geochem. Geophys. Geosystems*, doi:10.1002/2015GC005723.

Harpp, K., D. Fornari, D. J. Geist, and M. D. Kurz (2014), The geology and geochemistry of Isla Floreana, Galápagos: A different type of late stage ocean island volcanism, *Galápagos Nat. Lab. Earth Sci. AGU Monogr.*, *204*, 71–118.

Harpp, K. S., and W. M. White (2001), Tracing a mantle plume: isotopic and trace element variations of Galápagos seamounts, *Geochem. Geophys. Geosystems*, *2*, doi:10.1029/2000GC000137.

Hart, S. R., J. Blusztajn, H. J. B. Dick, P. S. Meyer, and K. Muehlenbachs (1999), The fingerprint of seawater circulation in a 500-meter section of ocean crust gabbros, *Geochim. Cosmochim. Acta*, *63*(23–24), 4059–4080, doi:10.1016/S0016-7037(99)00309-9.

Harvey, J., C. W. Dale, A. Gannoun, and K. W. Burton (2011), Osmium mass balance in peridotite and the effects of mantle-derived sulphides on basalt petrogenesis, *Geochim. Cosmochim. Acta*, *75*(19), 5574–5596, doi:10.1016/j.gca.2011.07.001.

Hauri, E. H., J. C. Lassiter, and D. J. DePaolo (1996), Osmium isotope systematics of drilled lavas from Mauna Loa, Hawaii, *J. Geophys. Res.-Solid Earth*, *101*(B5), PP. 11,793-11,806, doi:199610.1029/95JB03346.

Hoernle, K. A., R. Werner, J. P. Morgan, S. Garbe, J. Bryce, and J. Mrazek (2000), Existence of complex spatial zonation in the Galápagos plume, *Geology*, *28*(5), 435–438.

Jackson, M. G., and S. B. Shirey (2011), Re–Os isotope systematics in Samoan shield lavas and the use of Os-isotopes in olivine phenocrysts to determine primary magmatic compositions, *Earth Planet. Sci. Lett.*, *312*(1–2), 91–101, doi:10.1016/j.epsl.2011.09.046.

Kurz, M. D., J. Curtice, D. Fornari, D. J. Geist, and M. Moreira (2009), Primitive neon from the center of the Galápagos hotspot, *Earth Planet. Sci. Lett.*, *286*(1–2), 23–34.

Kvassnes, A. J. S., and T. L. Grove (2008), How partial melts of mafic lower crust affect ascending magmas at oceanic ridges, *Contrib. Mineral. Petrol.*, *156*(1), 49–71, doi:10.1007/s00410-007-0273-x.

Lassiter, J. C., and E. H. Hauri (1998), Osmium-isotope variations in Hawaiian lavas: evidence for recycled oceanic lithosphere in the Hawaiian plume, *Earth Planet. Sci. Lett.*, *164*(3–4), 483–496, doi:10.1016/S0012-821X(98)00240-4.

Levasseur, S., J.-L. Birck, and C. J. Allègre (1998), Direct measurement of femtomoles of osmium and the 187Os/186Os ratio in seawater, *Science*, *282*(5387), 272–274, doi:10.1126/science.282.5387.272.

Meisel, T., R. J. Walker, A. J. Irving, and J.-P. Lorand (2001), Osmium isotopic compositions of mantle xenoliths: a global perspective, *Geochim. Cosmochim. Acta*, *65*(8), 1311–1323, doi:10.1016/S0016-7037(00)00566-4.

Nicolas, A., D. Mainprice, and F. Boudier (2003), High-temperature seawater circulation throughout crust of oceanic ridges: A model derived from the Oman ophiolites, *J. Geophys. Res. Solid Earth*, *108*(B8), 2371, doi:10.1029/2002JB002094.

Nishimura, K. (2012), A mathematical model of trace element and isotopic behavior during simultaneous assimilation and imperfect fractional crystallization, *Contrib. Mineral. Petrol.*, *164*(3), 427–440, doi:10.1007/s00410-012-0745-5.

Peterson, M. E., A. E. Saal, E. Nakamura, H. Kitagawa, M. D. Kurz, and A. M. Koleszar (2014), Origin of the "ghost plagioclase" signature in Galápagos melt inclusions: New evidence from Pb isotopes, *J. Petrol.*, doi:10.1093/petrology/egu054.

Peucker-Ehrenbrink, B., W. Bach, S. R. Hart, J. S. Blusztajn, and T. Abbruzzese (2003), Rhenium-osmium isotope systematics and platinum group element concentrations in oceanic crust from DSDP/ODP Sites 504 and 417/418, *Geochem. Geophys. Geosystems*, *4*(7), n/a-n/a, doi:10.1029/2002GC000414.

Peucker-Ehrenbrink, B., K. Hanghoj, T. Atwood, and P. B. Kelemen (2012), Rhenium-osmium isotope systematics and platinum group element concentrations in oceanic crust, *Geology*, *40*(3), 199–202, doi:10.1130/G32431.1.

Reisberg, L., A. Zindler, F. Marcantonio, W. White, D. Wyman, and B. Weaver (1993), Os isotope systematics in ocean island basalts, *Earth Planet. Sci. Lett.*, *120*(3–4), 149–167, doi:10.1016/0012-821X(93)90236-3.

Richards, M., E. Contreras-Reyes, C. Lithgow-Bertelloni, M. Ghiorso, and L. Stixrude (2013), Petrological interpretation of deep crustal intrusive bodies beneath oceanic hotspot provinces, *Geochem. Geophys. Geosystems*, *14*(3), 604–619, doi:10.1029/2012GC004448.

Righter, K., J. T. Chesley, D. Geist, and J. Ruiz (1998), Behavior of Re during magma fractionation: an example from Volcán Alcedo, Galápagos, *J. Petrol.*, *39*(4), 785–795, doi:10.1093/petroj/39.4.785.

Saal, A. E., M. D. Kurz, S. . Hart, J. S. Blusztajn, G. D. Lane, K. Sims, and D. J. Geist (2000), U series isotopic variability in Galápagos lavas, evidence of a mildly buoyant plume, *AGU Fall Meet. Abstr.*, V22C–03.

Saal, A. E., M. D. Kurz, S. R. Hart, J. S. Blusztajn, J. Blichert-Toft, Y. Liang, and D. J. Geist (2007), The role of lithospheric gabbros on the composition of Galápagos lavas, *Earth Planet. Sci. Lett.*, *257*, 391–406.

Sallarès, V., and P. Charvis (2003), Crustal thickness constraints on the geodynamic evolution of the Galápagos Volcanic Province, *Earth Planet. Sci. Lett.*, *214*(3–4), 545–559, doi:10.1016/S0012-821X(03)00373-X.

Sallarès, V., P. Charvis, E. R. Flueh, and J. Bialas (2003), Seismic structure of Cocos and Malpelo Volcanic Ridges and implications for hot spot-ridge interaction, *J. Geophys. Res. Solid Earth*, *108*(B12), n/a–n/a, doi:10.1029/2003JB002431.

Skovgaard, A. C., M. Storey, J. Baker, J. Blusztajn, and S. R. Hart (2001), Osmium–oxygen isotopic evidence for a recycled and strongly depleted component in the Iceland mantle plume, *Earth Planet. Sci. Lett.*, *194*(1–2), 259–275, doi:10.1016/S0012-821X(01)00549-0.

Vidito, C., C. Herzberg, E. Gazel, D. Geist, and K. Harpp (2013), Lithological structure of the Galápagos Plume, *Geochem. Geophys. Geosystems*, *14*(10), 4214–4240, doi:10.1002/ggge.20270.

Villagómez, D. R., D. R. Toomey, D. J. Geist, E. E. E. Hooft, and S. C. Solomon (2014), Mantle flow and multistage melting beneath the Galápagos hotspot revealed by seismic imaging, *Nat. Geosci.*, 10.1038/ngeo2062, doi:10.1038/ngeo2062.

White, W. M., A. R. McBirney, and R. A. Duncan (1993), Petrology and geochemistry of the Galápagos Islands - Portrait of a pathological mantle plume, *J. Geophys. Res.-Solid Earth*, *98*(B11), 19533–19563.

Widom, E., and S. B. Shirey (1996), Os isotope systematics in the Azores: implications for mantle plume sources, *Earth Planet. Sci. Lett.*, *142*(3–4), 451–465, doi:10.1016/0012-821X(96)00111-2.

Yang, A. Y., T.-P. Zhao, M.-F. Zhou, X.-G. Deng, G.-Q. Wang, and J. Li (2013), Os isotopic compositions of MORBs from the ultra-slow spreading Southwest Indian Ridge: Constraints on the assimilation and fractional crystallization (AFC) processes, *Lithos*, *179*, 28–35, doi:10.1016/j.lithos.2013.07.020.

Figure captions

Figure 1. (a) Distribution of volcanic islands in the Galápagos Archipelago and their relationship to the Galápagos Spreading Centre (GSC), and Galápagos plume stem imaged at a depth of 200 km [*Villagómez et al.*, 2014]. At depths shallower than ~150 km plume material is dispersed laterally towards the GSC. (b) Comparison of regional variations of γOs ([$^{187}Os/^{188}Os_{sample(t)}/^{187}Os/^{188}Os_{PUM(t)}$]-1) x 100 PUM(t) is present-day primitive mantle= 0.1296 [*Meisel et al.*, 2001]) in Galápagos basalts with thickness of the Galápagos crust. Dashed black line shows the boundary between thick, strong lithosphere in the west and thin, weak lithosphere in the east of Galápagos [*Feighner and Richards*, 1994]. Bathymetric contours highlight the location of the Galápagos platform and surrounding seamounts. Abbreviations for sample locations on Isabela are as follows: CA, Cerro Azul; D, Volcan Darwin; E, Volcan Ecuador.

Figure 2. Variation of (a) MgO and (b) Ni with Os; (c) MgO with $^{187}Os/^{188}Os$ and (d) Cr with Os in Galápagos basalts. In (a) solid curve shows predicted crystal fractionation trend for a melt similar to submarine Fernandina picrite AHA19A, which has 14 wt. % MgO and 419 μg g^{-1} Ni [*Geist et al.*, 2006] and an estimated Os content of 200 pg g^{-1}. Fractionation curves were calculated using the thermodynamic modelling program Petrolog3 [*Danyushevsky and Plechov*, 2011]. For an early crystallisaing assemblage of olivine + Cr spinel + sulfide a *D* value for Os of 15; together with D_{Os} clinopyroxene = 0.3 and D_{Os} plagioclase = 0.3 provided the best fit to the observed whole-rock data. Tick marks at 5%, 10% and 20% are for fractionation of olivine + Cr spinel + sulfide. In (b) *D* values for Ni are from Beattie *et al.* [1991]. $^{187}Os/^{188}Os$ for primitive mantle is from Meisel et al. [2001]. Data sources are given in a Supplementary File. Specific symbols refer to locations given in Figure 1.

Figure 3. (a) and (b) Co-variations in Os-, Sr- and Nd-isotopes in Galápagos basalts and global ocean islands. Compositions of Galápagos mantle reservoirs are as follows: PLUME, $^{187}Os/^{188}Os$=0.1296, $^{87}Sr/^{86}Sr$=0.70328, $^{143}Nd/^{144}Nd$=0.51289; Depleted Galápagos Mantle (DGM), $^{187}Os/^{188}Os$=0.12776, $^{87}Sr/^{86}Sr$=0.70243, $^{143}Nd/^{144}Nd$=0.51317; Floreana (FLO) $^{187}Os/^{188}Os$=0.147, $^{87}Sr/^{86}Sr$=0.70450, $^{143}Nd/^{144}Nd$=0.51283. The enriched Wolf-Darwin component, which is prevalent in islands northwest of the main Galápagos platform, makes a negligible contribution to basalts analysed for $^{187}Os/^{188}Os$. Note that the $^{187}Os/^{188}Os$ of PLUME and DGM are assumed to be the same as primitive and MORB-source mantle, respectively [*Meisel et al.*, 2001; *Gannoun et al.*, 2007]. Mixing curves at 20% increments between PLUME, DGM, FLO and lower crust with the $^{187}Os/^{188}Os$ composition of Blusztajn *et al.* [2000] shown in (c) and sulfide-bearing lower oceanic crust for Galápagos with the Sr composition of [*Hart et al.*, 1999] shown in (d). Note that the effect of assimilation on Os isotopes is more significant than on $^{87}Sr/^{86}Sr$, which is consistent with the Sr-Nd isotope variations primarily reflecting mantle source heterogeneity. Data are from: Table 1 and

sources are given in a Supplementary File. Specific symbols refer to locations given in Figure 1.

Figure 4. Plot of $^{206}Pb/^{204}Pb$ versus $^{187}Os/^{188}Os$ for Galápagos basalts together with published analyses for global OIBs. On the basis that FLO is a mixture of PLUME and HIMU-like mantle and has a $^{206}Pb/^{204}Pb$ of 21.2 [*Harpp and White*, 2001] we infer the $^{187}Os/^{188}Os$ of the FLO reservoir to be 0.147. Bulk mixing curves were calculated using reservoirs with the following values: lower crust (Os=100 pg g^{-1}, $^{187}Os/^{188}Os$ = 0.32 (see text for discussion); DGM, Depleted Galápagos Mantle ($^{187}Os/^{188}Os$ = 0.126, $^{206}Pb/^{204}Pb$=18.1); PLUME ($^{187}Os/^{188}Os$ = 0.1296, $^{206}Pb/^{204}Pb$=18.9); 2 Ga recycled oceanic crust (Os=3.1 pg g^{-1}, $^{187}Os/^{188}Os$ =2.74, Pb=0.9 ng g^{-1}, $^{206}Pb/^{204}Pb$=21.53). The compositions of melts from these mantle reservoirs were assumed to have 200 pg g^{-1} Os and 0.8 ng g^{-1} Pb. Melts of sulfide-bearing Pacific lower oceanic crust were assumed to have: Os=100 pg g^{-1}; $^{187}Os/^{188}Os$ =0.32; Pb=0.5 ng g^{-1} and $^{206}Pb/^{204}Pb$=18.1 to 18.9. Data sources are given in a Supplementary File. Specific symbols refer to locations given in Figure 1.

Figure 5. Comparison of primitive-mantle-normalised multi-element patterns of basalts from western (red symbols) and eastern Galápagos (blue symbols) with lower oceanic crust (Oman gabbro) and upper oceanic crust (504B). The positive Sr anomaly in melt inclusions from E. Santiago and Fernandina has been interpreted as evidence of diffusive interaction of a depleted melt with a plagioclase-rich cumulate in the oceanic crust [*Peterson et al.*, 2014]. Analyses of melt inclusions from global OIBs believed to have melt contributions from recycled oceanic crust (Hawaii) and underlying young crust (Galápagos and Iceland) are shown for comparison. Osmium isotopic data are given where known for specific samples. Data are from: Table 1, Supplementary Table 1 and sources are given in a Supplementary File.

Figure 6. Variation of Os and $^{187}Os/^{188}Os$ in Galápagos basalts. Data are from Table 1. Curves show the results of Assimilation Fractional Crystallisation modelling [*Nishimura*, 2012] of a primitive Galápagos magma with 200 pg g^{-1} Os and $^{187}Os/^{188}Os$ of 0.129. (a) shows the effects of assimilating average upper and lower oceanic crust and also hypothetical lower oceanic crust containing hydrothermal sulfides and 100 pg g^{-1} Os; (b) shows the effects of assimilating high Re/Os 10 Ma lower crust with 10 pg g^{-1} Os [*Blusztajn et al.*, 2000] and (c) shoes the effect of assimilating hypothetical lower oceanic crust containing hydrothermal sulfides and 50 pg g^{-1} Os. Bulk D_{Os} was set to 15 for the early crystallising assemblage of olivine + Cr spinel + sulfide (see text for discussion). The ratio of assimilation to crystal fractionation (r_a) and the % mass of the residual magma relative to the initial mass are shown on all plots. The Os contents and $^{187}Os/^{188}Os$ for average upper and lower oceanic crust are from Peucker-Ehrenbrink *et al.* [2003, 2012]. Specific symbols refer to locations given in Figure 1.

Figure 7. Schematic illustrations to show the relationship between melt flux and $^{187}Os/^{188}Os$ beneath Fernandina and Genovesa which are located near and distal to the main zone of plume upwelling, respectively. The extent of crystal fractionation (F) and

rate of assimilation to fractionation (r_a) are estimated from AFC models. $^{187}Os/^{188}Os$ data are from Table 1. Upwelling velocities are from U-series data [*Saal et al.*, 2000]. Lithospheric thickness estimates are from Gibson & Geist [2010].

Figure 8. Comparison of $^{187}Os/^{188}Os$ in global MORB and OIBs according to age of the underlying lithosphere. Basalts are divided in to low Os and high Os groups based on a threshold of 50 pg g^{-1}, the canonical maximum value used to filter effects of crustal contamination. Note the general increase in range of $^{187}Os/^{188}Os$ in basalts with >50 pg g^{-1} and age of the underlying lithosphere. Galápagos basalts with >50 pg g^{-1} Os are unusual in that they have relatively high $^{187}Os/^{188}Os$ given the young age of the underlying lithosphere (as indicated by thick dashed line). Data sources are given in a Supplementary File.

Figure 9. Assimilation fractional crystallisation curves for: a) basalts erupted on young oceanic crust with typical average zero-aged upper and lower oceanic crust; and b) basalts erupted on old oceanic crust with $^{187}Os/^{188}Os$ of average lower oceanic crust age corrected to 150 Ma (0.221) and Os=55 pg g^{-1} [Blusztajn *et al.,* 2000]. The threshold of 30-50 pg g^{-1} Os below which contamination is thought to exert a significant influence on the $^{187}Os/^{188}Os$ of oceanic basalts [*Reisberg et al.*, 1993] is shown for reference. Data sources are the same as Figure 3. Data are from sources for ages of oceanic crust and buoyancy flux data beneath different islands are given in a Supplementary file.

Figure 1

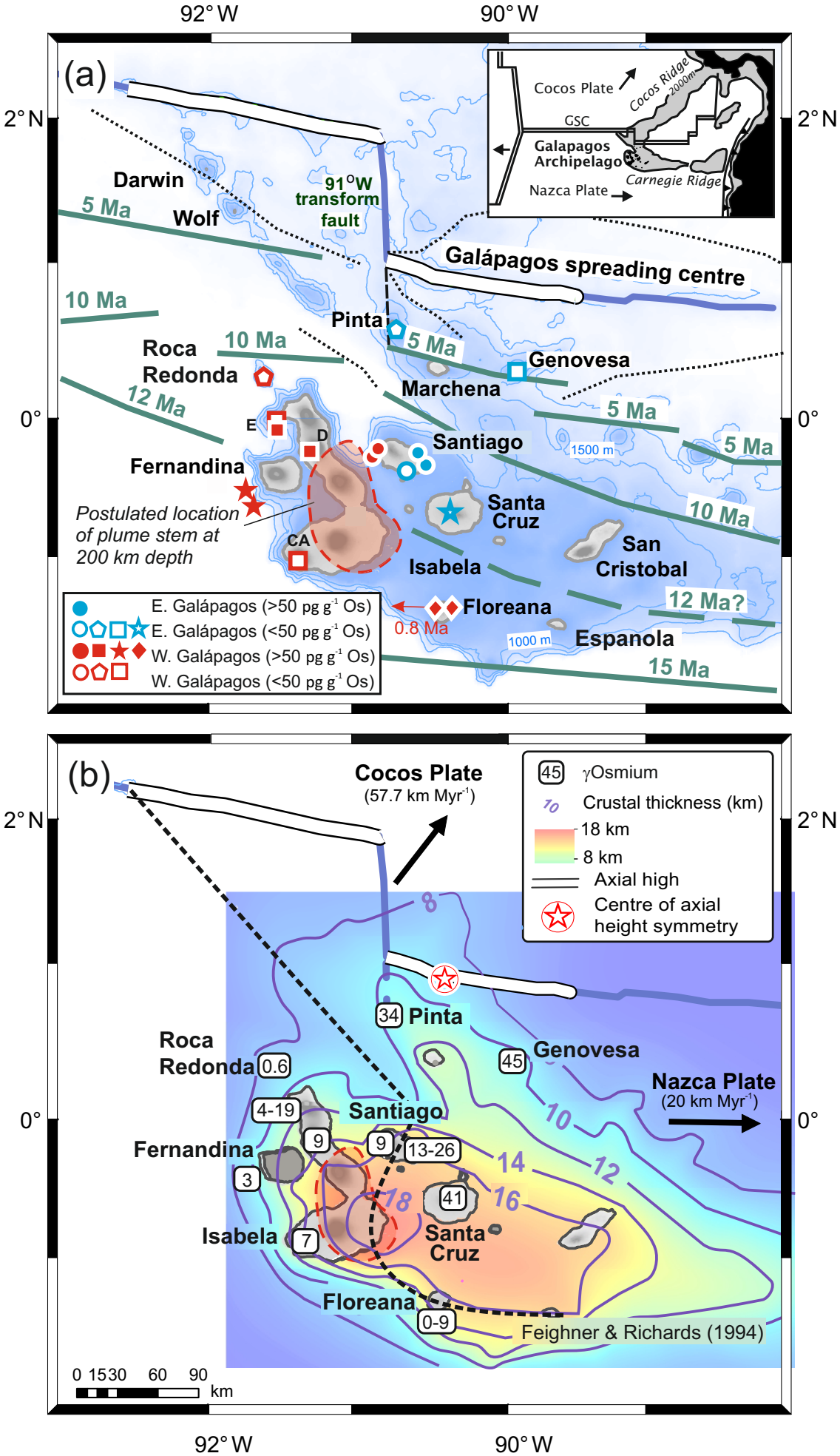
92° W
90° W
(a)
2° N
0°
Cocos Plate
Cocos Ridge
2000m
GSC
Galapagos Archipelago
Carnegie Ridge
Nazca Plate
Darwin
Wolf
91°W transform fault
5 Ma
Galápagos spreading centre
10 Ma
Pinta
5 Ma
Genovesa
Roca Redonda
10 Ma
Marchena
12 Ma
5 Ma
E
D
Santiago
1500 m
5 Ma
Fernandina
Postulated location of plume stem at 200 km depth
Santa Cruz
10 Ma
CA
San Cristobal
Isabela
12 Ma?
Floreana
0.8 Ma
1000 m
Espanola
15 Ma
E. Galápagos (>50 pg g-1 Os)
E. Galápagos (<50 pg g-1 Os)
W. Galápagos (>50 pg g-1 Os)
W. Galápagos (<50 pg g-1 Os)
(b)
Cocos Plate
(57.7 km Myr-1)
45 γOsmium
10 Crustal thickness (km)
18 km
8 km
Axial high
Centre of axial height symmetry
8
34 Pinta
Roca Redonda 0.6
45 Genovesa
Nazca Plate
(20 km Myr-1)
4-19
Santiago
10
Fernandina
9
9
13-26
14
12
3
18
41
16
Isabela 7
Santa Cruz
Floreana
0-9
Feighner & Richards (1994)
0 15 30 60 90
km

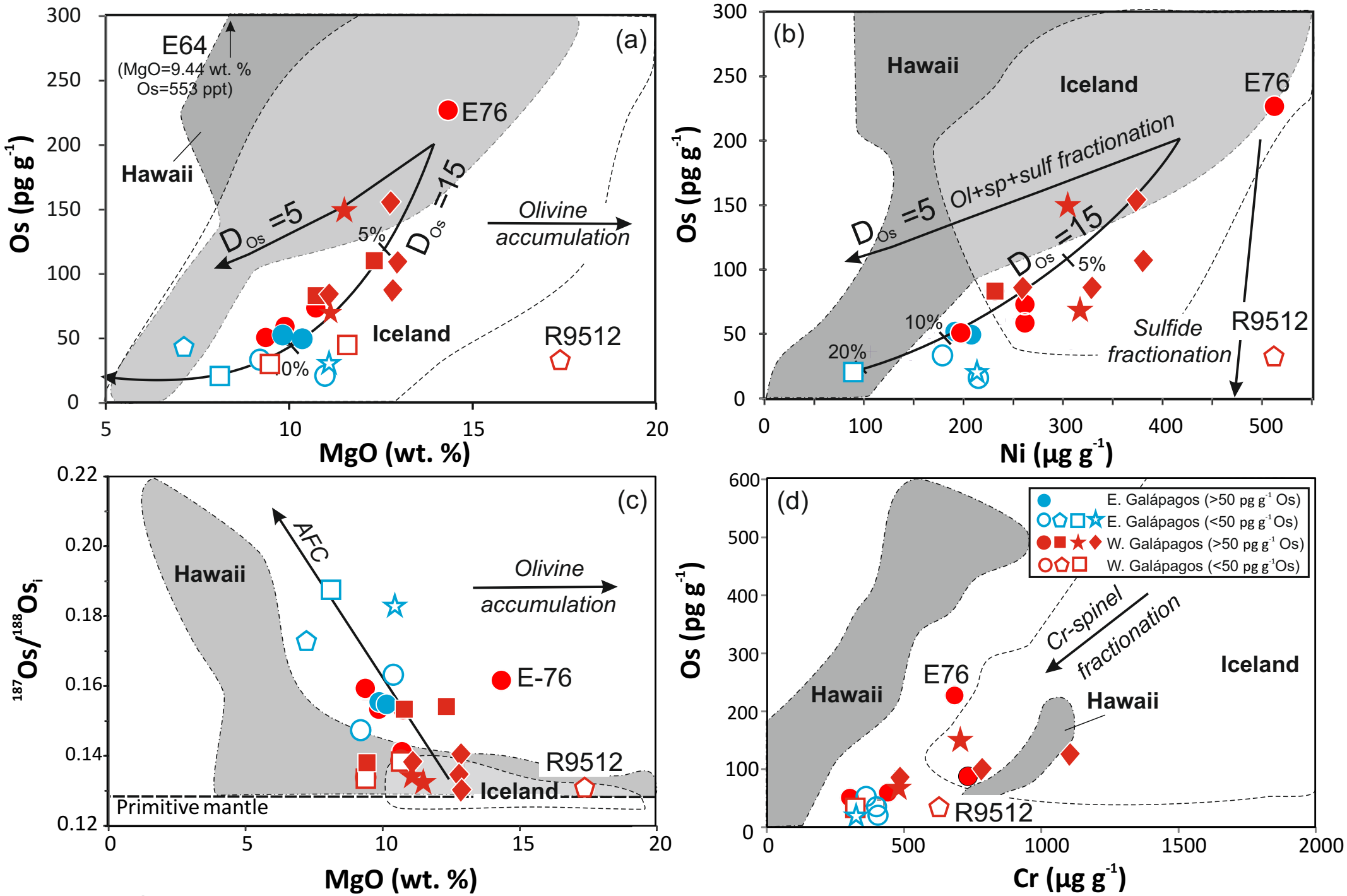
(a)
E64
(MgO=9.44 wt. %
Os=553 ppt)
E76
Hawaii
Iceland
R9512
Olivine
accumulation
D Os =5
D Os =15
5%
0%
Os (pg g-1)
MgO (wt. %)
(b)
Hawaii
Iceland
E76
Ol+sp+sulf fractionation
D Os =5
D Os =15
5%
10%
20%
Sulfide
fractionation
R9512
Os (pg g-1)
Ni (µg g-1)
(c)
AFC
Hawaii
Olivine
accumulation
E-76
R9512
Iceland
Primitive mantle
187Os/188Osi
MgO (wt. %)
(d)
E. Galápagos (>50 pg g-1 Os)
E. Galápagos (<50 pg g-1 Os)
W. Galápagos (>50 pg g-1 Os)
W. Galápagos (<50 pg g-1 Os)
Cr-spinel
fractionation
Hawaii
E76
Iceland
Hawaii
R9512
Os (pg g-1)
Cr (µg g-1)

Figure 2

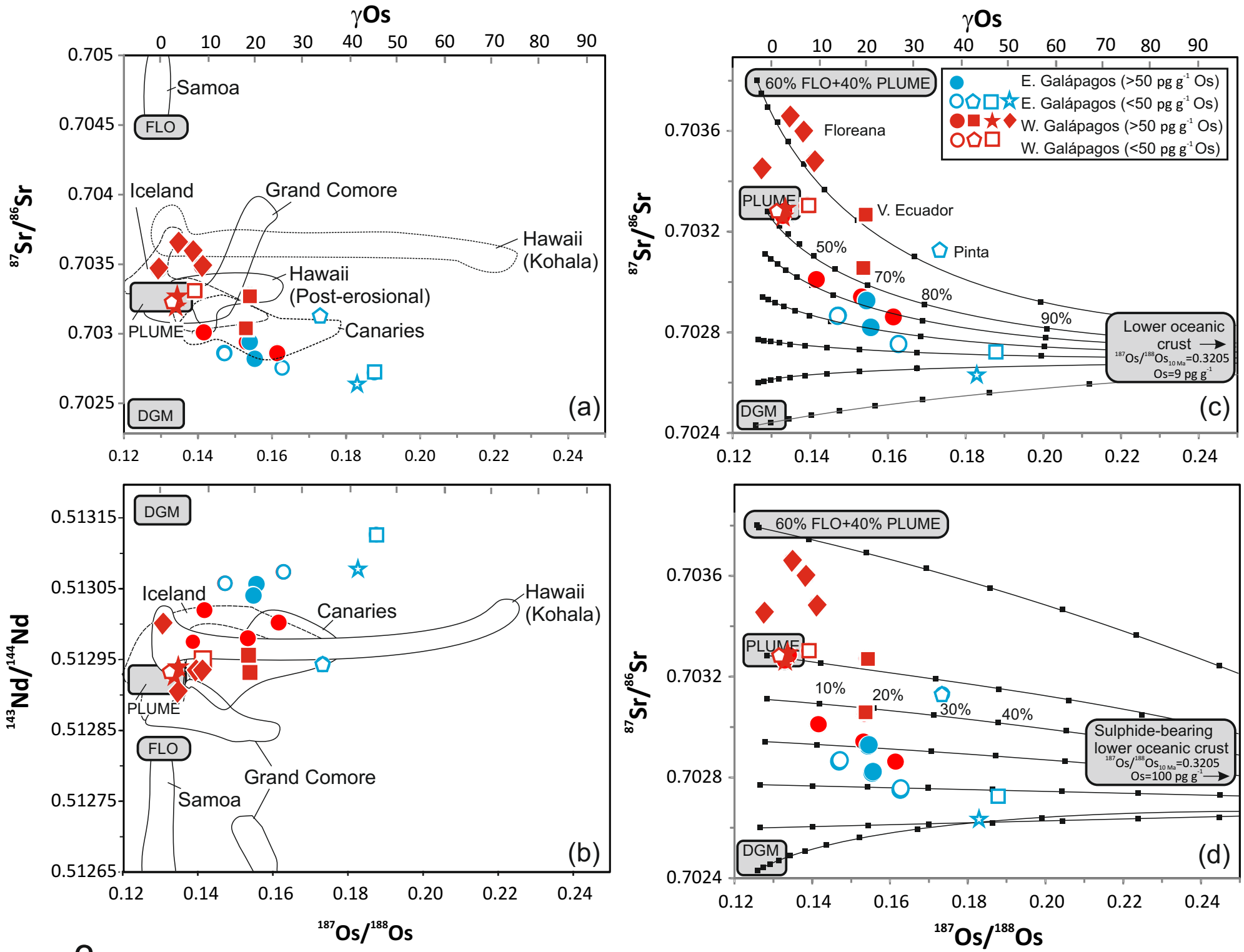
γOs
0 10 20 30 40 50 60 70 80 90
0.705
0.7045
0.704
0.7035
0.703
0.7025
87Sr/86Sr
Samoa
FLO
Iceland
Grand Comore
Hawaii (Kohala)
Hawaii (Post-erosional)
PLUME
Canaries
DGM
(a)
0.12 0.14 0.16 0.18 0.20 0.22 0.24
60% FLO+40% PLUME
E. Galápagos (>50 pg g-1 Os)
E. Galápagos (<50 pg g-1 Os)
W. Galápagos (>50 pg g-1 Os)
W. Galápagos (<50 pg g-1 Os)
Floreana
V. Ecuador
Pinta
50%
70%
80%
90%
Lower oceanic crust
187Os/188Os10 Ma=0.3205
Os=9 pg g-1
(c)
0.7036
0.7032
0.7028
0.7024
0.51315
0.51305
0.51295
0.51285
0.51275
0.51265
143Nd/144Nd
(b)
187Os/188Os
10%
20%
30%
40%
Sulphide-bearing lower oceanic crust
187Os/188Os10 Ma=0.3205
Os=100 pg g-1
(d)

Figure 3

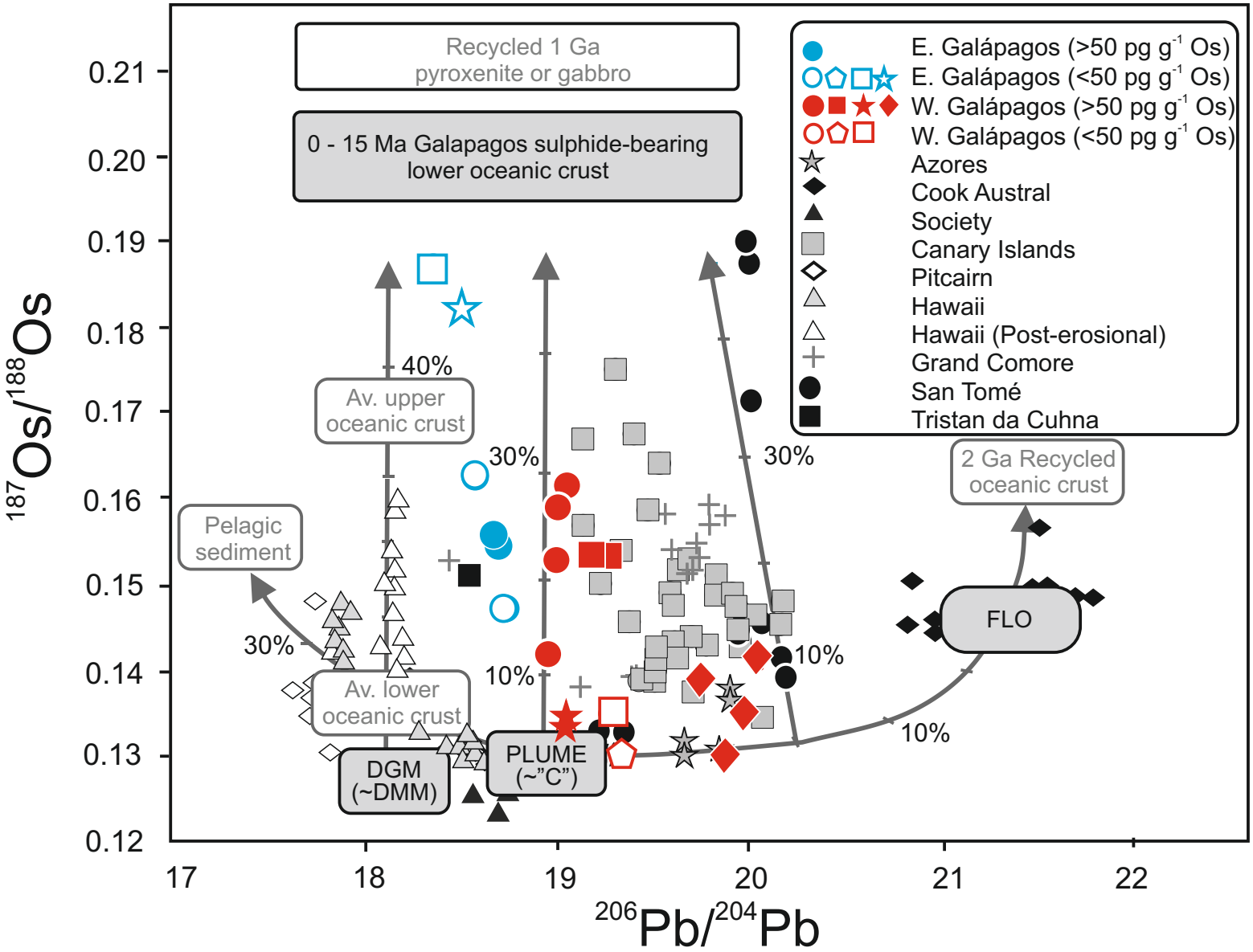
Recycled 1 Ga
pyroxenite or gabbro
0 - 15 Ma Galapagos sulphide-bearing
lower oceanic crust
E. Galápagos (>50 pg g-1 Os)
E. Galápagos (<50 pg g-1 Os)
W. Galápagos (>50 pg g-1 Os)
W. Galápagos (<50 pg g-1 Os)
Azores
Cook Austral
Society
Canary Islands
Pitcairn
Hawaii
Hawaii (Post-erosional)
Grand Comore
San Tomé
Tristan da Cuhna
Av. upper
oceanic crust
40%
30%
30%
2 Ga Recycled
oceanic crust
Pelagic
sediment
30%
10%
10%
FLO
Av. lower
oceanic crust
10%
DGM
(~DMM)
PLUME
(~"C")
0.21
0.20
0.19
0.18
0.17
0.16
0.15
0.14
0.13
0.12
17
18
19
20
21
22
187Os/188Os
206Pb/204Pb

Figure 4

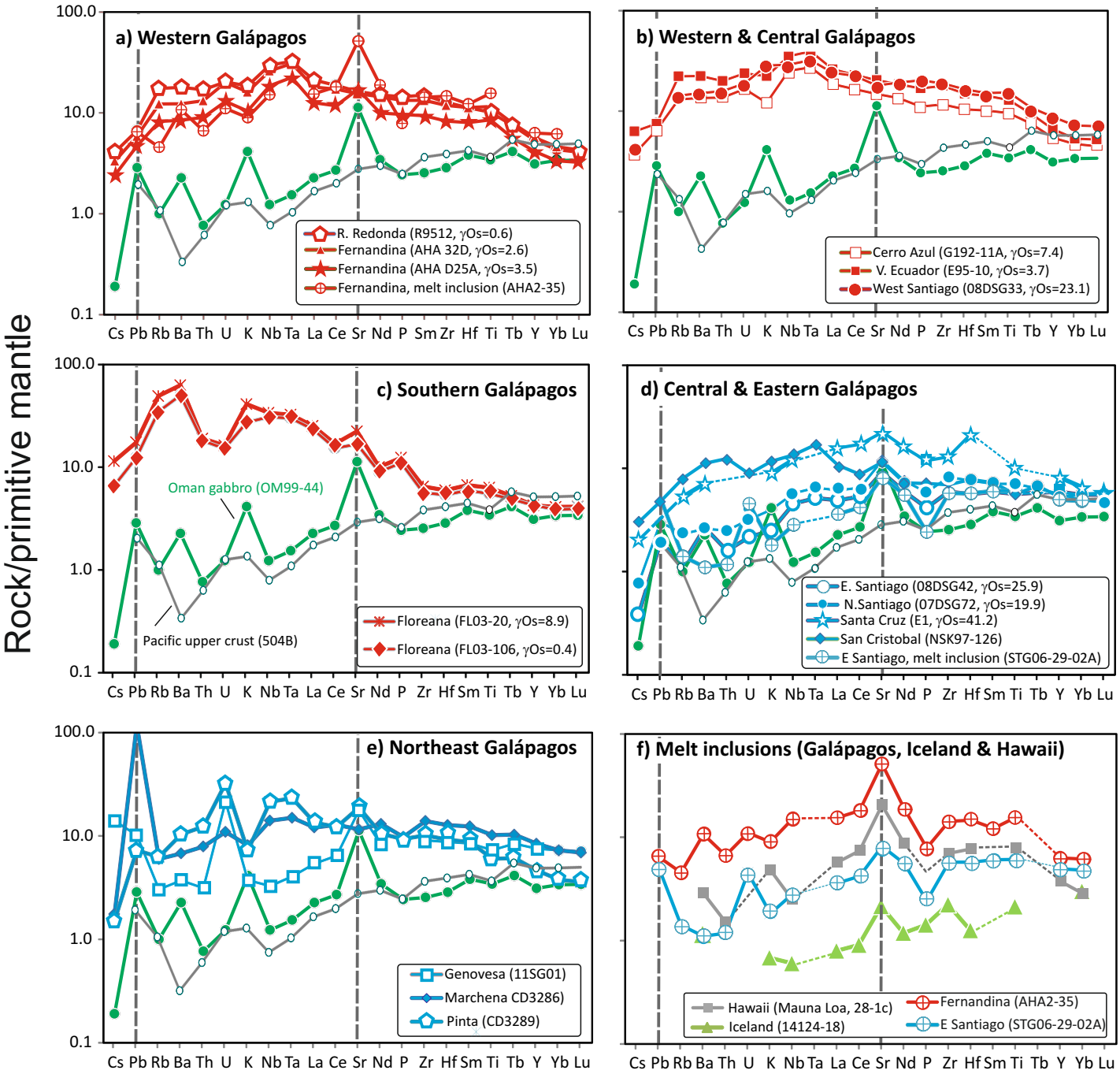
Rock/primitive mantle
a) Western Galápagos
R. Redonda (R9512, γOs=0.6)
Fernandina (AHA 32D, γOs=2.6)
Fernandina (AHA D25A, γOs=3.5)
Fernandina, melt inclusion (AHA2-35)
b) Western & Central Galápagos
Cerro Azul (G192-11A, γOs=7.4)
V. Ecuador (E95-10, γOs=3.7)
West Santiago (08DSG33, γOs=23.1)
c) Southern Galápagos
Oman gabbro (OM99-44)
Pacific upper crust (504B)
Floreana (FL03-20, γOs=8.9)
Floreana (FL03-106, γOs=0.4)
d) Central & Eastern Galápagos
E. Santiago (08DSG42, γOs=25.9)
N.Santiago (07DSG72, γOs=19.9)
Santa Cruz (E1, γOs=41.2)
San Cristobal (NSK97-126)
E Santiago, melt inclusion (STG06-29-02A)
e) Northeast Galápagos
Genovesa (11SG01)
Marchena CD3286)
Pinta (CD3289)
f) Melt inclusions (Galápagos, Iceland & Hawaii)
Hawaii (Mauna Loa, 28-1c)
Iceland (14124-18)
Fernandina (AHA2-35)
E Santiago (STG06-29-02A)
100.0
10.0
1.0
0.1
Cs Pb Rb Ba Th U K Nb Ta La Ce Sr Nd P Sm Zr Hf Ti Tb Y Yb Lu
Cs Pb Rb Ba Th U K Nb Ta La Ce Sr Nd P Zr Hf Sm Ti Tb Y Yb Lu

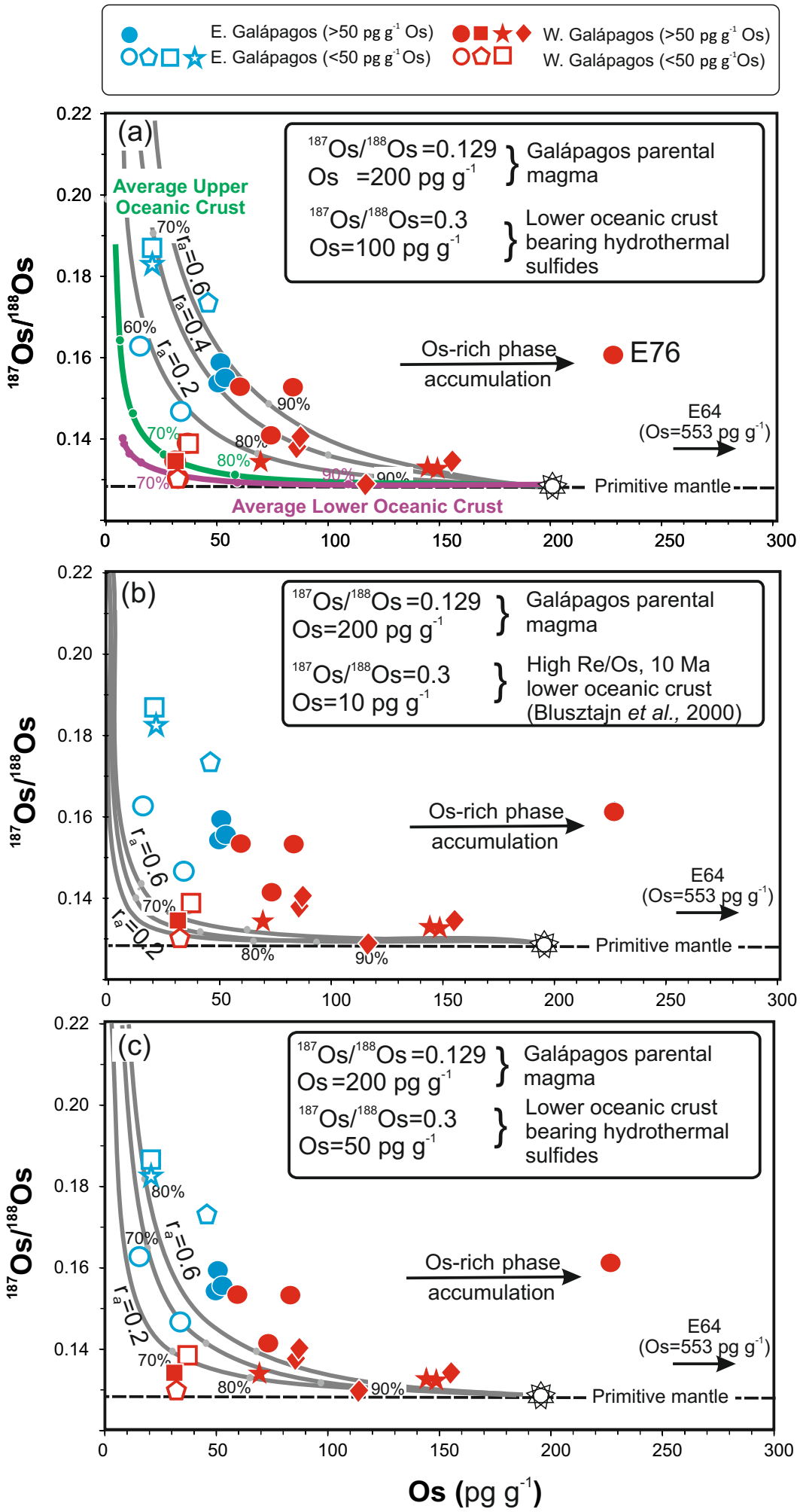
E. Galápagos (>50 pg g-1 Os)
E. Galápagos (<50 pg g-1 Os)
W. Galápagos (>50 pg g-1 Os)
W. Galápagos (<50 pg g-1 Os)
(a)
187Os/188Os =0.129
Os =200 pg g-1
Galápagos parental magma
187Os/188Os=0.3
Os=100 pg g-1
Lower oceanic crust bearing hydrothermal sulfides
Average Upper Oceanic Crust
Average Lower Oceanic Crust
Os-rich phase accumulation
E76
E64 (Os=553 pg g-1)
Primitive mantle
(b)
187Os/188Os =0.129
Os=200 pg g-1
Galápagos parental magma
187Os/188Os=0.3
Os=10 pg g-1
High Re/Os, 10 Ma lower oceanic crust (Blusztajn et al., 2000)
(c)
187Os/188Os =0.129
Os =200 pg g-1
Galápagos parental magma
187Os/188Os=0.3
Os=50 pg g-1
Lower oceanic crust bearing hydrothermal sulfides
187Os/188Os
Os (pg g-1)

Figure 6

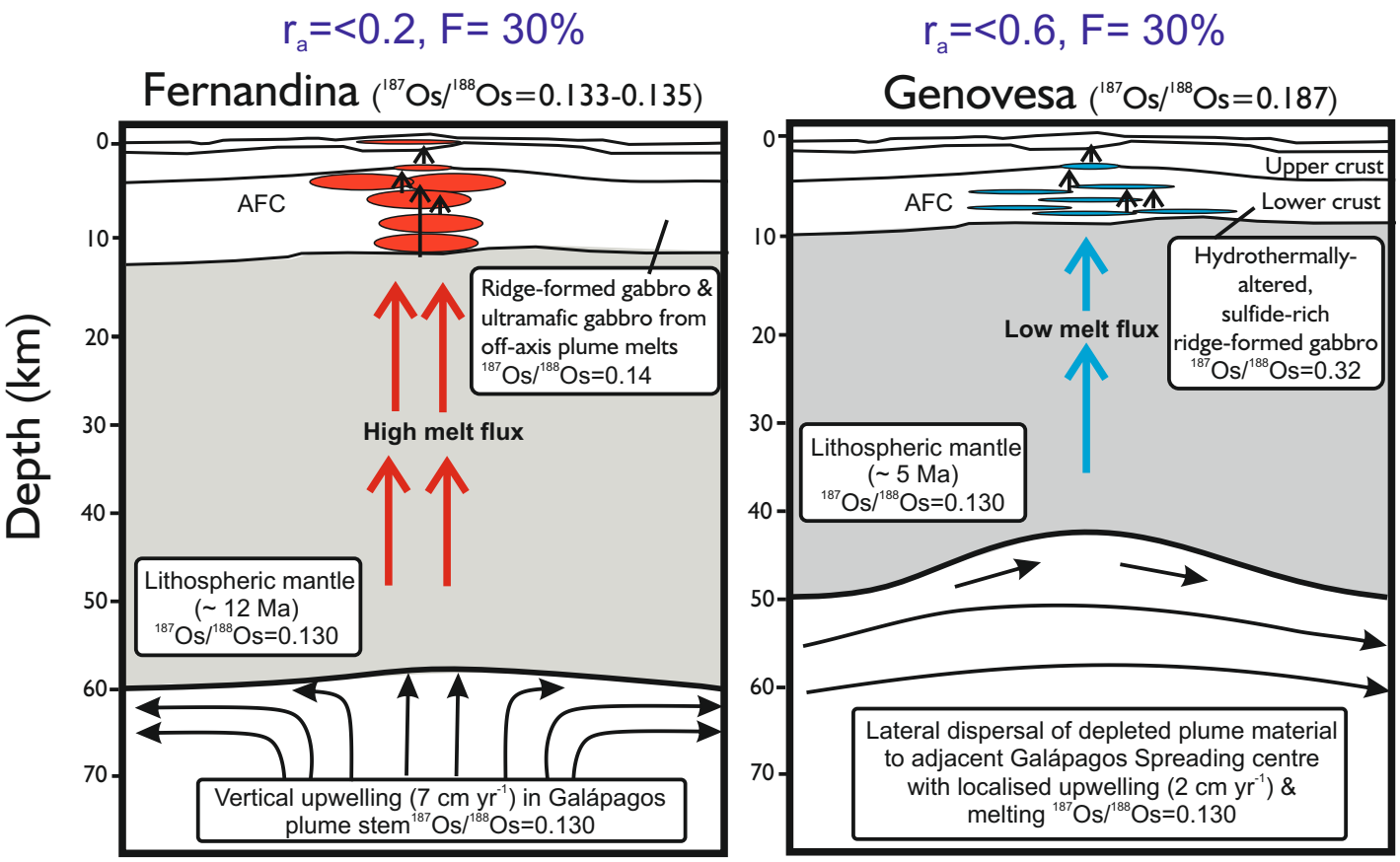
r_a=<0.2, F= 30%
Fernandina ($^{187}Os/^{188}Os$=0.133-0.135)
r_a=<0.6, F= 30%
Genovesa ($^{187}Os/^{188}Os$=0.187)
Depth (km)
0
10
20
30
40
50
60
70
AFC
Ridge-formed gabbro & ultramafic gabbro from off-axis plume melts $^{187}Os/^{188}Os$=0.14
High melt flux
Lithospheric mantle (~ 12 Ma) $^{187}Os/^{188}Os$=0.130
Vertical upwelling (7 cm yr^{-1}) in Galápagos plume stem $^{187}Os/^{188}Os$=0.130
Upper crust
Lower crust
AFC
Hydrothermally-altered, sulfide-rich ridge-formed gabbro $^{187}Os/^{188}Os$=0.32
Low melt flux
Lithospheric mantle (~ 5 Ma) $^{187}Os/^{188}Os$=0.130
Lateral dispersal of depleted plume material to adjacent Galápagos Spreading centre with localised upwelling (2 cm yr^{-1}) & melting $^{187}Os/^{188}Os$=0.130

Figure 7

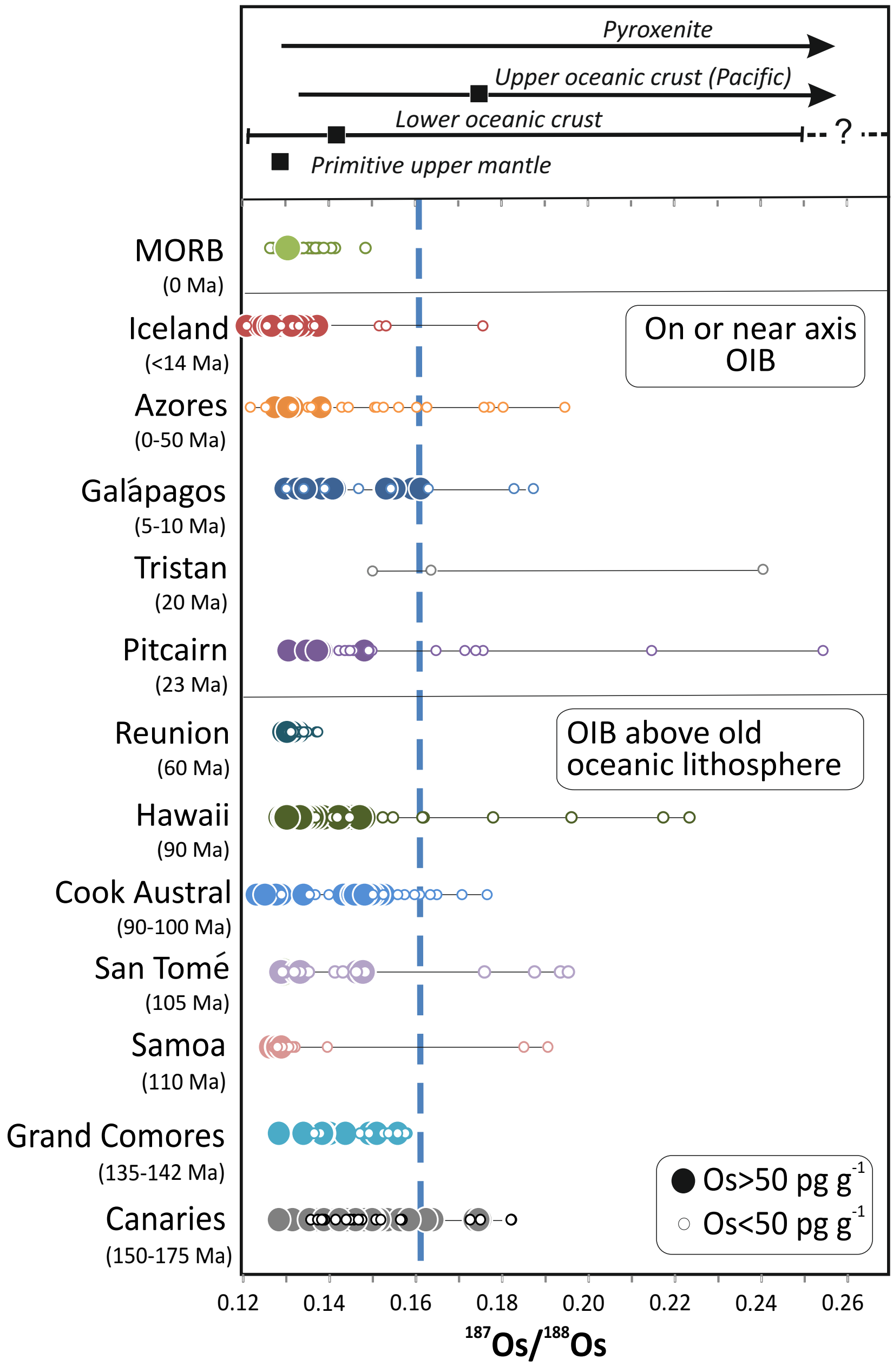
Pyroxenite
Upper oceanic crust (Pacific)
Lower oceanic crust
?
Primitive upper mantle
MORB
(0 Ma)
Iceland
(<14 Ma)
Azores
(0-50 Ma)
Galápagos
(5-10 Ma)
Tristan
(20 Ma)
Pitcairn
(23 Ma)
Reunion
(60 Ma)
Hawaii
(90 Ma)
Cook Austral
(90-100 Ma)
San Tomé
(105 Ma)
Samoa
(110 Ma)
Grand Comores
(135-142 Ma)
Canaries
(150-175 Ma)
On or near axis OIB
OIB above old oceanic lithosphere
Os>50 pg g-1
Os<50 pg g-1
0.12
0.14
0.16
0.18
0.20
0.22
0.24
0.26
187Os/188Os

Figure 8

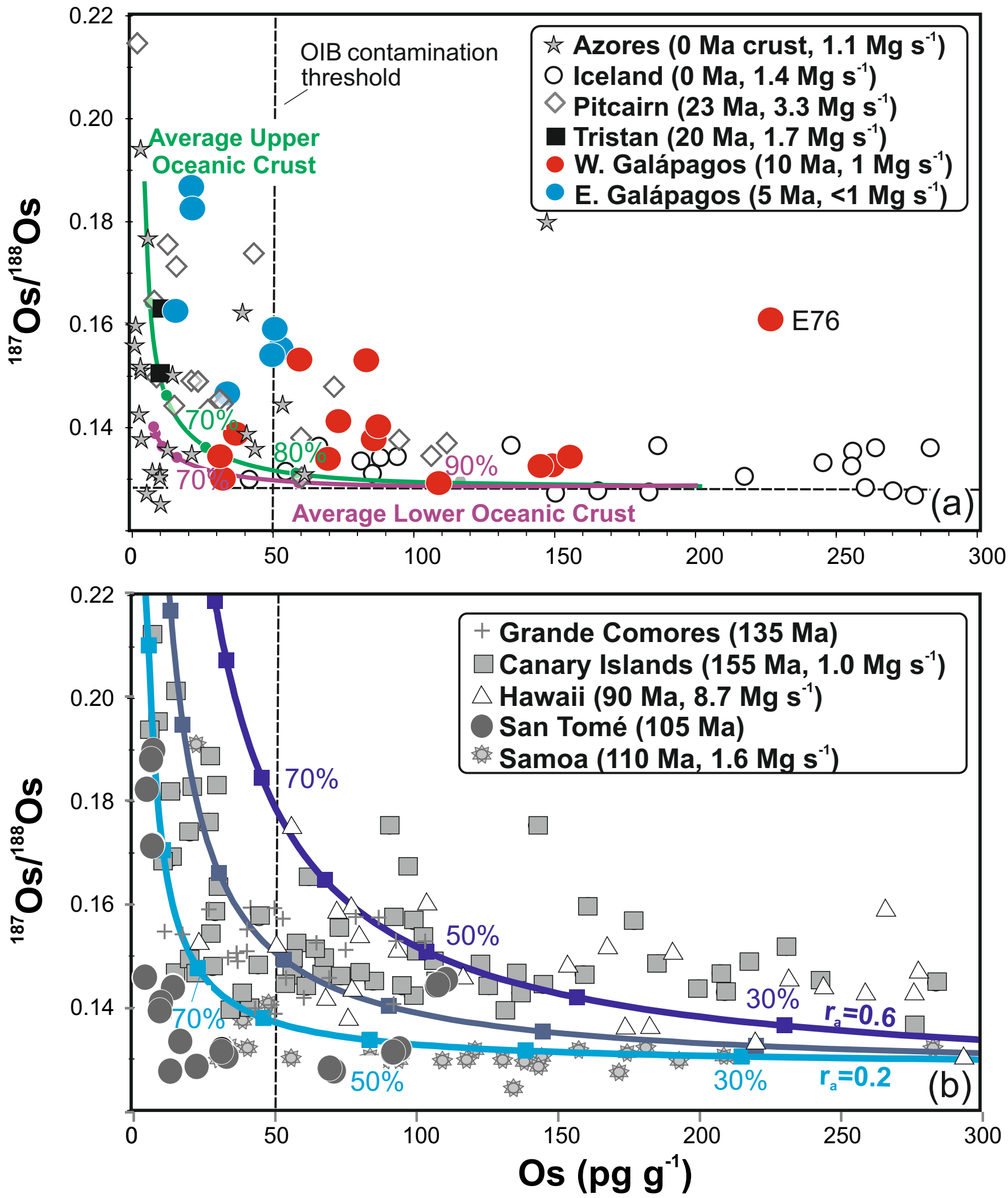
OIB contamination threshold
Azores (0 Ma crust, 1.1 Mg s-1)
Iceland (0 Ma, 1.4 Mg s-1)
Pitcairn (23 Ma, 3.3 Mg s-1)
Tristan (20 Ma, 1.7 Mg s-1)
W. Galápagos (10 Ma, 1 Mg s-1)
E. Galápagos (5 Ma, <1 Mg s-1)
Average Upper Oceanic Crust
Average Lower Oceanic Crust
E76
70%
80%
90%
(a)
187Os/188Os
Grande Comores (135 Ma)
Canary Islands (155 Ma, 1.0 Mg s-1)
Hawaii (90 Ma, 8.7 Mg s-1)
San Tomé (105 Ma)
Samoa (110 Ma, 1.6 Mg s-1)
70%
50%
30%
ra=0.6
ra=0.2
(b)
Os (pg g-1)

Figure 9

Table 1. Re-Os compositions of Galápagos basalts

	Sample No	Re (pg g^{-1})	Os (pg g^{-1})	$^{187}Os/^{188}Os$	2σ	γOs	MgO (wt. %)	$^{87}Sr/^{86}Sr$	$^{143}Nd/^{144}Nd$	$^{206}Pb/^{204}Pb$	$^{207}Pb/^{204}Pb$	$^{208}Pb/^{204}Pb$
Western Galápagos												
R. Redonda	R9512[a]	**84.3**	**32.2**	**0.13037**	**0.00051**	**0.60**	17.44	**0.703217**	**0.512951**	**19.336**	**15.612**	**39.076**
Fernandina	AHA D25A[a]	**457**	**69.4**	**0.13412**	**0.00014**	**3.49**	11.09	**0.703249**	**0.512929**	**19.055**	**15.556**	**38.706**
Fernandina	AHA 32D[a]	**910**	**149**	**0.13291**	**0.00007**	**2.55**	11.5	**0.703218**	**0.512933**	**19.065**	**15.563**	**38.726**
Fernandina	AHA 32D (repeat)[a]	**709**	**142**	**0.13249**	**0.00011**	**2.23**						
V. Ecuador	E95 10[a]	**265**	**31.6**	**0.13441**	**0.00023**	**3.71**	9.36					
V. Ecuador	E95-02[b]		**109**	**0.15393**	**0.00051**	**18.8**	12.29	0.703271	0.512934	19.289	15.601	39.037
V. Ecuador	E97-134[b]		**83.8**	**0.15340**	**0.00029**	**18.4**	10.74	0.703050	0.512956	19.209	15.592	38.888
Cerro Azul	G192-11A[a]	**478**	**36.5**	**0.13918**	**0.00020**	**7.39**	10.66	0.703302	0.512953	19.377	15.561	38.993
V. Darwin	E-64[b]		**552**	**0.13803**	**0.00018**	**6.50**	9.44					
Southern Galápagos												
Floreana	FL03-20[a]	**284**	**87.7**	**0.14109**	**0.00009**	**8.87**	12.85	0.7034850	0.512951	20.061	15.658	39.782
Floreana	FL03-106[a]	**253**	**109**	**0.13014**	**0.00013**	**0.42**	12.91	**0.703447**	**0.51300**	**19.886**	**15.648**	**39.604**
Floreana	E-110[b]		**86.1**	**0.13853**	**0.00025**	**6.89**	11.07	0.7036000	0.512975	19.785	15.636	39.516
Floreana	FL-3[b]		**154**	**0.13471**	**0.00045**	**3.94**	12.79	0.7036600	0.512905	20.002	15.657	39.739
Central Galapagos												
W. Santiago	08DSG33[a]	**150**	**50.6**	**0.15951**	**0.00020**	**23.1**	9.37			**19.129**	**15.588**	**38.785**
W. Santiago	07DSG61[a]	**314**	**73.6**	**0.14157**	**0.00012**	**9.23**	10.73	0.703009	0.513019	18.981	15.582	38.632
W. Santiago	E-76[b]		**227**	**0.16144**	**0.00036**	**24.6**	14.34	0.702860	0.513002	19.050	15.580	38.656
W. Santiago	E-20[b]		**59.2**	**0.15322**	**0.00032**	**18.2**	9.89	0.702940	0.512980	19.022	15.582	38.726
E. Santiago	07DSG72[a]	**498**	**52.5**	**0.15538**	**0.00016**	**19.9**	9.83	0.702819	0.513057	18.690	18.690	38.263
E. Santiago	08DSG42[a]	**277**	**15.7**	**0.16321**	**0.00044**	**25.9**	10.37	0.702926	0.513040	18.718	15.535	38.275
E. Santiago	08DSG16[a]	**157**	**34.2**	**0.14707**	**0.00023**	**13.5**	9.19	0.702864	0.513057	18.749	15.546	38.329
E. Santiago	08DSG04[a]	**327**	**49.9**	**0.15453**	**0.00016**	**19.2**	10.09	0.702752	0.513073	18.594	15.535	38.175
Santa Cruz	E-1[b]		**21.2**	**0.18303**	**0.00047**	**41.2**	10.43	0.702630	0.513077	18.514	15.520	38.048
North East Galápagos												
Genovesa	E-169[b]		**21.3**	**0.18751**	**0.00078**	**44.7**	8.09	0.702720	0.513127	18.387	15.511	37.941
Pinta	P-24[b]		**46.0**	**0.17318**	**0.00035**	**33.6**	7.23	0.703130	0.512943			

Analyses in bold are from this work. Sources of additional data are given in Table S4.

[a] denotes Re-Os analyses performed at the University of Durham and [b] analyses at the University of Mainz. Good reproducibility is demonstrated by duplicate analysis of basalt AHA-32D, for which the standard deviation (2σ) on the $^{187}Os/^{188}Os$ and Os concentrations were <0.5% and 7%, respectively. The variation in Re content was greater, at 35% (Table 1). Repeat analyses of the reference material TDB-1 provide a longer-term test of reproducibility which included the second analytical session (Durham): This gave a standard deviation (2σ) of ~20% for Os content and 4% for Re (n = 4), giving rise to a 20% variation in $^{187}Os/^{188}Os$ due to ingrowth over >1000 Ma.

Because of the relatively young age of basalts from western Galápagos (<1 Ma) and imprecise but young ages (<4 Ma) for basalts from the rest of the archipelago we have not corrected measured $1^{87O}s/1^{88O}s$ for in-growth of $1^{87O}s$. This does not significantly affect our findings as the correction for in-growth of $1^{87O}s$ to a 4 Ma sample with a Re/Os of ~18 (17 ppt Os and 300 ppt Re) and $1^{87O}s/1^{88O}s$ of 0.15 would involve a reduction in $1^{87O}s/1^{88O}s$ by only ~0.006.

Supplementary information related to '*The influence of melt flux and crustal processing on Re-Os isotope systematics of ocean island basalts: constraints from Galápagos*'

by Gibson, S.A., Dale, C.W. , Geist, D.J., Day J.A., Brügmann, G. & Harpp, K.

Table of contents

Supplementary Table 1

Sample	Location	Latitude	Longitude	Olivine		Fo max	Reference
				Euhedral phenocrysts	Large strained macrocrysts		
Western Galápagos							
Roca Redonda							
R9512		0.2696	-91.6249		x	83	Standish et al. [1998], Vidito et al. [2013]
Fernandina (submarine)							
AHA-D25A		-0.2720	-91.4460		x		Geist et al. [2006]
AHA-D32D		-0.3348	-91.4246	x	x		Geist et al. [2006]
Isabela							
V. Ecuador							
E95-10	East Rift	-0.0072	-91.5141		x		Geist et al. [2008]
E95-02	East Rift	-0.0118	-91.5195				Geist et al. [2008]
E97-134	Caldera Rim	-0.0014	-91.5808				Geist et al. [2008]
V. Darwin							
E-64							McBirney & Williams [1969]
Cerro Azul							
G192-11A		-0.8603	-91.5052	x	x	89	Kurz & Geist [1999]
Eastern Galápagos							
Santa Cruz							
E-1	Academy Bay (Shield)	-0.7429	-90.3041				McBirney & Williams [1969]
Southern Galápagos							
Floreana							
FLO3-20	Reversed flow	-1.2752	-90.3532	x	x		Harpp et al. [2014]
FLO3-106	Reversed flow	-1.2831	-90.4708				Harpp et al. [2014]
E-110	Flank Series	-1.2927	-90.4755				McBirney & Williams [1969]
FL-3	Main Series						Bow [1979]
Northern Galápagos							
Pinta							
P24						88	White et al. [1993], Vidito et al. [2013]
Genovesa							
E-169							White et al. [1993]
Central Galápagos							
Isla Santiago							
East							
08DSG04	SW of Puerto Martinez	-0.3320	-90.5720	x		87	Gibson et al. [2012]
07DSG72	Flamingo Bay	-0.2255	-90.6071	x		86	Gibson et al. [2012]
08DSG42	Cerro Inn	-0.2775	-90.5887	x		86	Gibson et al. [2012]
08DSG16	Poza Tiburones	-0.3441	-90.6741	x		-	Gibson et al. [2012]
West							
08DSG33	SE of Puerto Nuevo	-0.2902	-90.8387	x		85	Gibson et al. [2012]
E-76	Buccaneer Cove	-0.1658	-90.8237		x	88	McBirney & Williams [1969], Vidito et al.
E-20	James Bay						McBirney & Williams [1969]
07DSG61	James Bay	-0.2155	-90.8359	x	x	86	Gibson et al. [2012]

Table S2. Electron microprobe data for olivines from Isla Santiago, Galapagos

	MgO	SiO_2	Al_2O_3	CaO	TiO_2	Cr_2O_3	MnO	FeO	NiO	P_2O_5	Total	Fo
07DSG61												
1 / 1 .	45.25	40.67	0.07	0.26	0.02	0.05	0.17	14.00	0.27	0.01	100.78	85.21
2 / 1 .	43.43	40.05	0.05	0.25	0.02	0.03	0.22	16.13	0.24	0.01	100.43	82.75
3 / 1 .	44.16	39.66	0.06	0.24	0.02	0.09	0.25	15.04	0.27	0.02	99.81	83.95
4 / 1 .	44.17	40.14	0.10	0.23	0.01	0.03	0.21	14.72	0.35	0.02	99.98	84.25
5 / 1 .	44.43	40.15	0.07	0.24	0.00	0.06	0.19	14.79	0.27	0.03	100.24	84.26
6 / 1 .	43.66	40.07	0.05	0.24	0.02	0.06	0.22	15.42	0.20	0.01	99.94	83.46
7 / 1 .	46.16	40.54	0.06	0.24	0.01	0.08	0.20	12.89	0.33	0.01	100.52	86.46
8 / 1 .	44.10	39.84	0.06	0.26	0.01	0.05	0.26	15.45	0.25	0.03	100.31	83.57
9 / 1 .	44.47	40.34	0.03	0.26	0.01	0.03	0.23	14.78	0.30	0.01	100.46	84.28
07DSG72												
1 / 1 .	45.22	40.20	0.08	0.30	0.02	0.03	0.20	13.73	0.27	0.02	100.06	85.44
2 / 1 .	45.80	40.37	0.09	0.30	0.02	0.07	0.25	13.84	0.30	0.01	101.04	85.50
3 / 1 .	45.63	39.86	0.07	0.29	0.02	0.05	0.21	13.56	0.27	0.01	99.96	85.71
4 / 1 .	48.68	38.71	0.56	0.30	0.23	0.04	0.16	13.70	0.25	0.01	102.64	86.36
5 / 1 .	44.58	41.48	0.29	0.31	0.00	0.00	0.18	13.65	0.28	0.01	100.78	85.33
6 / 1 .	45.69	40.74	0.10	0.29	0.01	0.04	0.23	13.76	0.26	0.00	101.11	85.54
7 / 1 .	44.35	39.62	0.09	0.28	0.02	0.04	0.23	15.24	0.24	0.04	100.15	83.83
8 / 1 .	45.98	40.68	0.11	0.28	0.01	0.03	0.17	13.48	0.26	0.00	101.00	85.88
9 / 1 .	43.51	39.99	0.08	0.29	0.02	0.06	0.23	16.16	0.15	0.00	100.48	82.76
10 / 1 .	41.59	42.69	0.61	0.33	0.02	0.04	0.19	14.27	0.18	0.02	99.95	83.85
11 / 1 .	45.87	40.10	0.09	0.28	0.02	0.06	0.19	13.42	0.30	0.02	100.35	85.90
12 / 1 .	44.84	40.30	0.08	0.32	0.02	0.01	0.23	14.31	0.22	0.03	100.38	84.81
13 / 1 .	45.79	40.37	0.08	0.29	0.01	0.09	0.16	13.80	0.29	0.01	100.89	85.54
14 / 1 .	45.56	40.17	0.09	0.30	0.00	0.03	0.19	13.79	0.29	0.01	100.43	85.48
15 / 1 .	45.25	40.27	0.08	0.30	0.02	0.06	0.22	13.92	0.27	0.01	100.41	85.28
16 / 1 .	45.73	40.73	0.08	0.28	0.01	0.04	0.22	13.26	0.31	0.00	100.67	86.00
17 / 1 .	45.78	40.62	0.07	0.28	0.02	0.04	0.17	13.50	0.30	0.00	100.78	85.80
18 / 1 .	42.04	42.99	0.71	0.29	0.01	0.02	0.22	13.68	0.28	0.02	100.26	84.56
19 / 1 .	46.85	38.66	0.74	0.37	0.01	0.05	0.17	13.35	0.27	0.13	100.61	86.21
20 / 1 .	45.46	40.27	0.10	0.29	0.01	0.02	0.20	13.60	0.27	0.00	100.21	85.63
08DSG04												
1 / 1 .	38.71	38.59	0.05	0.37	0.03	0.03	0.36	22.37	0.11	0.02	100.65	75.51
2 / 1 .	46.17	40.58	0.06	0.28	0.01	0.07	0.17	13.16	0.29	0.01	100.78	86.21
3 / 1 .	46.21	40.00	0.08	0.26	0.01	0.05	0.17	12.86	0.32	0.00	99.95	86.50
4 / 1 .	46.18	39.80	0.08	0.27	0.01	0.06	0.20	12.90	0.30	0.03	99.84	86.45
5 / 1 .	46.27	40.13	0.08	0.28	0.01	0.04	0.18	12.99	0.31	0.02	100.32	86.39
6 / 1 .	46.17	39.98	0.07	0.28	0.01	0.05	0.19	12.75	0.34	0.00	99.84	86.58
7 / 1 .	46.33	40.20	0.07	0.28	0.01	0.00	0.17	13.03	0.34	0.00	100.44	86.37
8 / 1 .	46.13	40.05	0.08	0.28	0.01	0.04	0.18	13.09	0.30	0.01	100.16	86.26
9 / 1 .	46.22	40.35	0.08	0.28	0.02	0.08	0.22	12.96	0.32	0.02	100.55	86.40
10 / 1 .	45.64	39.87	0.08	0.27	0.01	0.07	0.19	13.47	0.31	0.00	99.90	85.79
11 / 1 .	39.78	38.48	0.05	0.32	0.02	0.04	0.26	21.02	0.16	0.04	100.18	77.13
12 / 1 .	46.38	39.80	0.07	0.27	0.01	0.05	0.21	12.87	0.32	0.01	99.97	86.53
13 / 1 .	46.26	39.74	0.08	0.27	0.01	0.03	0.21	12.89	0.30	0.02	99.82	86.48
14 / 1 .	46.36	40.45	0.08	0.27	0.01	0.05	0.14	13.13	0.35	0.00	100.85	86.29
15 / 1 .	46.17	40.29	0.07	0.28	0.01	0.04	0.16	12.75	0.28	0.01	100.07	86.58
16 / 1 .	45.49	40.29	0.07	0.26	0.02	0.04	0.26	14.41	0.32	0.00	101.15	84.90
17 / 1 .	46.24	40.44	0.08	0.28	0.01	0.06	0.18	13.00	0.34	0.00	100.64	86.37
18 / 1 .	45.94	40.59	0.08	0.28	0.01	0.05	0.18	13.00	0.32	0.00	100.46	86.30
19 / 1 .	42.44	39.59	0.07	0.23	0.00	0.04	0.26	17.33	0.19	0.00	100.15	81.36
20 / 1 .	46.30	40.54	0.08	0.28	0.01	0.07	0.21	12.54	0.34	0.00	100.39	86.81
21 / 1 .	46.23	40.38	0.07	0.29	0.01	0.05	0.18	12.92	0.33	0.00	100.47	86.44
22 / 1 .	46.37	39.98	0.08	0.28	0.01	0.05	0.11	12.77	0.32	0.00	99.97	86.61
23 / 1 .	45.04	40.06	0.07	0.25	0.01	0.03	0.21	14.48	0.25	0.02	100.42	84.72
24 / 1 .	46.17	40.67	0.12	0.27	0.02	0.07	0.19	12.96	0.28	0.00	100.75	86.39
25 / 1 .	45.49	40.24	0.09	0.24	0.02	0.07	0.18	12.85	0.24	0.01	99.42	86.32
26 / 1 .	45.68	40.27	0.07	0.28	0.00	0.02	0.15	13.47	0.33	0.01	100.29	85.80
27 / 1 .	45.27	40.18	0.06	0.26	0.01	0.03	0.16	14.14	0.29	0.00	100.40	85.08
28 / 1 .	45.71	40.42	0.26	0.29	0.02	0.10	0.18	12.95	0.30	0.01	100.24	86.28
08DSG33												
1 / 1 .	43.75	39.57	0.07	0.22	0.02	0.06	0.25	16.01	0.32	0.03	100.29	82.96
2 / 1 .	43.32	39.30	0.08	0.24	0.02	0.03	0.26	16.03	0.31	0.04	99.63	82.80
3 / 1 .	43.54	39.19	0.06	0.22	0.02	0.02	0.16	15.89	0.35	0.01	99.46	83.00
4 / 1 .	42.11	39.30	0.02	0.15	0.02	0.02	0.29	18.60	0.24	0.01	100.76	80.13
5 / 1 .	43.17	39.93	0.04	0.22	0.03	0.00	0.22	16.56	0.26	0.05	100.49	82.28
6 / 1 .	43.73	39.59	0.08	0.22	0.01	0.03	0.17	16.03	0.32	0.03	100.20	82.94
7 / 1 .	42.45	39.46	0.04	0.26	0.02	0.00	0.25	17.57	0.29	0.05	100.40	81.15
8 / 1 .	43.99	39.75	0.03	0.15	0.01	0.00	0.18	15.94	0.33	0.01	100.38	83.10
9 / 1 .	41.05	39.10	0.05	0.17	0.03	0.00	0.27	20.03	0.25	0.02	100.95	78.51
10 / 1 .	42.90	39.70	0.04	0.16	0.00	0.00	0.24	17.37	0.29	-0.01	100.69	81.48
11 / 1 .	43.94	40.12	0.04	0.21	0.02	0.02	0.22	15.52	0.32	0.00	100.41	83.46
12 / 1 .	42.42	39.69	0.06	0.23	0.02	0.04	0.19	18.03	0.27	0.03	100.99	80.74
13 / 1 .	43.34	39.75	0.06	0.24	0.03	0.02	0.20	16.74	0.30	0.02	100.70	82.19
14 / 1 .	43.02	39.70	0.00	0.07	0.01	0.00	0.24	17.56	0.22	0.00	100.84	81.36
15 / 1 .	40.80	39.19	0.05	0.17	0.03	0.01	0.28	20.26	0.16	0.04	100.98	78.21
16 / 1 .	45.24	40.36	0.08	0.25	0.01	0.02	0.17	14.52	0.37	0.01	101.04	84.74
17 / 1 .	39.05	38.78	0.02	0.06	0.00	0.02	0.32	22.49	0.11	0.02	100.87	75.57
18 / 1 .	40.22	39.43	0.03	0.13	0.02	0.04	0.28	20.43	0.21	0.02	100.80	77.82
19 / 1 .	44.20	39.48	0.08	0.21	0.02	0.03	0.20	15.55	0.37	0.03	100.17	83.51
20 / 1 .	40.90	39.11	0.04	0.14	0.02	0.00	0.21	20.01	0.23	0.01	100.67	78.46
21 / 1 .	44.04	39.45	0.07	0.22	0.03	0.07	0.19	15.56	0.34	0.03	100.00	83.45
22 / 1 .	40.80	38.91	0.05	0.17	0.03	0.00	0.33	20.29	0.19	0.04	100.81	78.19
08DSG42												
1 / 1 .	45.62	39.91	0.09	0.31	0.01	0.08	0.23	13.15	0.32	0.02	99.74	86.07
2 / 1 .	45.11	40.45	0.14	0.34	-0.01	0.02	0.12	13.28	0.28	0.02	99.77	85.82
3 / 1 .	45.28	40.59	0.08	0.29	0.01	0.04	0.08	13.60	0.27	0.02	100.29	85.57
4 / 1 .	45.43	40.12	0.07	0.30	0.01	0.03	0.17	12.95	0.29	0.01	99.38	86.21
5 / 1 .	44.88	40.28	0.06	0.19	0.02	0.03	0.22	14.55	0.24	0.05	100.54	84.61
6 / 1 .	45.78	40.39	0.06	0.29	0.00	0.07	0.20	13.15	0.28	-0.01	100.22	86.12
7 / 1 .	45.70	40.46	0.07	0.30	0.00	0.03	0.21	13.30	0.29	0.00	100.37	85.96
8 / 1 .	45.51	40.38	0.06	0.30	0.01	0.06	0.24	13.45	0.26	-0.01	100.28	85.77
9 / 1 .	45.52	40.44	0.08	0.32	0.01	0.02	0.16	13.48	0.28	0.00	100.31	85.75
10 / 1 .	45.38	40.51	0.06	0.32	0.03	0.00	0.11	13.64	0.27	0.00	100.32	85.57
11 / 1 .	45.40	40.36	0.08	0.30	0.01	0.05	0.21	12.98	0.28	0.01	99.67	86.17
12 / 1 .	45.44	40.34	0.07	0.30	0.02	0.07	0.27	13.11	0.21	0.00	99.84	86.06
13 / 1 .	45.54	40.39	0.08	0.32	0.01	0.06	0.17	13.09	0.32	0.01	99.99	86.11
14 / 1 .	45.47	40.46	0.06	0.29	0.01	0.02	0.15	13.33	0.23	0.03	100.05	85.87
15 / 1 .	43.40	39.52	0.05	0.22	0.02	0.06	0.30	15.96	0.25	0.01	99.78	82.89
16 / 1 .	45.79	40.84	0.06	0.27	0.00	0.06	0.27	13.21	0.29	0.00	100.79	86.07
17 / 1 .	45.84	40.81	0.06	0.30	0.01	0.00	0.21	13.51	0.27	0.00	101.02	85.81
18 / 1 .	45.15	39.82	0.06	0.31	0.00	0.01	0.17	13.54	0.26	0.02	99.34	85.60
19 / 1 .	45.57	40.41	0.08	0.31	0.01	0.09	0.19	13.42	0.26	0.03	100.37	85.81
20 / 1 .	45.38	39.75	0.06	0.29	0.00	0.03	0.24	13.67	0.26	0.00	99.69	85.54

Supplementary Table3: International rock standards analysed by ICP-MS in the Department of Earth Sciences at the University of Cambridge. Standards were analysed during the same run as Galapagos samples

	AGV-2 lit	AGV-2	AGV-2	AGV-2 avg	% RSD	%REC	**BCR-2 lit**	BCR-2	BCR-2	BCR-2 avg	% RSD	%REC	**BHVO-2 lit**	BHVO-2	BHVO-2	BHVO-2 avg	% RSD	%REC
Sc	13	19.63	19.34	19.49	1.1	150	33	41.12	41.73	41.43	1.0	126	32	38.07	39.19	38.63	2.0	121
Ti	6295	6214.30	6223.43	6219	0.1	99	13549	13260.75	13613.89	13437	1.9	99	16367	16044.64	16225.36	16135	0.8	99
V	120	115.06	113.51	114	1.0	95	416	381.39	387.08	384.24	1.0	92	317	352.08	363.02	358	2.2	113
Cr	16	14.20	13.65	13.93	2.8	87	18	13.81	13.31	13.56	2.6	75	280	282.39	281.17	282	0.3	101
Mn	770	1025.32	1050.03	1038	1.7	135	1520	1604.84	1542.54	1574	2.8	104	1290	1345.26	1409.77	1378	3.3	107
Co	16	15.33	16.35	15.84	4.5	99	37	36.15	36.96	36.56	1.6	99	45	44.60	44.25	44.42	0.6	99
Ni	19.4	18.38	17.53	17.95	3.3	93	17.7	11.97	11.88	11.92	0.5	67	119	116.10	118.40	117	1.4	99
Cu	53	51.66	54.09	52.87	3.3	100	21	28.06	26.58	27.32	3.8	130	127	140.04	138.18	139	0.9	110
Zn	86	84.23	84.19	84	0.0	98	127	124.80	127.00	125.90	1.2	99	103	108.57	109.24	109	0.4	106
Ga	20	20.30	20.48	20.39	0.6	102	20.6	21.38	21.18	21.28	0.7	103	21.7	21.01	21.26	21.13	0.8	97
Rb	66.3	79.84	79.70	79.77	0.1	120	46.9	54.16	53.47	53.81	0.9	115	9.08	10.76	10.68	10.72	0.5	118
Sr	661	667.58	683.18	675	1.6	102	340	344.55	342.57	344	0.4	101	396	416.69	409.84	413	1.2	104
Y	20	20.62	20.38	20.50	0.8	103	37	36.55	36.09	36.32	0.9	98	26	26.02	26.88	26.45	2.3	102
Zr	230	242.30	242.92	243	0.2	105	188	186.68	183.18	185	1.3	98	172	169.74	177.48	174	3.2	101
Nb	14.5	14.08	14.09	14.09	0.0	97	12.6	12.24	12.17	12.21	0.4	97	18.1	18.41	18.57	18.49	0.6	102
Sn	2.3	1.96	2.00	1.98	1.5	86	2	2.06	2.08	2.07	0.6	104	1.7	1.68	1.71	1.70	1.1	100
Cs	1.2	1.14	1.16	1.15	1.3	96	1.07	1.10	1.10	1.10	0.4	103	0.09	0.10	0.10	0.10	4.6	111
Ba	1130	1126.70	1128.89	1128	0.1	100	677	662.57	655.86	659	0.7	97	131	128.17	131.60	130	1.9	99
La	37.9	38.02	38.37	38.20	0.6	101	24.9	25.11	24.96	25.04	0.4	101	15.2	15.36	15.26	15.31	0.4	101
Ce	68.6	69.62	69.65	69.64	0.0	102	52.9	52.17	51.78	51.97	0.5	98	37.5	36.99	37.66	37.32	1.3	100
Pr	7.84	7.98	7.98	7.98	0.0	102	6.57	6.54	6.59	6.56	0.5	100	5.29	5.12	5.24	5.18	1.6	98
Nd	30.5	30.42	31.07	30.75	1.5	101	28.7	28.43	28.26	28.34	0.4	99	24.5	24.62	24.70	24.66	0.2	101
Sm	5.49	5.49	5.63	5.56	1.7	101	6.58	6.56	6.49	6.53	0.7	99	6.07	6.09	6.24	6.17	1.8	102
Eu	1.53	1.51	1.55	1.53	1.7	100	1.96	1.96	1.95	1.96	0.2	100	2.07	2.10	2.10	2.10	0.3	101
Gd	4.52	4.50	4.59	4.55	1.4	101	6.75	6.61	6.72	6.67	1.2	99	6.24	6.34	6.39	6.36	0.5	102
Tb	0.641	0.65	0.66	0.65	0.8	102	1.07	1.08	1.07	1.07	0.4	100	0.936	0.96	0.97	0.97	1.2	103
Dy	3.47	3.60	3.62	3.61	0.3	104	6.41	6.42	6.49	6.45	0.8	101	5.31	5.42	5.41	5.42	0.1	102
Ho	0.653	0.69	0.69	0.69	0.3	106	1.3	1.36	1.32	1.34	2.5	103	0.972	1.02	1.03	1.02	0.7	105
Er	1.81	1.88	1.88	1.88	0.0	104	3.66	3.68	3.68	3.68	0.1	101	2.54	2.60	2.57	2.59	0.7	102
Tm	0.26	0.27	0.28	0.27	1.2	106	0.54	0.54	0.54	0.54	0.1	100	0.33	0.35	0.35	0.35	0.9	105
Yb	1.62	1.65	1.68	1.67	1.2	103	3.38	3.38	3.44	3.41	1.2	101	2	2.01	2.03	2.02	0.8	101
Lu	0.247	0.25	0.26	0.26	2.5	104	0.503	0.52	0.50	0.51	3.3	102	0.274	0.28	0.29	0.29	0.7	104
Hf	5	5.19	5.21	5.20	0.3	104	4.9	4.82	4.85	4.84	0.4	99	4.36	4.35	4.41	4.38	1.0	100
Ta	0.87	0.84	0.87	0.85	2.0	98	0.74	0.76	0.78	0.77	1.4	104	1.14	1.17	1.15	1.16	1.0	102
Pb	13.2	13.42	13.56	13.49	0.7	102	11	10.29	10.12	10.21	1.2	93	1.6	1.71	1.74	1.73	1.1	108
Th	6.1	6.18	6.22	6.20	0.5	102	5.7	5.82	5.82	5.82	0.1	102	1.22	1.21	1.22	1.21	0.2	99
U	1.86	1.92	1.93	1.92	0.7	103	1.69	1.70	1.69	1.69	0.4	100	0.39	0.42	0.43	0.42	0.6	109

Table S4. Whole rock analyses of Galápagos samples

	Western Galapagos																		Eastern Galapagos						
	R. Redonda[1]	**Fernandina[2]**	**Fernandina[2]**	**Fernandina**	**V. Ecuador[3]**	**V. Ecuador[3]**	**V. Ecuador[3]**	**V. Darwin[4]**	**Cerro Azul[5]**	**Floreana[6]**	**Floreana[6]**	**Floreana[4,7]**	**Floreana[4]**	**W. Santiago[8]**	**W. Santiago[8]**	**W. Santiago[8]**	**W. Santiago[4,7]**	**W. Santiago[4,7]**	**E. Santiago[8]**	**E. Santiago[8]**	**E. Santiago[8]**	**Santa Cruz[4,7]**	**Genovesa[4]**	**Genovesa**	**Pinta[4]**
	R9512	AHA D25A	AHA 32D	32D (repeat)	E95 10	E95-02	E97-134	E-64	G192-11A	FL03-20	FL03-106	E-110	FL-3	07DSG61	08DSG33	07DSG72	E-76	E-20	08DSG42	08DSG16	08DSG04	E-1	E-169	11SG01	P-24
Major elements (wt.%)																									
SiO2	46.17	47.64	47.79		47.41	47.71	47.84		47.53	47.47	47.77	45.79	46.87	46.81	46.59	46.97	45.80	47.16	47.00	46.62	46.25	46.14	48.65		48.06
TiO2	1.99	1.90	2.45		2.62	2.47	3.19		2.00	1.28	1.33	2.15	1.21	1.93	2.50	1.42	1.73	2.28	1.14	1.76	1.93	16.10	16.25		16.49
Al2O3	12.29	16.06	14.03		15.67	13.84	13.42		14.45	14.42	14.44	15.15	14.46	14.36	16.00	16.59	13.99	15.15	16.69	15.87	15.97	2.01	1.36		2.08
Fe2O3												6.96	7.17	12.40	13.37	11.68	1.64	1.40	11.15	12.50	13.24	9.07	7.57		3.91
FeO												3.90	2.12				9.14	10.48				2.26	3.03		6.45
FeO*	11.36	8.95	10.46		10.79	11.04	10.86		10.52	8.15	8.53														
MnO	0.18	0.15	0.12		0.18	0.18	0.10		0.17	0.17	0.18	0.17	0.18	0.17	0.18	0.18	0.17	0.16	0.17	0.19	0.19	0.19	0.18		0.17
MgO	17.44	11.09	11.5		9.36	12.29	10.74	9.44	10.66	12.85	12.91	11.07	12.79	10.73	9.37	9.83	14.34	9.89	10.37	9.19	10.09	10.43	8.09		7.15
CaO	7.58	11.57	10.54		10.13	10.05	9.81		11.37	11.04	10.70	9.52	10.68	10.55	9.58	11.65	10.12	9.47	11.62	10.49	10.15	9.19	12.01		12.01
Na2O	2.73	2.13	2.39		0.63	0.40	2.63		0.33	3.24	2.91	0.91	1.11	2.40	3.06	2.31	2.91	2.88	2.26	3.07	2.81	0.26	0.11		0.43
K2O	0.52	0.33	0.46		2.99	2.44	0.29		2.44	1.13	0.98	3.42	2.60	0.24	0.49	0.12	0.24	0.37	0.07	0.37	0.17	3.64	2.64		2.77
P2O5	0.29	0.19	0.27		0.34	0.25	0.21		0.20	0.24	0.25	0.36	0.81	0.19	0.34	0.12	0.15	0.27	0.09	0.33	0.18	0.24	0.10		0.31
LOI							1.17							-0.63	-0.71	-0.66			-0.54	-0.53	-0.78	0.48	0.01		0.19
Total	100.54	99.68	100.04		100.12	100.67	100.26		99.67	99.99	100.00	99.42	100.00	99.16	100.77	100.20	100.23	99.51	100.02	99.87	100.20	100.01	100.01		100.00
Trace elements (ppm)																									
Ba	**118.1**	**55.94**	**81.14**		**147.7**				**89.24**	**415**	**331**	316.0	620	44.32	100.0	17.19	37.4	56.5	17.61	74.07	31.95	47.3		24.46	
Be	**0.93**	**0.61**	**0.78**		**1.00**				**0.67**	**0.83**	**0.61**				1.99				0.65	1.15	1.05			0.47	
Co	**72.82**	**54.21**	**58.67**		**54.43**				**51.64**	**54.45**	**63.56**			63.04	58.04	55.12			61.36	55.62	56.99			47.19	
Cr	**625**	**485**	**705**		**322**				**514**	**733**	**1107**	484		695	303	338	684	441	409	405	335	311		199	
Cs	**0.09**	**0.05**	**0.07**		**0.13**				**0.08**	**0.24**	**0.14**			0.04	0.09	0.02			0.01	0.09	0.02			0.29	
Cu	**54.54**	**68.81**	**98.11**		**77.37**				**83.10**	**84.54**	**95.07**	60.9		107.0	77.85	126.9	47.4	68.2	77.85	93.47	81.92	76		115.59	
Ga	**15.81**	**17.79**	**18.84**		**20.19**				**17.59**	**13.38**	**12.09**			19.91	22.25	17.72			18.02	20.90	20.04			16.78	
Hf	**3.59**	**2.35**	**3.36**		**4.22**				**2.95**	**1.69**	**1.53**			3.31	4.66	2.15			1.59	5.10	2.93			2.48	
Mn	**1386**	**1120**	**1394**		**1443**				**1418**	**1378**	**1349**			1147	1577	1428			1546		1517			1537	
Nb	**19.56**	**12.22**	**17.16**		**23.17**				**16.58**	**22.24**	**20.27**	25.6		8.44	19.06	3.78	8.2	13.2	3.007	15.95	5.93	8.1		2.16	
Ni	**470**	**303**	**326**		**204**				**220**	**304**	**410**			261	202	191	510.0	204.0	207	215	215	211.4		58	
P	**1299**	**869**	**1197**		**1517**				**999**	**1114**	**991**			899	1826	661			532	179	849			1852	
Pb	**1.00**	**0.71**	**0.88**		**1.12**				**0.97**	**2.63**	**1.87**			1.04	1.08	0.45			0.29	1.42	0.75			1.53	
Rb	**10.49**	**4.93**	**7.36**		**13.34**				**7.86**	**29.56**	**20.82**	22.1	20	4.50	8.57	1.39	3.4	6.0	0.714	6.01	2.04	3.20		1.83	
Sc	**40.70**	**30.54**	**34.38**		**34.37**				**40.11**	**39.82**	**39.62**	27.2		36.30	37.09	41.30	26.1	25.3	38.55	33.19		30.3		70.99	
Sn	**1.36**	**0.85**	**1.25**		**1.73**				**1.28**	**0.61**	**0.56**			1.95		0.92				2.20				0.98	
Sr	**325**	**340**	**308**		**406**				**295**	**444**	**334**	483.60	505.0	612	359	238	286	473	182	310	271	431		352	
Ta	**1.20**	**0.83**	**1.14**		**1.46**				**1.01**	**1.20**	**1.11**			0.55	1.19	0.24			0.191	0.95	0.38			0.15	
Th	**1.35**	**0.72**	**1.05**		**1.59**				**1.08**	**1.51**	**1.44**			0.57	1.26	0.20			0.127	1.05	0.284			0.25	
U	**0.41**	**0.26**	**0.41**		**0.48**				**0.34**	**0.33**	**0.31**			0.20	0.38	0.07			0.04	0.37	0.092			0.44	
V	**222**	**261**	**351**		**307**				**323**	**291**	**260**	216		125	268	294			299	257	260	190		358	
Y	**23.02**	**17.81**	**24.52**		**28.49**				**23.38**	**18.30**	**18.26**	23.7		28.26	37.78	24.33	21.3	32.1	25.486	40.45	30.906	33.8		32.38	
Zn	**96.47**	**84.27**	**108.06**		**105.5**				**89.07**	**66.72**	**64.28**			100.5	112.3	82.50	90.2	102	81.04	104.1	97.05	76.4		87.32	
Zr	**157.3**	**98.52**	**139.71**		**187.6**				**122.4**	**68.17**	**59.32**	109.5		133.6	198.6	86.70	108.5	173.5	62.60	253.1	130.3	220		95.16	
La	**13.75**	**8.17**	**11.69**		**16.95**				**12.02**	**16.34**	**15.17**	16.8	14.9	7.98	15.63	3.97	7.2	11.4	3.19	14.87	6.55	9.79		3.50	
Ce	**31.36**	**19.74**	**28.82**		**38.35**				**27.73**	**28.31**	**25.68**	31.7	26.3	20.26	37.64	10.90	17.9	28.2	8.94	37.68	18.69	28.2		10.81	
Pr	**4.13**	**2.71**	**3.91**		**5.11**				**3.70**	**3.17**	**2.89**			3.05	5.09	1.82	2.6		1.42	5.05	2.91			1.85	
Nd	**18.85**	**12.50**	**18.10**		**23.18**				**16.84**	**12.57**	**11.24**	15.7	11.4	15.55	24.10	9.46	12.0	19.1	7.46	23.59	14.77	20.1		10.23	
Sm	**4.56**	**3.25**	**4.58**		**5.76**				**4.12**	**2.72**	**2.42**	3.63	2.49	4.55	6.15	2.87	3.3	5.2	2.41	6.29	4.17	5.17		3.44	
Eu	**1.61**	**1.21**	**1.61**		**1.97**				**1.45**	**0.97**	**0.89**			1.52	2.13	1.10	1.2	1.8	0.93	2.14	1.55			1.34	
Gd	**4.77**	**3.50**	**5.03**		**6.05**				**4.55**	**3.16**	**3.05**			5.20	6.80	3.70	4.0	6.1	3.30	6.96	5.03			4.76	
Tb	**0.74**	**0.56**	**0.78**		**0.94**				**0.75**	**0.52**	**0.49**			0.86	1.08	0.63	0.7		0.58	1.13	0.83			0.83	
Dy	**4.37**	**3.32**	**4.72**		**5.46**				**4.35**	**3.33**	**3.09**			5.00	6.41	4.00	4.0	5.8	3.80	7.01	5.13			5.54	
Ho	**0.84**	**0.65**	**0.90**		**1.05**				**0.88**	**0.71**	**0.66**			0.99	1.30	0.85	0.8		0.85	1.41	1.08			1.21	
Er	**2.26**	**1.77**	**2.41**		**2.81**				**2.40**	**1.99**	**1.86**			2.59	3.53	2.33	2.1	3.1	2.49	4.04	3.00			3.46	
Tm	**0.32**	**0.24**	**0.33**		**0.41**				**0.34**	**0.30**	**0.28**			0.36	0.51	0.35	0.3		0.38	0.59	0.44			0.51	
Yb	**1.91**	**1.48**	**2.04**		**2.35**				**2.08**	**1.81**	**1.71**	2.22	1.79	2.20	3.17	2.17	1.8	2.7	2.46	3.76	2.80	2.85		3.20	
Lu	**0.28**	**0.22**	**0.29**		**0.35**				**0.30**	**0.28**	**0.27**			0.32	0.48	0.32	0.3	0.4	0.38	0.56	0.42			0.48	
$^{87}Sr/^{86}Sr$	0.703217	**0.703249**	**0.703218**			0.703271	0.703050		0.703302	0.703485	**0.703447**	0.703600	0.703660	0.703009		0.702819	0.702860	0.702940	0.702926	0.702864	0.702752	0.702630	0.702720		0.703130
$^{143}Nd/^{144}Nd$	0.512951	**0.512929**	**0.512933**			0.512934	0.512956		0.512953	0.512951	**0.513001**	0.512975	0.512905	0.513019		0.513057	0.513002	0.512980	0.513040	0.513057	0.513073	0.513077	0.513127		0.512943
$^{206}Pb/^{204}Pb$	**19.336**	**19.055**	**19.065**			19.289	19.209		19.377	20.061	**19.886**	19.785	20.002	18.981	**19.129**	18.690	19.050	19.022	18.718	18.749	18.594	18.514	18.387		
$^{207}Pb/^{204}Pb$	**15.612**	**15.556**	**15.563**			15.601	15.592		15.561	15.658	**15.648**	15.636	15.657	15.582	**15.588**	18.690	15.580	15.582	15.535	15.546	15.535	15.52	15.511		
$^{208}Pb/^{204}Pb$	**39.076**	**38.706**	**38.726**			39.037	38.888		38.993	39.782	**39.604**	39.516	39.739	38.632	**38.785**	38.263	38.656	38.726	38.275	38.329	38.175	38.048	37.941		
Re (ppt)	**84.3**	**457**	**910**	**709**	**265**				**478**	**284**	**253**			**314**	**150**	**498**			**277**	**157**	**327**				
Os (ppt)	**32.2**	**69.4**	**149**	**142**	**31.6**	**109**	**83.8**	**552**	**36.5**	**87.7**	**109**	**86.1**		**73.6**	**50.6**	**52.5**	**227**	**59.2**	**15.7**	**34.2**	**49.9**	**21.2**	**21.3**		**46.0**
$^{187}Os/^{188}Os$	**0.13037**	**0.13412**	**0.13291**	**0.13249**	**0.13441**	**0.15393**	**0.15340**	**0.13803**	**0.13918**	**0.14109**	**0.13014**	**0.13853**	**0.1347095**	**0.14157**	**0.15951**	**0.15538**	**0.16144**	**0.15322**	**0.16321**	**0.14707**	**0.15453**	**0.18303**	**0.18751**		**0.17318**
2σ	**0.00051**	**0.00014**	**0.00007**	**0.00011**	**0.00023**	**0.00051**	**0.00029**	**0.00018**	**0.00020**	**0.00009**	**0.00013**	**0.00025**	**0.00045**	**0.00012**	**0.00020**	**0.00016**	**0.00036**	**0.00032**	**0.00044**	**0.00023**	**0.00016**	**0.00047**	**0.00078**		**0.00035**
γOs	**0.60**	**3.49**	**2.55**	**2.23**	**3.71**	**18.8**	**18.4**	**6.50**	**7.39**	**8.87**	**0.42**	**6.89**	**3.94**	**9.23**	**23.1**	**19.9**	**24.6**	**18.2**	**25.9**	**13.5**	**19.2**	**41.2**	**44.7**		**33.6**

Analyses in bold are from this work

Additional data are from: [1]Standish et al. (1998); [2]Geist et al (2006); [3]Geist et al (2008); [4]White et al. (1993); [5]Kurz & Geist (1999); [6]Harpp et al. (2014); [7]Fitton et al. (2007); [8]Gibson et al. (2012)

$^{87}Sr/^{86}Sr$ data are renormalised using deviation of measured value for NBS 987 Sr standard (0.710757, 17 ppm uncertainty) from accepted value of 0.710240.

$^{143}Nd/^{144}Nd$ data are renormalised using deviation of measured value for Johnson & Matthey Nd standard (0.511097, 27 ppm uncertainty) from accepted value of 0.511110.

Following the method outlined in Gibson et al. (2012), Pb isotope ratios were adjusted for mass fractionation effects using a thallium doping method: The $^{205}Tl/^{203}Tl$ ratio used for mass fractionation correction was determined by minimising the offsets of all measured Pb isotope ratios for the standard NBS 981, relative to the accepted values. The $^{205}Tl/^{203}Tl$ ratio used was 2.38852. Resulting ratios for the NBS 981 Pb standard were are follows (with uncertainties and accepted values in brackets): $^{206}Pb/^{204}Pb$ = 16.9415 (117 ppm; 16.9405), $^{207}Pb/^{204}Pb$ = 15.4995 (93 ppm; 15.4963), $^{208}Pb/^{204}Pb$ = 36.7196 (121 ppm; 36.7219). NBS 981 accepted values from Galer et al. (1997).

Because of the relatively young age of basalts from western Galápagos (<1 Ma) and imprecise but young ages (<4 Ma) for basalts from the rest of the archipelago [*Simkin and Siebert* , 1994; *Geist et al.* , 2014a] we have not corrected measured $^{187}Os/^{188}Os$ for in-growth of ^{187}Os. This does not significantly affect our findings as the correction for in-growth of ^{187}Os to a 4 Ma sample with a Re/Os of ~18 (17 ppt Os and 300 ppt Re) and $^{187}Os/^{188}Os$ of 0.15 would involve a reduction in $^{187}Os/^{188}Os$ by only ~0.006.

Supplementary Figures

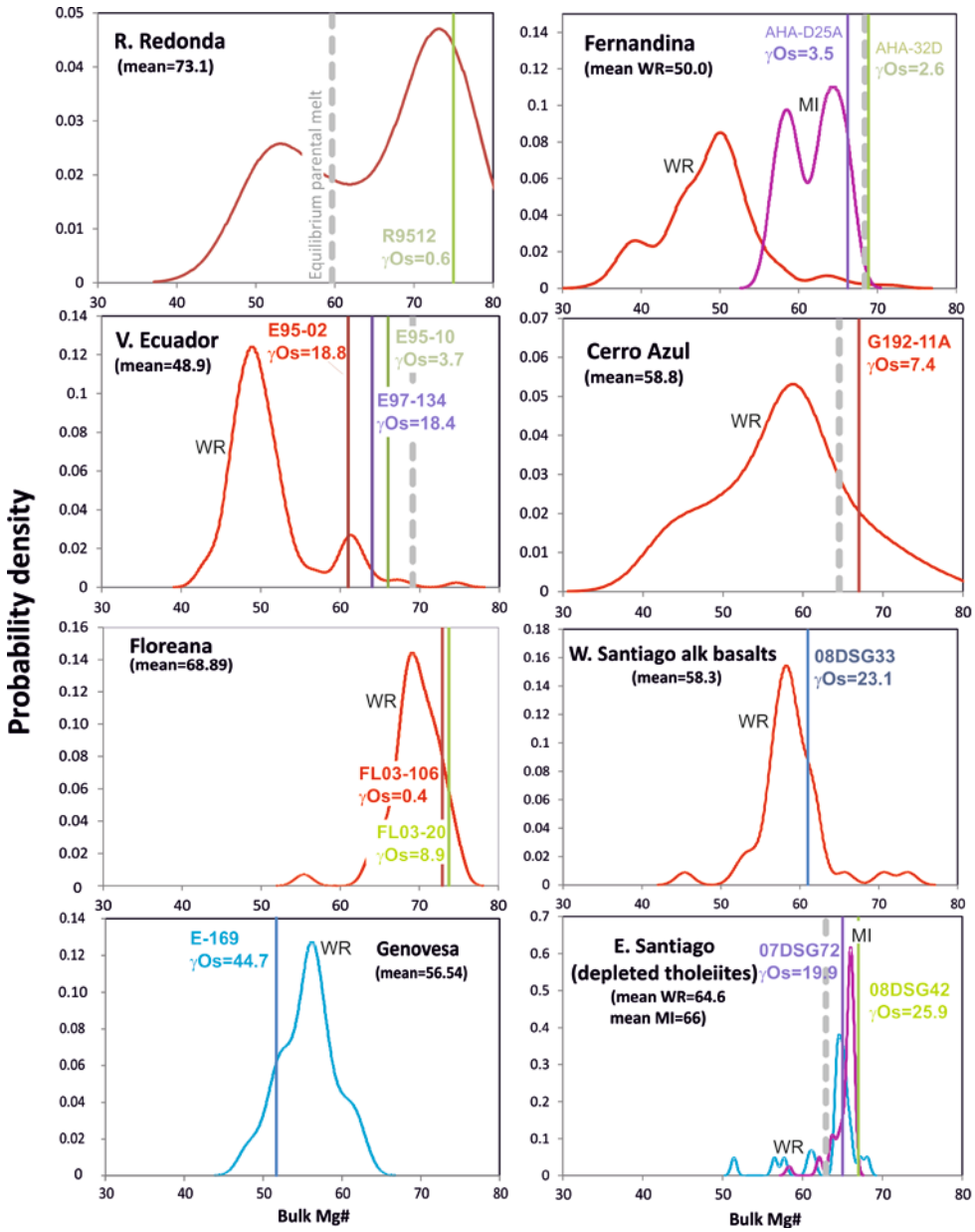

Figure S1. Kernel density probability plots of bulk-rock Mg# in Galápagos basalts. The Mg# of samples analysed in this study are shown as single solid lines. Olivine-hosted melt inclusion (MI) data are available for Fernandina and eastern Santiago (depleted tholeiites) and are shown for comparison. Equilibrium parental melt compositions based on Fo contents of olivines in analysed samples and $K_{D(Fe\text{-}Mg)}$=0.3 are illustrated by dashed lines. The regional variation in Mg# is consistent with the observation of McBirney & Williams [1969] that lavas in central and northeastern parts of the Archipelago are more evolved than those erupted in the south and west. Data are from: Geist et al. [2002]; Geist et al. [2006]; Gibson & Geist [2010]; Gibson et al. [2012]; Harpp et al. [2014a]; Harpp et al. [2014b]; Naumann et al. [2002]; Saal et al. [2007]; Standish et al. [1998]; White et al. [1993].

(a)

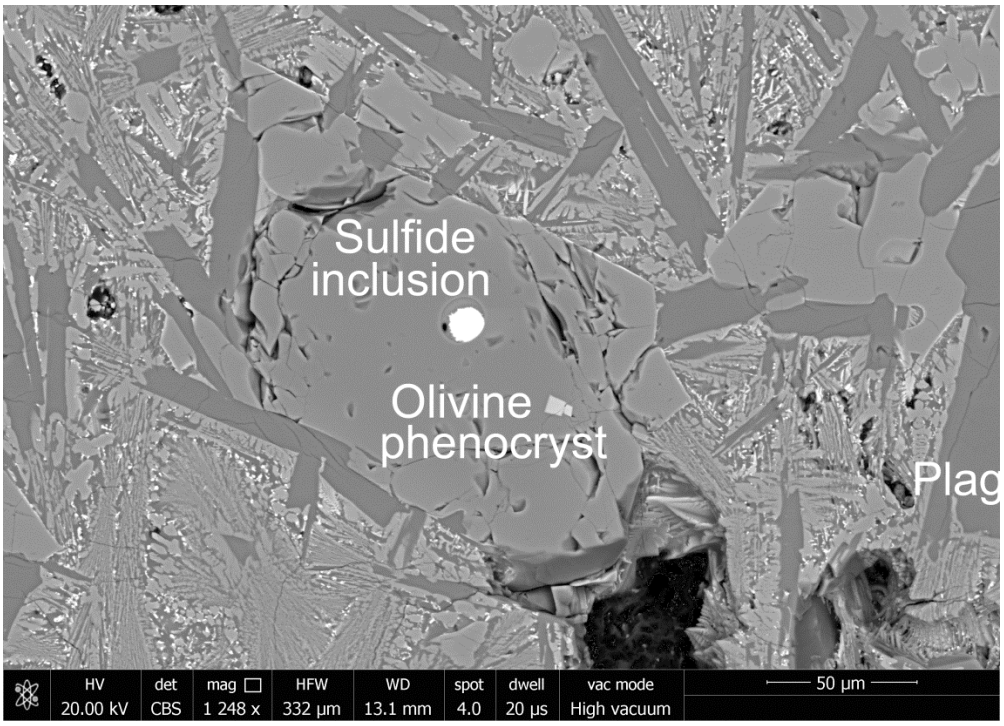

(b)

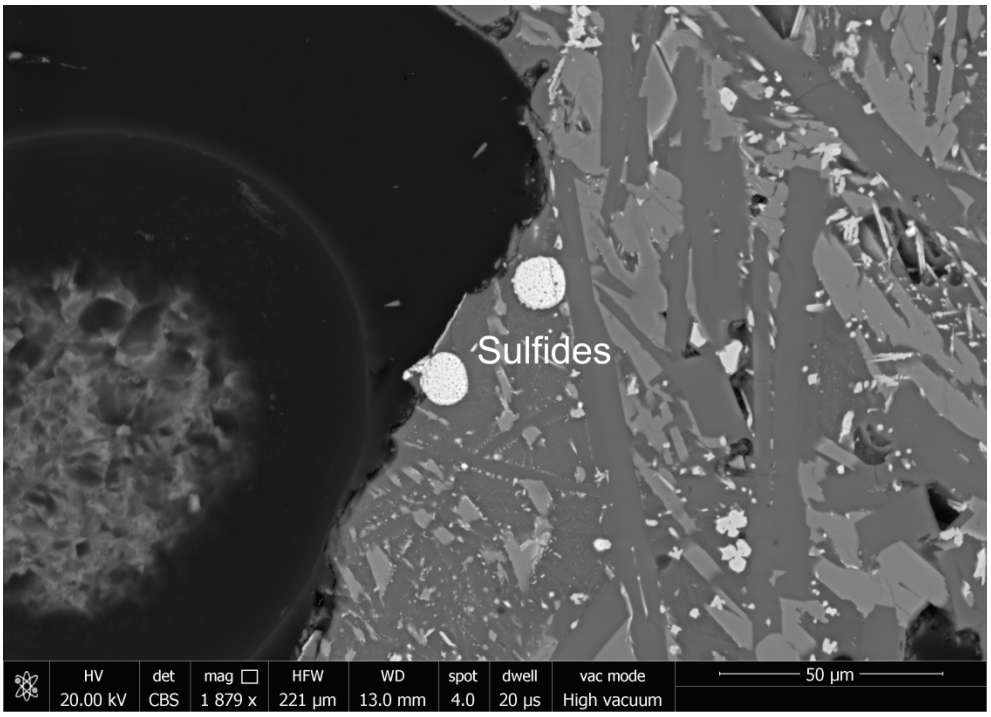

Figure S2. BSE images showing the nature and occurrence of sulfides in Galápagos basalts. Image (a) is of an olivine-hosted, sulfide inclusion in a basalt from Cerro Azul (Isabela; GI 92_11A) and (b) is a sulfide bleb surrounded by glass found in a Fernandina sub-marine basalt (AHA32D).

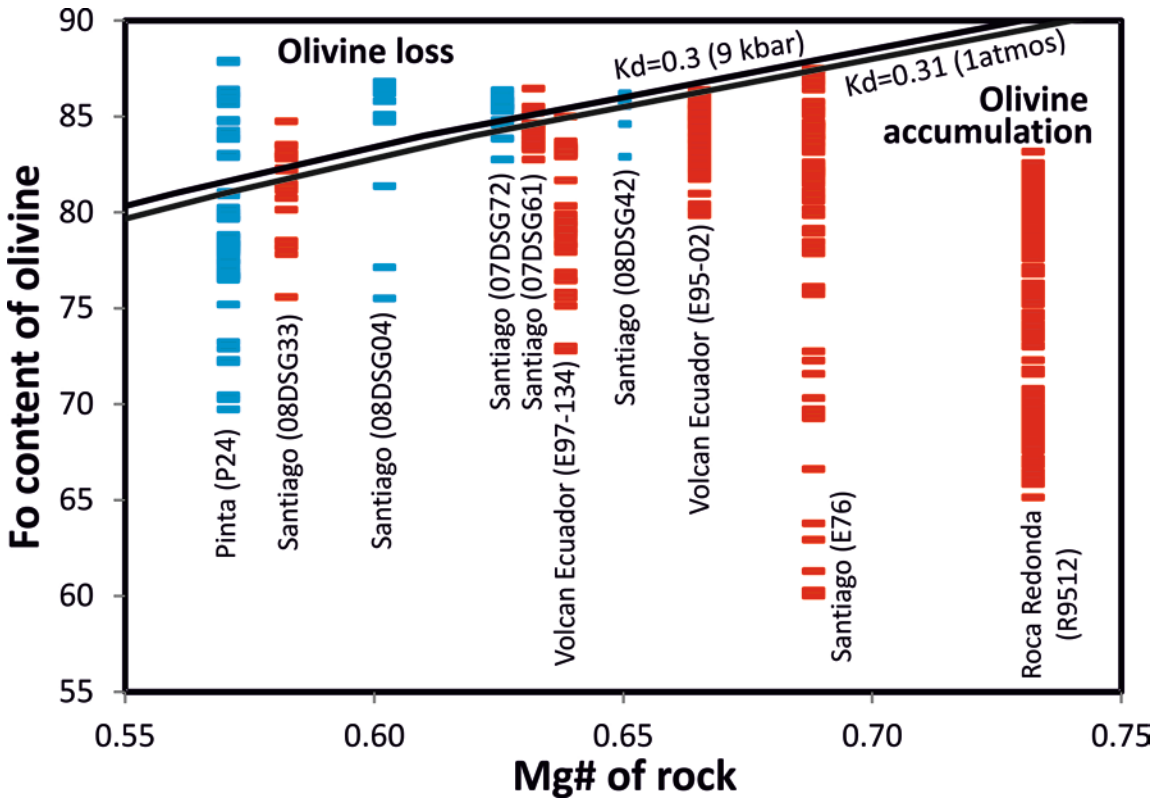

Figure S3. Bulk-rock Mg# [(Mg/(Mg+Fe)] versus forsterite (Fo) content of olivine in samples used in this study. Samples with blue and red dashes are from eastern and western Galápagos, respectively. Equilibrium curves are shown for crystallisation at 9 kbar and 1 atmosphere where $K_{D(Fe\text{-}Mg)}$=0.3 and 0.31, respectively [*Ulmer*, 1989]. Electron microprobe data are from this work (Supplementary Table 2) and Vidito *et al.* [2013]. Samples that plot to the right of the curves have experienced olivine accumulation. This is consistent with petrographic observations.

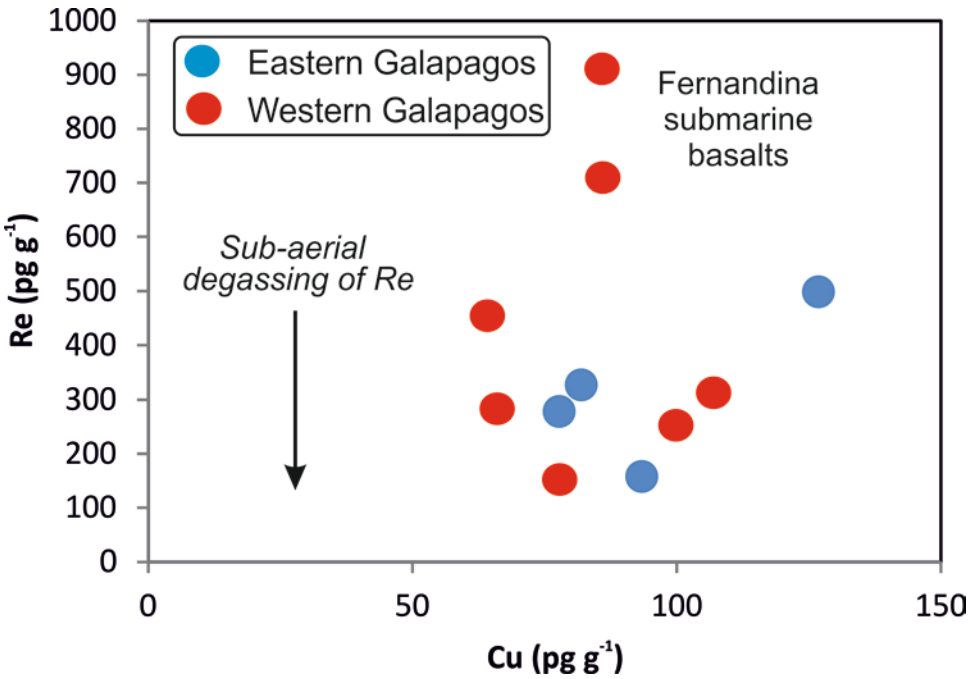

Figure S4. Variation in Cu and Re in Galápagos basalts. Cu has similar compatibility to Re in fractionating basaltic magmas [*Peach et al.*, 1990]. The scatter in Re is interpreted as a consequence of loss during sub-aerial degassing. Data are from Table 1.

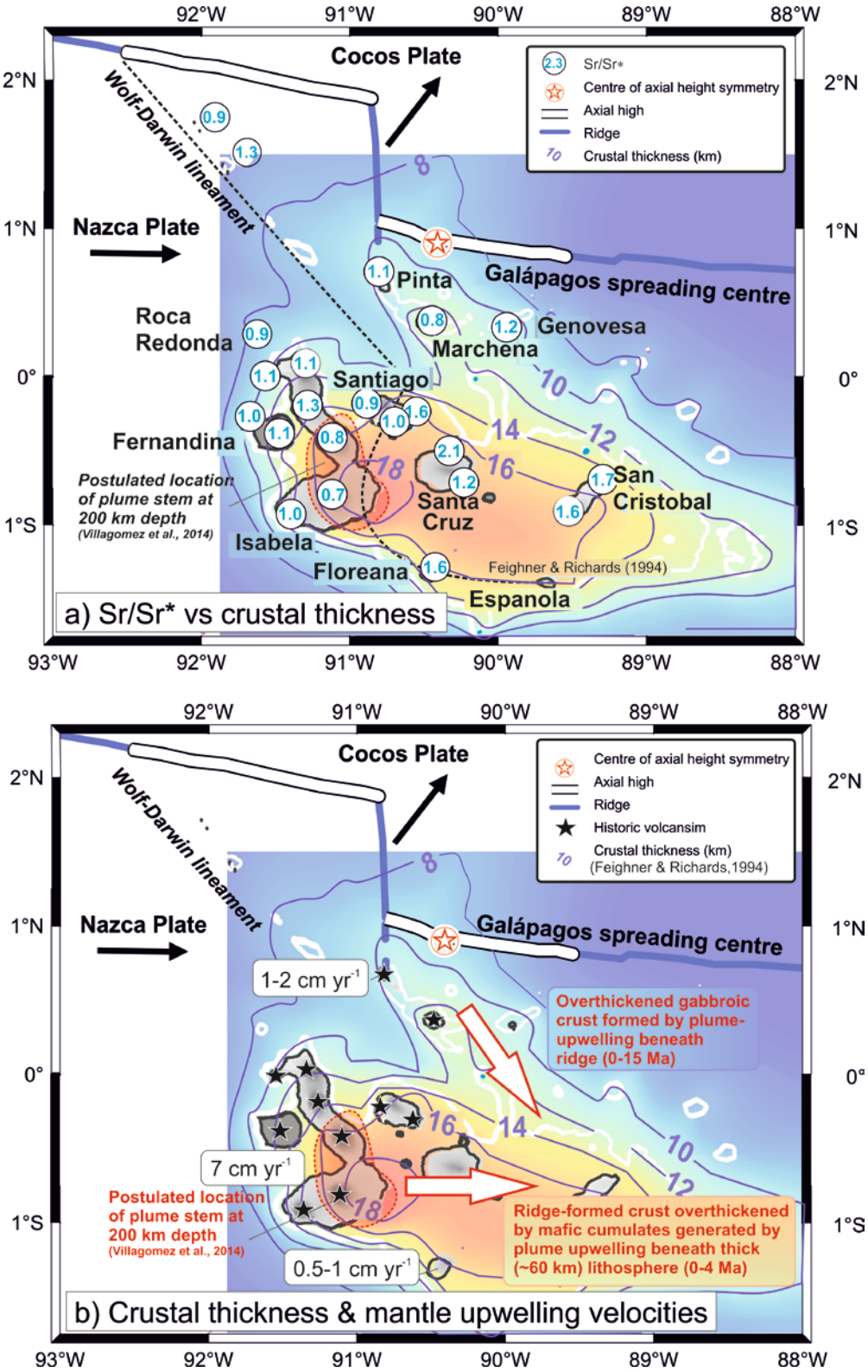

Figure S5. Comparison of regional variations of a) Sr/Sr* in Galápagos basalts and b) upwelling rates and crustal lithology with thickness of the Galápagos crust. Dashed black line shows the boundary between thick strong lithosphere in the west and thin, weak lithosphere in the east of Galápagos [*Feighner and Richards*, 1994]. The 1000m bathymetric contour (thick white line) illustrates the location of the Galápagos platform [*Smith and Sandwell*, 1997]. Data are from: this work; Gibson *et al.* [2010; 2012]; Harpp *et al.* [2014b] and Saal *et al.* [2007].

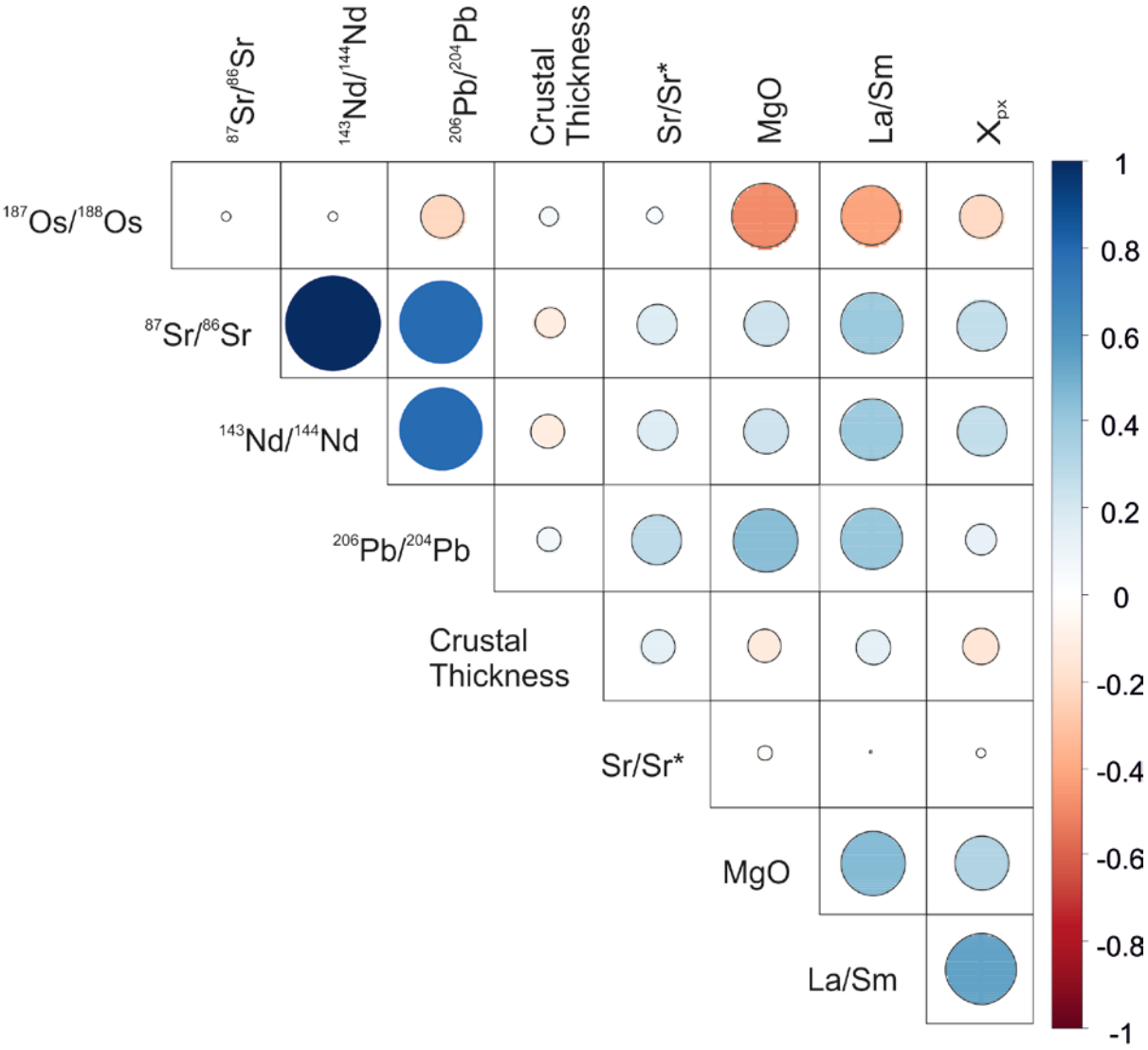

Figure S6. Correlation matrix showing relationships between $^{187}Os/^{188}Os$, Sr-, Nd and Pb-isotopic ratios, crustal thickness, Sr/Sr*, MgO, La/Sm, and proportion of pyroxenite in the source (X_{px}) of Galápagos basalts. The latter are estimated from olivine compositions [*Gurenko et al.*, 2009]. Circle radius is proportional to the strength of the linear correlation (circle diameter increases with linear correlation) and the colour scale shows Pearson's product moment coefficients. Data are from: This work; Feighner & Richards [1994]; Harpp & White [2001, p.200]; Saal *et al.* [2007]; Gibson *et al.* [2012]; Vidito *et al.* [2013].

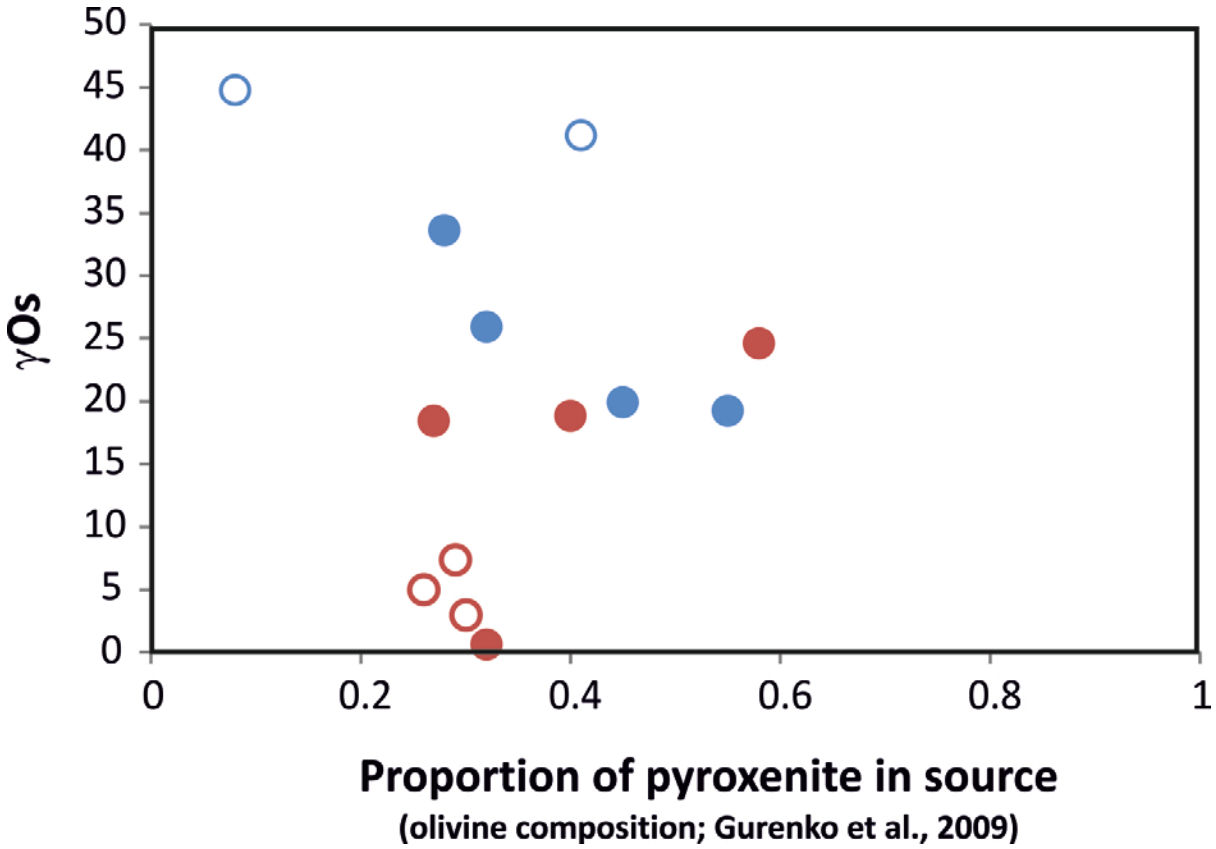

Figure S7. Variation in proportion of pyroxenite in the source of Galapagos magmas based on olivine chemistry (Gurenko et al., 2009) versus γOs value for the same sample (this work). Closed symbols are for samples with >50 pg g^{-1} Os and open symbols for samples with <50 pg g^{-1} Os.

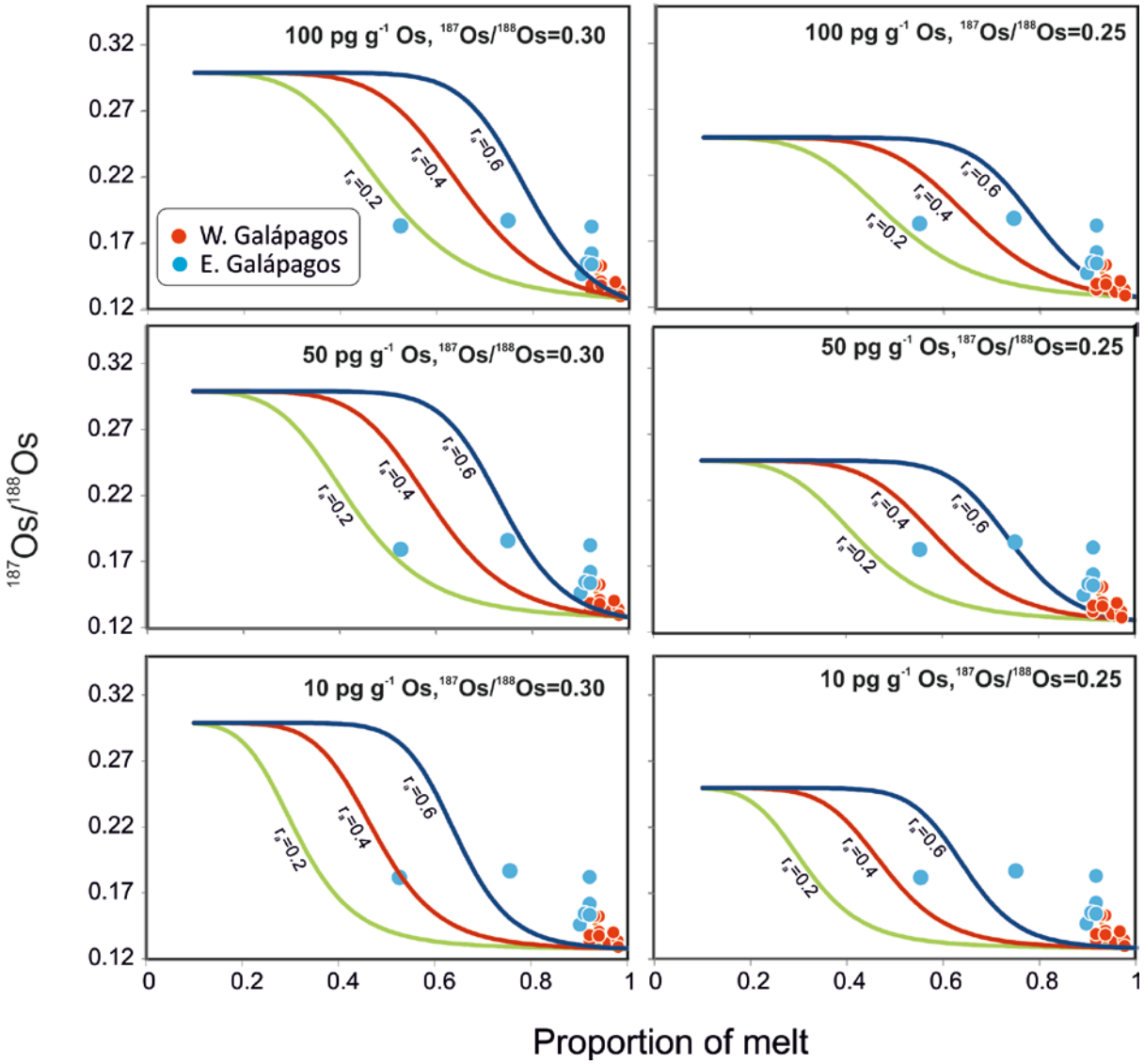

Figure S8. Simulations of assimilation during fractional crystallisation using hypothetical end members and variable rates of assimilation and crystallisation (r_a). Amounts of fractional crystallisation of Galápagos samples are calculated from Ni contents. The $^{187}Os/^{188}Os$ and Os content of the crust was varied between 0.25 to 0.3 and 10 to 100 pg g^{-1}, respectively. The primitive Galápagos melt was assumed to have an $^{187}Os/^{188}Os$ of 0.129 and Os content of 200 pg g^{-1}. Data are from Table 1.

Data sources for Figures 2 to 9

Figure 2. Data sources: Canary Islands [*Day et al.*, 2010]; Grand Comores [*Class and Goldstein*, 1997; *Class et al.*, 2009]; Hawaii [*Crocket*, 2000; *Jamais et al.*, 2008; *Ireland et al.*, 2009]; Iceland [*Skovgaard et al.*, 2001]; MORB [*Gannoun et al.*, 2007] and Samoa [*Jackson and Shirey*, 2011].

Figure 3. Data sources: Bennett et al. [1996]; Class et al. [2009]; Day et al. [2009, 2010]; Eisele et al. [2002]; Hannan & Graham [1996]; Harpp & White [2001]; Hauri & Hart [1993]; Ireland [2009]; Jackson et al. [2007]; Jamais et al. [2008]; Lassiter & Hauri [1998]; Lassiter et al. [2000]; Peucker-Ehrenbrink *et al.* [2003, 2012]; Skovgaard et al. [2001] and Widom et al. [1999].

Figure 4: Data sources are the same as Figure 3 and Rocha Júnior et al. [2012].

Figure 5. Bach et al. [2003]; Fitton [2007]; Gurenko & Chaussidon [1995]; Sobolev et al. [2000]; Koleszar et al. [2009]; Gibson [2010]; Peucker-Ehrenbrink et al. [2012]; White et al. [1993]. Normalisation factors are from McDonough and Sun [1995].

Figur 8. Data are from sources given in Figures 3 & 4; Bizimis et al. [2007]; Blusztajn et al. [2000]; Brandon et al. [2007]; Dale et al. [2007]; Debaille et al. [2009]; Gaffney et al. [2004]; Gannoun et al. [2007]; Jackson and Shirey [2011]; Lassiter et al. [2003]; Marchesi et al. [2014]; Meisel et al. [2001]; Reisberg et al. [1993]; Schaefer et al. [2002].

Figure 9. Data sources for ages of oceanic crust: Watts & Cochran [1974], Calmant *et al.* [1990], McNutt *et al.* [1997], Class *et al.* [1998] & Watts [1994]. Buoyancy flux data are from Sleep [1990].

References

Bach, W., B. Peucker-Ehrenbrink, S. R. Hart, and J. S. Blusztajn (2003), Geochemistry of hydrothermally altered oceanic crust: DSDP/ODP Hole 504B – Implications for seawater-crust exchange budgets and Sr- and Pb-isotopic evolution of the mantle, *Geochem. Geophys. Geosystems*, *4*(3), 8904, doi:10.1029/2002GC000419.

Bennett, V. C., T. M. Esat, and M. D. Norman (1996), Two mantle-plume components in Hawaiian picrites inferred from correlated Os–Pb isotopes, *Nature*, *381*(6579), 221–224, doi:10.1038/381221a0.

Bizimis, M., M. Griselin, J. C. Lassiter, V. J. M. Salters, and G. Sen (2007), Ancient recycled mantle lithosphere in the Hawaiian plume: Osmium–Hafnium isotopic evidence from peridotite mantle xenoliths, *Earth Planet. Sci. Lett.*, *257*(1–2), 259–273, doi:10.1016/j.epsl.2007.02.036.

Blusztajn, J., S. R. Hart, G. Ravizza, and H. J. B. Dick (2000), Platinum-group elements and Os isotopic characteristics of the lower oceanic crust, *Chem. Geol.*, *168*(1–2), 113–122, doi:10.1016/S0009-2541(00)00186-8.

Brandon, A. D., D. W. Graham, T. Waight, and B. Gautason (2007), 186Os and 187Os enrichments and high-3He/4He sources in the Earth's mantle: Evidence from Icelandic picrites, *Geochim. Cosmochim. Acta*, *71*(18), 4570–4591, doi:10.1016/j.gca.2007.07.015.

Calmant, S., J. Francheteau, and A. Cazenave (1990), Elastic layer thickening with age of the oceanic lithosphere: A tool for prediction of the age of volcanoes or oceanic crust, *Geophys. J. Int.*, *100*(1), 59–67, doi:10.1111/j.1365-246.

Class, C., and S. L. Goldstein (1997), Plume-lithosphere interactions in the ocean basins: constraints from the source mineralogy, *Earth Planet. Sci. Lett.*, *150*(3–4), 245–260, doi:10.1016/S0012-821X(97)00089-7.

Class, C., S. L. Goldstein, R. Altherr, and P. Bachelery (1998), The process of plume-lithosphere interactions in the ocean basins--the case of Grande Comore, *J. Petrol.*, *39*(5), 881–903, doi:10.1093/petroj/39.5.881.

Class, C., S. L. Goldstein, and S. B. Shirey (2009), Osmium isotopes in Grande Comore lavas: A new extreme among a spectrum of EM-type mantle endmembers, *Earth Planet. Sci. Lett.*, *284*(1–2), 219–227, doi:10.1016/j.epsl.2009.04.031.

Crocket, J. H. (2000), PGE in fresh basalt, hydrothermal alteration products, and volcanic incrustations of Kilauea volcano, Hawaii, *Geochim. Cosmochim. Acta*, *64*(10), 1791–1807, doi:10.1016/S0016-7037(00)00340-9.

Dale, C. W., A. Gannoun, K. W. Burton, T. W. Argles, and I. J. Parkinson (2007), Rhenium–osmium isotope and elemental behaviour during subduction of oceanic crust and the implications for mantle recycling, *Earth Planet. Sci. Lett.*, *253*(1–2), 211–225, doi:10.1016/j.epsl.2006.10.029.

Day, J. M. D., D. G. Pearson, C. G. Macpherson, D. Lowry, and J.-C. Carracedo (2009), Pyroxenite-rich mantle formed by recycled oceanic lithosphere: Oxygen-osmium isotope evidence from Canary Island lavas, *Geology*, *37*(6), 555–558.

Day, J. M. D., D. G. Pearson, C. G. Macpherson, D. Lowry, and J. C. Carracedo (2010), Evidence for distinct proportions of subducted oceanic crust and lithosphere in HIMU-type mantle beneath El Hierro and La Palma, Canary Islands, *Geochim. Cosmochim. Acta*, *74*(22), 6565–6589, doi:10.1016/j.gca.2010.08.021.

Debaille, V., R. G. Trønnes, A. D. Brandon, T. E. Waight, D. W. Graham, and C.-T. A. Lee (2009), Primitive off-rift basalts from Iceland and Jan Mayen: Os-isotopic evidence for a mantle source containing enriched subcontinental lithosphere, *Geochim. Cosmochim. Acta*, *73*(11), 3423–3449, doi:10.1016/j.gca.2009.03.002.

Eisele, J., M. Sharma, S. J. G. Galer, J. Blichert-Toft, C. W. Devey, and A. W. Hofmann (2002), The role of sediment recycling in EM-1 inferred from Os, Pb, Hf, Nd, Sr isotope and trace element systematics of the Pitcairn hotspot, *Earth Planet. Sci. Lett.*, *196*(3–4), 197–212, doi:10.1016/S0012-821X(01)00601-X.

Fitton, J. G. (2007), The OIB Paradox, *Geol. Soc. Am. Spec. Publ.*, *430*, 387–412.

Gaffney, A. M., B. K. Nelson, and J. Blichert-Toft (2004), Geochemical constraints on the role of oceanic lithosphere in intra-volcano heterogeneity at West Maui, Hawaii, *J. Petrol.*, *45*(8), 1663–1687, doi:10.1093/petrology/egh029.

Gannoun, A., K. W. Burton, I. J. Parkinson, O. Alard, P. Schiano, and L. E. Thomas (2007), The scale and origin of the osmium isotope variations in mid-ocean ridge basalts, *Earth Planet. Sci. Lett.*, *259*(3-4), 541–556, doi:10.1016/j.epsl.2007.05.014.

Gibson, S. A. (2010), Darwin the geologist in Galápagos: An early insight into sub-volcanic magmatic processes, *Proc. Californian Acad. Sci.*, *61*, 69–88.

Gurenko, A. A., and M. Chaussidon (1995), Enriched and depleted primitive melts included in olivine from Icelandic tholeiites: origin by continuous melting of a single mantle column, *Geochim. Cosmochim. Acta*, *59*(14), 2905–2917, doi:10.1016/0016-7037(95)00184-0.

Hanan, B. B., and D. W. Graham (1996), Lead and helium isotope evidence from oceanic basalts for a common deep source of mantle plumes, *Science*, *272*(5264), 991–995, doi:10.1126/science.272.5264.991.

Harpp, K. S., and W. M. White (2001), Tracing a mantle plume: isotopic and trace element variations of Galápagos seamounts, *Geochem. Geophys. Geosystems*, *2*, doi:10.1029/2000GC000137.

Hauri, E. H., and S. R. Hart (1993), ReOs isotope systematics of HIMU and EMII oceanic island basalts from the south Pacific Ocean, *Earth Planet. Sci. Lett.*, *114*(2–3), 353–371, doi:10.1016/0012-821X(93)90036-9.

Ireland, T. J., R. J. Walker, and M. O. Garcia (2009), Highly siderophile element and 187Os isotope systematics of Hawaiian picrites: Implications for parental melt composition and source heterogeneity, *Chem. Geol.*, *260*(1–2), 112–128, doi:10.1016/j.chemgeo.2008.12.009.

Jackson, M. G., and S. B. Shirey (2011), Re–Os isotope systematics in Samoan shield lavas and the use of Os-isotopes in olivine phenocrysts to determine primary magmatic compositions, *Earth Planet. Sci. Lett.*, *312*(1–2), 91–101, doi:10.1016/j.epsl.2011.09.046.

Jackson, M. G., S. R. Hart, A. A. P. Koppers, H. Staudigel, J. Konter, J. Blusztajn, M. D. Kurz, and J. A. Russell (2007), The return of subducted continental crust in Samoan lavas, *Nature*, *448*, 684–687, doi:10.1038/nature06048.

Jamais, M., J. C. Lassiter, and G. Brügmann (2008), PGE and Os-isotopic variations in lavas from Kohala Volcano, Hawaii: Constraints on PGE behavior and melt/crust interaction, *Chem. Geol.*, *250*(1–4), 16–28, doi:10.1016/j.chemgeo.2008.01.028.

Koleszar, A. M., A. E. Saal, E. H. Hauri, A. N. Nagle, Y. Liang, and M. D. Kurz (2009), The volatile contents of the Galápagos plume; evidence for H2O and F open system behavior in melt inclusions, *Earth Planet. Sci. Lett.*, *287*(3-4), 442–452.

Lassiter, J. C., and E. H. Hauri (1998), Osmium-isotope variations in Hawaiian lavas: evidence for recycled oceanic lithosphere in the Hawaiian plume, *Earth Planet. Sci. Lett.*, *164*(3-4), 483–496, doi:10.1016/S0012-821X(98)00240-4.

Lassiter, J. C., E. H. Hauri, P. W. Reiners, and M. O. Garcia (2000), Generation of Hawaiian post-erosional lavas by melting of a mixed lherzolite/pyroxenite source, *Earth Planet. Sci. Lett.*, *178*(3-4), 269–284, doi:10.1016/S0012-821X(00)00084-4.

Lassiter, J. C., J. Blichert-Toft, E. H. Hauri, and H. G. Barsczus (2003), Isotope and trace element variations in lavas from Raivavae and Rapa, Cook–Austral islands: constraints on the nature of HIMU- and EM-mantle and the origin of mid-plate volcanism in French Polynesia, *Chem. Geol.*, *202*(1-2), 115–138, doi:10.1016/j.chemgeo.2003.08.002.

Marchesi, C., C. W. Dale, C. J. Garrido, D. G. Pearson, D. Bosch, J.-L. Bodinier, F. Gervilla, and K. Hidas (2014), Fractionation of highly siderophile elements in refertilized mantle: Implications for the Os isotope composition of basalts, *Earth Planet. Sci. Lett.*, *400*, 33–44, doi:10.1016/j.epsl.2014.05.025.

McNutt, M. K., D. W. Caress, J. Reynolds, K. A. Jordahl, and R. A. Duncan (1997), Failure of plume theory to explain midplate volcanism in the southern Austral islands, *Nature*, *389*(6650), 479–482, doi:10.1038/39013.

Meisel, T., R. J. Walker, A. J. Irving, and J.-P. Lorand (2001), Osmium isotopic compositions of mantle xenoliths: a global perspective, *Geochim. Cosmochim. Acta*, *65*(8), 1311–1323, doi:10.1016/S0016-7037(00)00566-4.

Peucker-Ehrenbrink, B., W. Bach, S. R. Hart, J. S. Blusztajn, and T. Abbruzzese (2003), Rhenium-osmium isotope systematics and platinum group element concentrations in oceanic crust from DSDP/ODP Sites 504 and 417/418, *Geochem. Geophys. Geosystems*, *4*(7), n/a–n/a, doi:10.1029/2002GC000414.

Peucker-Ehrenbrink, B., K. Hanghoj, T. Atwood, and P. B. Kelemen (2012), Rhenium-osmium isotope systematics and platinum group element concentrations in oceanic crust, *Geology*, *40*(3), 199–202, doi:10.1130/G32431.1.

Reisberg, L., A. Zindler, F. Marcantonio, W. White, D. Wyman, and B. Weaver (1993), Os isotope systematics in ocean island basalts, *Earth Planet. Sci. Lett.*, *120*(3–4), 149–167, doi:10.1016/0012-821X(93)90236-3.

Rocha-Júnior, E. R. V., I. S. Puchtel, L. S. Marques, R. J. Walker, F. B. Machado, A. J. R. Nardy, M. Babinski, and A. M. G. Figueiredo (2012), Re–Os isotope and highly siderophile element systematics of the Paraná continental flood basalts (Brazil), *Earth Planet. Sci. Lett.*, *337–338*, 164–173, doi:10.1016/j.epsl.2012.04.050.

Schaefer, B. F., S. Turner, I. Parkinson, N. Rogers, and C. Hawkesworth (2002), Evidence for recycled Archaean oceanic mantle lithosphere in the Azores plume, *Nature*, *420*(6913), 304–307, doi:10.1038/nature01172.

Skovgaard, A. C., M. Storey, J. Baker, J. Blusztajn, and S. R. Hart (2001), Osmium–oxygen isotopic evidence for a recycled and strongly depleted component in the Iceland

mantle plume, *Earth Planet. Sci. Lett.*, *194*(1–2), 259–275, doi:10.1016/S0012-821X(01)00549-0.

Watts, A. B. (1994), Crustal structure, gravity anomalies and flexure of the lithosphere in the vicinity of the Canary Islands, *Geophys. J. Int.*, *119*(2), 648–666, doi:10.1111/j.1365-246X.1994.tb00147.x.

Watts, A. B., and J. R. Cochran (1974), Gravity anomalies and flexure of the lithosphere along the Hawaiian-Emperor seamount chain, *Geophys. J. R. Astron. Soc.*, *38*(1), 119–141, doi:10.1111/j.1365-246X.1974.tb04112.x.

White, W. M., A. R. McBirney, and R. A. Duncan (1993), Petrology and geochemistry of the Galápagos Islands - Portrait of a pathological mantle plume, *J. Geophys. Res.-Solid Earth*, *98*(B11), 19533–19563.

Widom, E., K. A. Hoernle, S. B. Shirey, and H.-U. Schmincke (1999), Os isotope systematics in the Canary Islands and Madeira: Lithospheric contamination and mantle plume signatures, *J. Petrol.*, *40*(2), 279–296, doi:10.1093/petroj/40.2.279.

Analytical Techniques

1.1 Electron Microprobe Analysis

Olivine, orthopyroxene, clinopyroxene, garnet, spinel and phlogopite were analysed for major and some trace elements using a Cameca SX 100 electron microprobe equipped with five wavelength-dispersive spectrometers and one energy-dispersive spectrometer in the Department of Earth Sciences at the University of Cambridge. All samples were analysed at 15kV and currents of 10nA and 100nA were employed for major and trace elements, respectively. The count time was 30 seconds and the beam diameter was 1μm.

Electron microprobe detection limits for olivine

Element	Xray Peak	Crystal	Peak Time (s)	Background time (s)	Background offset1	Background offset 2	Slope/background	Calibration	Detection Limit (max) ppm	Detection Limit (max) wt%oxide
Major:										
Na	Na Kα1	LATP	20	10	-600	400		Jadite	215	0.058
Mg	Mg Kα1	TAP	20	10	-550	350		Periclase	705	0.118
Si	Si Kα1	TAP	20	10	-500	300		Diopside	510	0.109
Fe	Fe Kα1	LIF	20	10	-250	300		Fe	1234	0.158
Trace:										
Al	Al Kα1	TAP	50	25	-500	300		Corrundum	46	0.017
Ca	Ca Kα1	LPET	40	20	-300	250		Diopside	46	0.006
Ti	Ti Kα1	LPET	40	20	-350	250		Ti	58	0.010
Cr	Cr Kα1	LIF	40	20	-200	300		Cr	219	0.064
Mn	Mn Kα1	LIF	40	20		300	1.0221	Mn	287	0.037
Ni	Ni Kα1	LIF	40	20	-250	300		Ni	322	0.041

1.2 Inductively Coupled Plasma – Mass Spectrometry

All samples were analysed on a PerkinElmer SCIEX Elan DRC II quadrupole ICP-MS (Inductively Coupled Plasma – Mass Spectrometer), in the Department of Earth Sciences at the University of Cambridge, for the REE, Ba, Co, Cs, Cu, Ga, Hf, Nb, Pb, Rb, Sc, Sr, Ta, Th, U, V, Y, Zn and Zr. Be, Li and Sn were also analysed in a small subset of samples. For each sample, 0.1g of powder was digested in a sealed Savillex vial using an Evapoclean system and the HF/HNO_3 technique of Jarvis & Jarvis (1992) before dilution to 3.5% HNO_3. Blanks were prepared with each set of samples. Samples were spiked with In, Re, and Rh to monitor internal drift. Solutions were analysed at a final dilution factor of 5000x using a quartz Meinhard nebuliser and quartz cyclonic spray chamber, with platinum sampler and skimmer cones. ICP-MS sensitivity in this configuration was 4.5 x 105 cps/ppb In with CeO/Ce = 0.03 ± 0.002. Appropriate corrections were made using oxide/metal ratios calculated by analysing pure single-element standard solutions. Instrument calibration was performed using certificate, and high accuracy and precision literature values, for matrix-matched international rock standards AGV-1, BIR-1 and BHVO-2 (see table of standards in Supplementary File) and also in-house standards. Total procedural blanks for all elements were negligible for all analytes (see table of standards in Supplementary File). Solutions were run on two different days. Analytical accuracy and reproducibility were estimated from repeated measurements of

international rock standards AGV-2 and BCR-2 using preferred values from GeoReM (Jochum et al., 2005). BHVO-2 was also analysed repeatedly to check instrument performance and accuracy of the linear calibration. One standard and one blank were analysed at several intervals throughout the whole run to monitor signal drift and contamination within the instrument. % Recovery (REC) is the difference between the literature and experimental values and is given in Table S3. Reproducibility, based on replicate digestions of standards and samples within batches, varied from 0.5% to 3% for most analytes (see Table S3).

1.3 Strontium, neodymium and lead isotope chemistry and multi-collector inductively coupled plasma mass spectrometry

The methods for the collection of isotope data for Sr, Nd (n = 3) and Pb (n = 5) follow the techniques covered in detail in Gibson et al. (2012), and thus are not repeated here. Standard values, precision and corrections applied are listed in the notes to Table S4.

1.4 Rhenium-osmium isotope chemistry and mass spectrometry

Chemistry. Whole-rock powders were digested and analysed over two periods: During 2000 at the Max-Planck-Institut für Chemie in Mainz, and from July to September 2013 at the Arthur Holmes Isotope Geology Laboratory, Department of Earth Sciences, Durham University. The first analytical session, at Mainz, employed a Carius Tube digestion technique following the methods described in Puchtel *et al.* (2001): Approximately 2 g of each sample powder was digested and equilibrated with a ^{190}Os-^{185}Re spike for at least 24 hours, using ~16 mol l^{-1} HNO_3 and ~12 mol l^{-1} HCl, in 3:2 proportions. Osmium was extracted from the sample using bromine and then purified by microdistillation (Birck et al., 1997). Rhenium was separated from the solution using an anion exchange technique similar to Rehkämper & Halliday (1997). At Durham, approximately 1.5g of each sample powder was digested and equilibrated with a ^{190}Os-^{185}Re spike for at least 16 hours in an Anton-Paar high pressure asher (Dale et al., 2012), using 5 mL ~16 mol l^{-1} HNO_3 and 2.5 mL ~12 mol l^{-1} HCl. Osmium was triple-extracted using CCl_4, and then back-extracted into 9 mol l^{-1} HBr (Cohen and Waters, 1996). After drying down, the residue was transferred to the inverted lid of a conical vial and microdistilled (Birck et al., 1997). Rhenium was separated using an anion exchange column method (after Pearson and Woodland, 2000).

Mass spectrometry. At both Durham and Mainz, osmium was loaded onto Pt filaments, ionised as OsO_3^-, and analysed by negative-thermal ionisation mass spectrometry (N-TIMS) using either a Finnigan MAT 262 (Mainz) or a ThermoFinnigan Triton (Durham). All Os isotope beams, and mass 233, corresponding to $^{185}ReO_3^-$, were measured sequentially using an axial secondary electron multiplier. Data were corrected offline for oxygen isotope interferences, spike-unmixing and mass fractionation (using ^{192}Os/^{188}Os ratios of 3.082678 at Mainz and 3.08271 at Durham, but the difference in value used is insignificant at the level of precision required and measured on ^{187}Os/^{188}Os). Counts on mass 233 were typically insignificant for the precision required (<5 cps), with no correlation with mass 235, and thus no correction was made. Repeated analyses of Os standard solutions gave average ^{187}Os/^{188}Os values of 0.10696

± 0.00005 for 35 pg loads (n = 73) of an in-house standard solution at Mainz and 0.16108 ± 0.00016 for 10 pg aliquots (n = 23) of DROsS at Durham, in good agreement with the value of 0.160924 ± 04 measured on much larger aliquots by TIMS and MC-ICP-MS at Durham (Luguet et al., 2008; Nowell et al., 2008).

At Mainz, Re was analysed as ReO_4^- ions by N-TIMS on a Finnigan MAT 262. Repeated measurements of a Johnson Matthey Re standard gave an external uncertainty of 0.1% (2 s.d.; n=57). No mass fractionation correction was made. At Durham, Re was measured at Durham by inductively-coupled plasma mass spectrometry (ICP–MS) on a ThermoFinnigan Element 2. A Romil standard Re solution (1 ng g^{-1}) was analysed at the start, middle and end of each session to quantify the degree of mass fractionation, and a correction was then applied. In either case, the effect of mass fractionation (always less than 2% on the sample concentration) is insignificant in comparison to the other uncertainties on the Re measurements.

Blanks & reproducibility. Total procedural blanks for the two laboratories over the two time periods were: 0.2 - 1.5 pg Os and 0.1 - 0.5 pg Re (n = 8), with a $^{187}Os/^{188}Os$ of 0.14 - 0.17 for Mainz, and 0.25 - 1.9 pg Os and 0.5 - 1.2 pg Re (n = 3) for Durham, with a $^{187}Os/^{188}Os$ of 0.145 - 0.17. Good reproducibility is demonstrated by duplicate analysis of the Fernandina basalt AHA-32D, for which the standard deviation (2σ) on the $^{187}Os/^{188}Os$ and Os concentrations were <0.5% and 7%, respectively. The variation in Re content was greater at 35% (Table 1). Repeat analyses of the CANMET diabase reference material TDB-1 provided a longer-term test of reproducibility which included the second analytical session (Durham): This gave a standard deviation (2σ) of ~20% for Os content and 4% for Re (n = 4), giving rise to a 20% variation in $^{187}Os/^{188}Os$ due to ingrowth over >1000 Ma, but a much smaller variation in terms of the deviation from the trend for this sample on a Re-Os isochron diagram, which provides a better test of accuracy and precision on low-level heterogeneous reference materials. See Ishikawa *et al.* (2014) for the complete long term dataset and discussion of heterogeneity within this sample powder.

References

Birck, J.L., Barman, M.R., Capmas, F., 1997. Re-Os isotopic measurements at the femtomole level in natural samples. Geostand. Newsl. 20, 19-27.

Cohen, A.S., Waters, F.G., 1996. Separation of osmium from geological materials by solvent extraction for analysis by thermal ionisation mass spectrometry. Anal. Chim. Acta 332, 269-275.

Dale, C.W., Macpherson, C.G., Pearson, D.G., Hammond, S.J., Arculus, R.J., 2012. Inter-element fractionation of highly siderophile elements in the Tonga Arc due to flux melting of a depleted source. Geochimica et Cosmochimica Acta 89, 202-225.

Galer, S., 1997. Optimal triple spiking for high precision lead isotope ratio determination. Terr. Nova 9, 441.

Gibson, S.A., Geist, D.G., Day, J.A., Dale, C.W., 2012. Short wavelength heterogeneity in the Galapagos plume: Evidence from compositionally diverse basalts on Isla Santiago. Geochem. Geophys. Geosyst. 13, 9.

Ishikawa, A., Senda, R., Suzuki, K., Dale, C.W., Meisel, T., 2014. Re-evaluating digestion methods for highly siderophile element and ^{187}Os isotope analysis: evidence from geological reference materials. Chemical Geology 384, 27-46.

Luguet, A., Nowell, G.M., Pearson, D.G., 2008. ^{184}Os/^{188}Os and ^{186}Os/^{188}Os measurements by Negative Thermal Ionisation Mass Spectrometry (N-TIMS): Effects of interfering element and mass fractionation corrections on data accuracy and precision. Chemical Geology 248, 342-362.

Nowell, G.M., Luguet, A., Pearson, D.G., Horstwood, M.S.A., 2008. Precise and accurate 186Os/188Os and 187Os/188Os measurements by multi-collector plasma ionisation mass spectrometry (MC-ICP-MS) part I: Solution analyses. Chemical Geology 248, 363-393.

Pearson, D.G., Woodland, S.J., 2000. Solvent extraction/anion exchange separation and determination of PGEs (Os, Ir, Pt, Pd, Ru) and Re-Os isotopes in geological samples by isotope dilution ICP-MS. Chemical Geology 165, 87-107.

Puchtel, I.S., Brügmann, G.E., Hofmann, A.W., 2001. 187Os-enriched domain in an Archean mantle plume: evidence from 2.8 Ga komatiites of the Kostomuksha greenstone belt, NW Baltic Shield. Earth and Planetary Science Letters 186, 513-526.

Rehkämper, M., Halliday, A.N., 1997. Development and application of new ion-exchange techniques for the separation of the platinum group and other siderophile elements from geological samples. Talanta 44, 663-672.